Graduate Theses and Dissertations

Iowa State University Capstones, Theses and Dissertations

2010

Dynamic modeling and ascent flight control of Ares-I Crew Launch Vehicle

Wei Du
Iowa State University

Dynamic modeling and ascent flight control of Ares-I Crew Launch Vehicle

by

Wei Du

A dissertation submitted to the graduate faculty

in partial fulfillment of the requirements for the degree of

DOCTOR OF PHILOSOPHY

Major: Aerospace Engineering

Program of Study Committee:
Bong Wie, Major Professor
Ping Lu
Thomas J. Rudolphi
Zhijian Wang
John Basart

Iowa State University

Ames, Iowa

2010

TABLE OF CONTENTS

LIST OF TABLES

LIST OF FIGURES

ACKNOWLEDGEMENTS

I would first like to thank my supervisor, Dr. Bong Wie, for all his inspiration, guidance and financial support throughout my study at Iowa State University. Dr. Wie provided me a chance to make my dream, studying flight control system of a launch vehicle, come true. I was influenced by his research philosophy, which placed great emphasis on the fundamental knowledge and deep understanding of control theory. His words "there is no magic" and "what is the next logical question" motivated me to finish my Ph.D. program step by step.

Meeting Dr. Ping Lu was another great fortune for me. His organized course on optimal control and aerospace vehicle guidance reshaped my knowledge in those fields. Through discussions with him, his intuition and sense of potential research direction opened my mind.

My appreciation also goes to all my committee members Dr. Thomas Rudolphi, Dr. Zhijian Wang and Dr. John Basart for their valuable help and suggestions to my research. I would also like to thank Dr. Nicola Elia who is a faculty in the Department of Electrical and Computer Engineering. His big picture teaching style and enthusiasm in theoretical research made tedious theorems visible and colorful.

I am indebted to my colleagues at ISU, including Anand Gopa Kumar, Insu Chang, Morgan Baldwin, Matthew Hawkins, Zhongyuan Qian, Ying Zhou, De Huang, Haiyang Gao and a lot of people in the Department of Aerospace Engineering. And I am especially grateful to Matthew Hawkins for his help on polishing my writing.

My sincere thanks go to my parents for their advice and guidance throughout all my education. And I am also thankful to my parents-in-law for their spiritual support.

Lastly, I wish to thank my wife Zhimei for all her love, support and sacrifice. She has always stood beside me and encouraged me. To her I dedicate this dissertation.

ABSTRACT

This research focuses on dynamic modeling and ascent flight control of large flexible launch vehicles such as the Ares-I Crew Launch Vehicle (CLV). A complete set of six-degrees-of-freedom dynamic models of the Ares-I, incorporating its propulsion, aerodynamics, guidance and control, and structural flexibility, is developed. NASA's Ares-I reference model and the SAVANT Simulink-based program are utilized to develop a Matlab-based simulation and linearization tool for an independent validation of the performance and stability of the ascent flight control system of large flexible launch vehicles. A linearized state-space model as well as a non-minimum-phase transfer function model (which is typical for flexible vehicles with non-collocated actuators and sensors) are validated for ascent flight control design and analysis.

This research also investigates fundamental principles of flight control analysis and design for launch vehicles, in particular the classical "drift-minimum" and "load-minimum" control principles. It is shown that an additional feedback of angle-of-attack can significantly improve overall performance and stability, especially in the presence of unexpected large wind disturbances. For a typical "non-collocated actuator and sensor" control problem for large flexible launch vehicles, non-minimum-phase filtering of "unstably interacting" bending modes is also shown to be effective. The uncertainty model of a flexible launch vehicle is derived. The robust stability of an ascent flight control system design, which directly controls the inertial attitude-error quaternion and also employs the non-minimum-phase filters, is verified by the framework of structured singular value (μ) analysis. Furthermore, nonlinear coupled dynamic simulation results are presented for a reference model of the Ares-I CLV as another validation of the feasibility of the ascent flight control system design.

Another important issue for a single main engine launch vehicle is stability under mal-

function of the roll control system. The roll motion of the Ares-I Crew Launch Vehicle under nominal flight conditions is actively stabilized by its roll control system employing thrusters. This dissertation describes the ascent flight control design problem of Ares-I in the event of disabled or failed roll control. A simple pitch/yaw control logic is developed for such a technically challenging problem by exploiting the inherent versatility of a quaternion-based attitude control system. The proposed scheme requires only the desired inertial attitude quaternion to be re-computed using the actual uncontrolled roll angle information to achieve an ascent flight trajectory identical to the nominal flight case with active roll control. Another approach that utilizes a simple adjustment of the proportional-derivative gains of the quaternion-based flight control system without active roll control is also presented. This approach doesn't require the re-computation of desired inertial attitude quaternion. A linear stability criterion is developed for proper adjustments of attitude and rate gains. The linear stability analysis results are validated by nonlinear simulations of the ascent flight phase. However, the first approach, requiring a simple modification of the desired attitude quaternion, is recommended for the Ares-I as well as other launch vehicles in the event of no active roll control.

Finally, the method derived to stabilize a large flexible launch vehicle in the event of uncontrolled roll drift is generalized as a modified attitude quaternion feedback law. It is used to stabilize an axisymmetric rigid body by two independent control torques.

NOMENCLATURE

a	speed of sound = 1117 ft/s at sea level in the standard atmosphere
A_e	nozzle exit area = 122.137 ft^2
b	reference body length = 12.16 ft
(c_x, c_y, c_z)	components of the center of mass location in the structural reference frame with its origin at the top of vehicle = $(-220.31, 0.02, 0.01)$ ft at $t = 0$
C_A	axial force coefficient
$C_{Y\beta}$	side force curve slope with respect to β
C_{N0}	normal force coefficient at zero angle of attack
$C_{N\alpha}$	normal force curve slope with respect to α
$C_{Mr\beta}$	rolling moment curve slope
C_{Mp0}	pitching moment coefficient at zero angle of attack
$C_{Mp\alpha}$	pitching moment curve slope
$C_{My\beta}$	yawing moment curve slope
$\boldsymbol{C}^{B/I}$	direction cosine matrix of the frame B with respect to the frame I
C	lateral (side) force
D	drag (axial) force
F_{base}	base force
$(F_{aero.xb}, F_{aero.yb}, F_{aero.zb})$	body-axis components of aerodynamic force
$(F_{rkt.xb}, F_{rkt.yb}, F_{rkt.zb})$	body-axis components of solid rocket booster force
$(F_{rcs.xb}, F_{rcs.yb}, F_{rcs.zb})$	body-axis components of RCS force
$(F_{total.xb}, F_{total.yb}, F_{total.zb})$	body-axis components of total force

$(F_{total.xi}, F_{total.yi}, F_{total.zi})$	inertial components of total force
(g_x, g_y, g_z)	inertial components of the gravitational acceleration
$(\vec{i}, \vec{j}, \vec{k})$	basis vectors of the body-fixed reference frame B
$(\vec{i}_s, \vec{j}_s, \vec{k}_s)$	basis vectors of the structural reference frame S
$(\vec{I}, \vec{J}, \vec{K})$	basis vectors of the Earth-centered inertial reference frame I
$(\vec{I}_e, \vec{J}_e, \vec{K}_e)$	basis vectors of the Earth-fixed equatorial rotating reference frame E
J_2	Earth's second-order zonal coefficient $= 1.082631 \times 10^{-3}$
J_3	Earth's third-order zonal coefficient $= -2.55 \times 10^{-6}$
J_4	Earth's fourth-order zonal coefficient $= -1.61 \times 10^{-6}$
K_p	proportional gain
K_d	derivative gain
m	vehicle's mass
M	Mach number
N	normal force
p_0	local atmospheric pressure
p_e	nozzle exit pressure
(p, q, r)	body-axis components of $\vec{\omega}$
(q_1, q_2, q_3, q_4)	attitude quaternion of the vehicle with respect to an inertial reference frame
$(q_{1c}, q_{2c}, q_{3c}, q_{4c})$	desired attitude quaternion command from ascent guidance system
$(q_{1e}, q_{2e}, q_{3e}, q_{4e})$	attitude-error quaternion
$(\hat{q}_{1c}, \hat{q}_{2c}, \hat{q}_{3c}, \hat{q}_{4c})$	a modified set of desired attitude quaternion associated with $(\theta_1, \theta_{2c}, \theta_{3c})$
Q	dynamic pressure
R_e	Earth's equatorial radius $= 20,925,646$ ft
R_p	Earth's polar radius $= 20,855,486$ ft
$\vec{r}$	vehicle's position vector
r	magnitude of $\vec{r}$

S	reference area $= 116.2$ ft^2
T	total thrust
T_0	total vacuum thrust
T_∞	thrust at any lower level in the atomosphere
$(T_{aero.xb}, T_{aero.yb}, T_{aero.zb})$	body-axis components of aerodynamic torque
$(T_{rkt.xb}, T_{rkt.yb}, T_{rkt.zb})$	body-axis components of solid rocket torque
$(T_{rcs.xb}, T_{rcs.yb}, T_{rcs.zb})$	body-axis components of RCS torque
U	Earth's gravitational potential
(u, v, w)	body-axis components of $\vec{V}$
$\vec{V}$	vehicle's inertial velocity vector
V_e	exit velocity of the solid rocket booster
$\vec{V}_{rel}$	vehicle's velocity vector relative to the Earth-fixed reference frame
$\vec{V}_w$	velocity vector of the wind
$\vec{V}_m$	air stream velocity vector
V_m	magnitude of the air stream velocity
$(V_{m.xb}, V_{m.yb}, V_{m.zb})$	body-axis components of vehicle's air stream velocity vector
(x, y, z)	inertial components of vehicle's position vector $\vec{r}$
X_a	aerodynamic reference point location in the structural frame $= -275.6$ ft
X_g	gimbal attach point location in the structural frame $= -296$ ft
α	angle of attack
β	angle of sideslip
δ_y	pitch gimbal angle (rotation about the body y-axis)
δ_z	yaw gimbal angle (rotation about the body z-axis)
μ	Earth's gravitational parameter $= 1.407644176 \times 10^{16}$ ft^3/s^2
ϕ	Earth's geocentric latitude
$(\theta_1, \theta_2, \theta_3)$	Euler angles associated with (q_1, q_2, q_3, q_4) for
	$\mathbf{C}_1(\theta_1) \leftarrow \mathbf{C}_2(\theta_2) \leftarrow \mathbf{C}_3(\theta_3)$
$(\theta_{1c}, \theta_{2c}, \theta_{3c})$	Euler angles associated with $(q_{1c}, q_{2c}, q_{3c}, q_{4c})$

$(\theta_1, \theta_{2c}, \theta_{3c})$	a modified set of Euler angles
ρ	density of the air
$\boldsymbol{\eta}$	flexible-mode state vector
ζ	damping ratio of the flexible modes $= 0.005$
$\boldsymbol{\Omega} = diag(\omega_i)$	undamped natural frequency matrix of the flexible modes
$\vec{\omega}$	angular velocity vector of the vehicle
$\vec{\omega}_e = \omega_e \vec{K}$	angular velocity vector of the Earth where $\omega_e = 7.29 \times 10^{-5}$ rad/s

CHAPTER 1.   INTRODUCTION

1.1   Overview
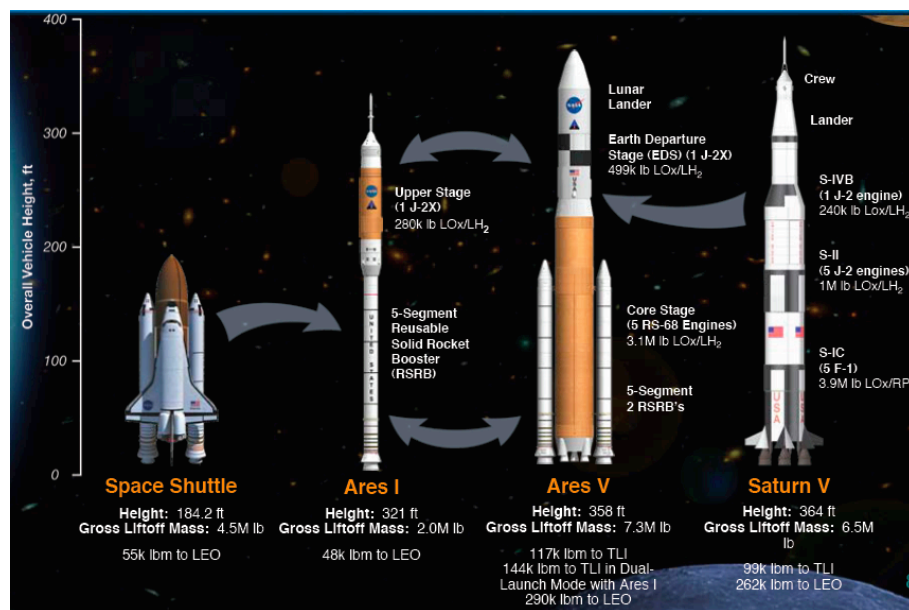
Figure 1.1   Comparison of Space Shuttle, Ares-I, Ares-V, and Saturn V launch vehicles [1].

The Ares-I Crew Launch Vehicle (CLV), being developed by the National Aeronautics and Space Administration (NASA) [1], is a large, slender, and aerodynamically unstable vehicle. It will be used to launch astronauts to Low Earth Orbit and rendezvous with the International Space Station (ISS) or NASA Exploration System Mission Directorate's earth departure stage for lunar or other future missions beyond Low Earth Orbit. In Figure 1.1, its overall configuration is compared to other launch vehicles, including the Ares-V Cargo Launch Vehicle and Saturn V. The Ares-I CLV is a two-stage rocket with a solid-propellant first stage derived from the Shuttle Reusable Solid Rocket Motor/Booster and an upper stage employing a J-2X

engine derived from the Saturn J-2 engines.

1.2 Ares-I Configuration
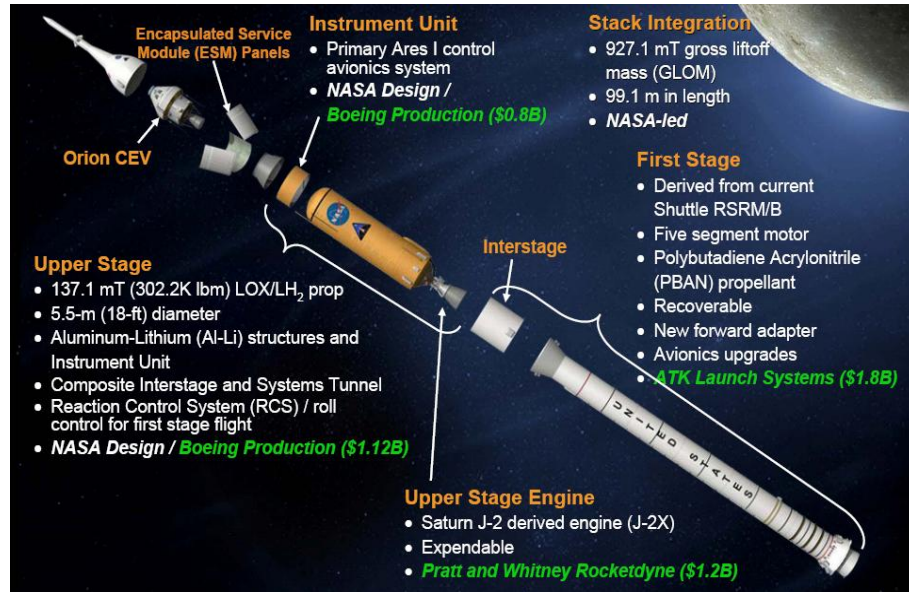
Figure 1.2   Ares-I CLV configuration [2].

Ares-I CLV has an "in-line" configuration as illustrated in Figure 1.2, as opposed to the Shuttle, which has the orbiter and crew placed beside the External Tank. In the event of an emergency, the Orion Crew Module can be blasted away from the launch vehicle using the Launch Abort System (LAS), which will fly directly upward, out of the way of the launch vehicle.

The first stage is a new 5-segment solid rocket booster (SRB), derived from a 4-segment space shuttle reusable solid rocket motor (RSRM). It will also include separation and recovery systems, and SRB nozzle gimbal capability for thrust vector control (TVC). The second stage or upper stage is powered by a liquid oxygen/liquid hydrogen constant-thrust J-2X engine. It also contains avionics and other subsystems. The upper stage and first stage are connected by the interstage, which also contains roll control system (RCS) [3] to prevent the vehicle from spinning as it accelerates upward from the thrust of the SRB.

In addition to the LAS, upper stage, and first stage, the stack includes a forward skirt

and instrument unit, which connects the Orion to the Ares-I and contains the flight computer for controlling the launch vehicle. The Ares-I navigation hardware will be located within an instrumentation ring near the top of the second stage and just behind crew exploration vehicle (CEV). An Inertial Measurement Unit (IMU) located in the instrument unit (at the top of upper stage) will provide inertial position and velocity information to the navigation system [4], and attitude quaternion and angular velocity to the Flight Control System (FCS). Pitch and yaw body rates are obtained from two Rate Gyro Assemblies (RGAs) located near the interstage and the first stage aft skirt (Figure 1.3).
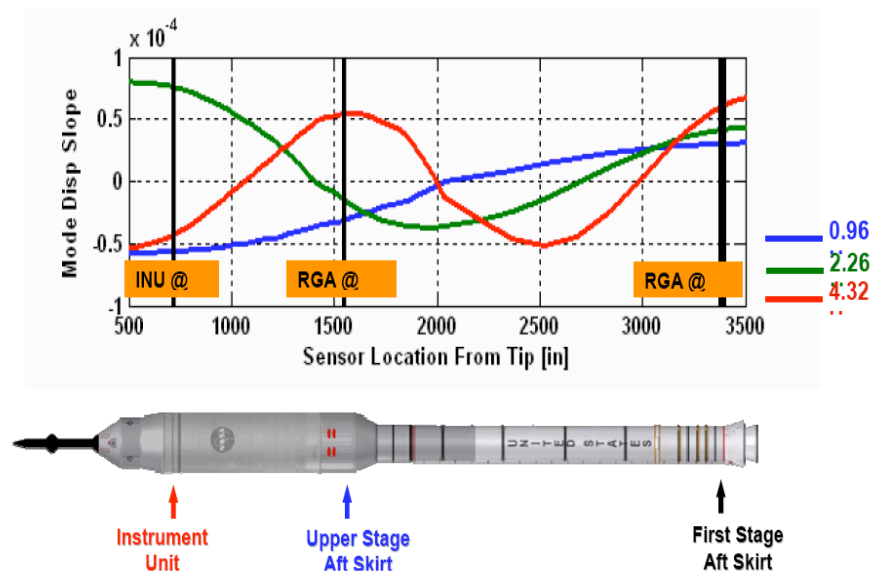
Figure 1.3   Flexible mode shapes and sensor locations of the Ares-I Crew
Launch Vehicle [1]. Currently, rate-gyro blending is not consid-
ered for the Ares-I.

1.3   Ares-I Mission Profile

As seen in Figure 1.4, ascent flight trajectory begins at lift-off and lasts until first stage separation. It takes approximately 120 seconds. This dissertation will focus on flight simulation and ascent flight control system analysis and design during the ascent flight phase. During this phase, Ares-I will experience velocities up to Mach 4.5 at an altitude of about 130,000 feet,
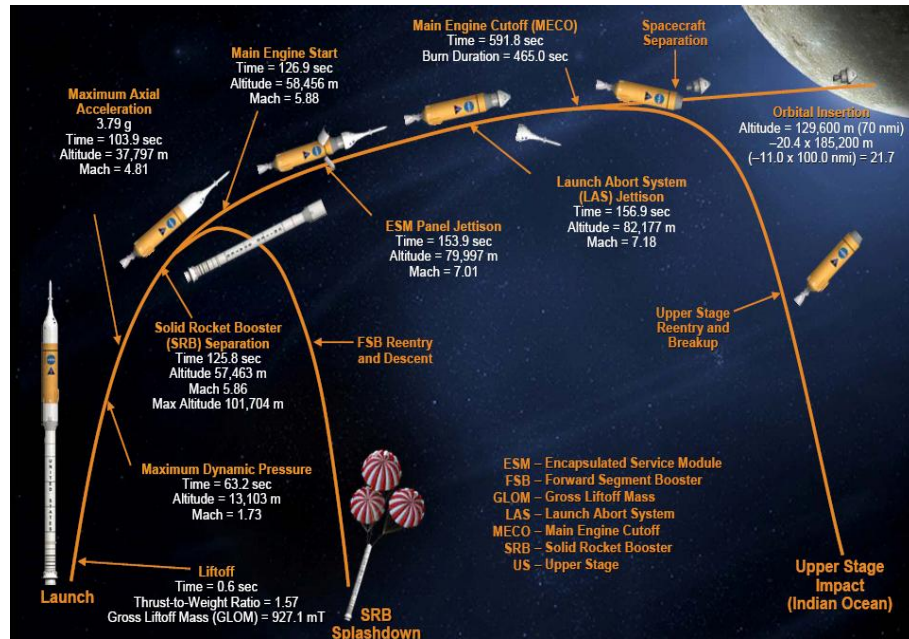
Figure 1.4   Ares-I CLV mission profile [2].

and a maximum dynamic pressure (Max Q) of approximately 800 pounds per square foot.

The ascent flight trajectory can be separated into three phases: vertical flight, transition turn and gravity turn. After SRB ignition, the launch vehicle flies vertically until it has cleared the launch tower. The vertical, stationary attitude flight of the launch vehicle lasts approximately 6 seconds, and then it commences a combined pitch/roll maneuver in order to head the crew window to the launch azimuth, which is defined as the angle between the vertical ascent trajectory plane (or the so-called pitch plane) and a vector pointing from the launch pad toward the North Pole. As a result, the required heads-down orientation of the crew can be maintained during the ascent flight phase [5]. This maneuver is also known as the transition turn [6]. The vehicle transitions from vertical rise to the gravity turn condition. It will fly a gravity turn trajectory until burn out of the SRB and separation [7]. The gravity turn maneuver is used to achieve an ascent trajectory with zero angle of attack and zero sideslip angle (e.g. flying into the relative wind) by minimizing structural bending loads.

Since a detailed discussion of the launch vehicle guidance and trajectory optimization of Ares-I CLV is beyond the scope of this dissertation, the reader is referred to the literature for

a more complete treatment [7, 8, 9].

1.4   Interaction Between Structures and Flight Control System
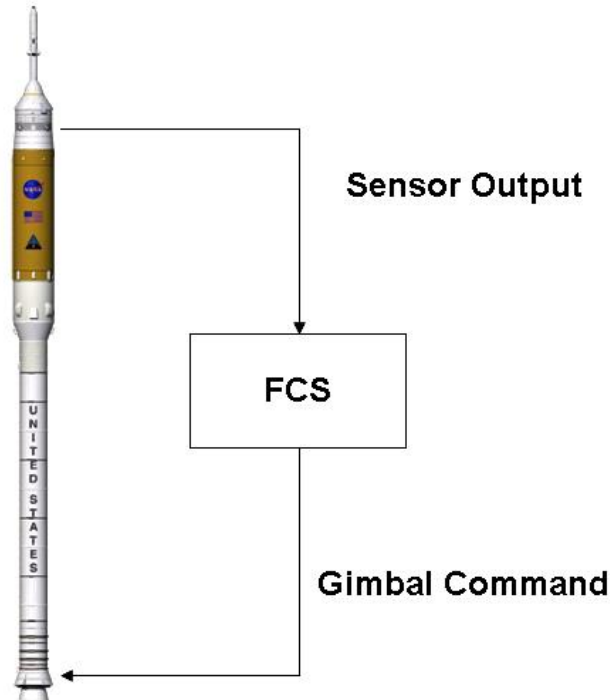
Figure 1.5   Interaction between the ascent flight control and the structural
bending mode.

A launch vehicle is essentially a long slender beam,thus it is structurally very flexible. IMUs
are placed along the vehicle body to sense angular displacement or rate for feedback control.
The IMU measures local elastic distortions as well as rigid body motion. As a result, one
significant risk for a large flexible launch vehicle ascent flight control system is the potential
for interaction between the ascent flight control and the structural bending mode. Because the
first bending mode frequency is usually close to the crossover regime of the rigid body control
system, the control system has the potential to excite the bending mode and destabilize the
vehicle dynamics [11].

This structural feedback problem can be illustrated by Figure 1.5. TVC actuators and

attitude sensors of launch vehicles are not collocated. The sensors pick up both rigid-body motion of the vehicle and motion caused by structural deformations at the location of the sensors. These deformations affect the command to the actuator (usually gimbaled rocket engines). Since engines apply forces to the launch vehicle's structure, energy can be fed into the structure at various frequencies. This will reinforce elastic oscillations, leading ultimately to structural failure of the vehicle.

Conventional roll-off filters and/or notch filters were often used in practice for the stabilization of such unstably interacting bending modes of large flexible launch vehicles [10, 12, 13, 14, 15]. However, in [16, 20, 21], use of non-minimum-phase (NMP) structural filters was shown to be very effective and robust in controlling flexible structures with non-collocated actuators and sensors. In Chapter 3 it will be shown that the NMP filters can stabilize, effectively and robustly, the bending modes of the Ares-I CLV.

1.5   Underactuated Control Problem

The active RCS of Ares-I CLV provides rotational azimuth control to perform a roll orientation maneuver after lift-off and to mitigate against adverse roll torques [22]. It was harvested from the Peacekeeper missile's fourth stage axial thruster system. The challenge for the roll control system is to be able to control large rolling moments, with continuously decreasing principal moment of inertia during flight. RCS failure is a potential threat to the safety of astronauts and launch vehicles. In Chapter 4, the problem of ascent flight control in the event of uncontrolled roll drift will be discussed. Furthermore, it could be generalized as a typical underactuated control problem [23, 24, 25, 26, 27]. In Chapter 5, methods developed to stabilize Ares-I will be generalized as a method to stabilize an axisymmetric rigid body using two control inputs.

CHAPTER 2.   6-DEGREE-OF-FEEDOM DYNAMIC MODELING

2.1   Introduction

A complete set of coupled dynamic models of the Ares-I CLV, incorporating its propulsion, aerodynamics, guidance and control, and structural flexibility will be described in this chapter. The Ares-I CLV is a large, slender, and aerodynamically unstable vehicle. NASA's reference model and SAVANT Simulink-based program [11, 28, 29], as well as various dynamic models of launch vehicles developed previously in the literature [10, 16, 30, 31, 32], were utilized to develop a Matlab-based simulation and linearization tool for an independent validation of the performance and stability of the ascent flight control system of the Ares-I CLV. The block diagram of the Matlab-based simulation program is shown in Figure 2.1.
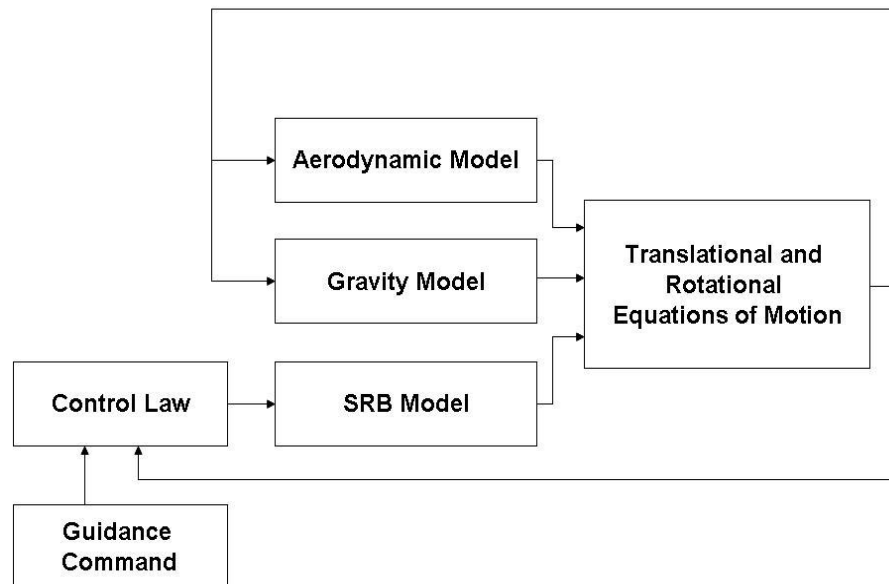
Figure 2.1   Ares-I CLV 6-DOF simulation block diagram.

2.2　Reference Frames and Rotational Kinematics

Various reference frames, which are essential for describing the six-degrees-of-freedom dynamic model of launch vehicles, are discussed in this section.

2.2.1　Earth-Centered Inertial Reference Frame
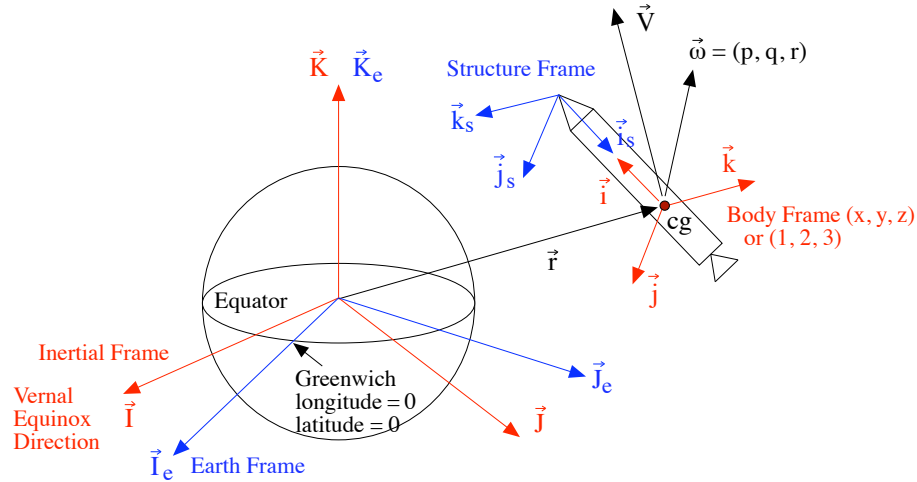
Figure 2.2　Illustration of Earth-centered inertial reference frame $\{\vec{I}, \vec{J}, \vec{K}\}$, Earth-fixed reference frame $\{\vec{I}_e, \vec{J}_e, \vec{K}_e\}$, structural reference frame $\{\vec{i}_s, \vec{j}_s, \vec{k}_s\}$, and body-fixed reference frame $\{\vec{i}, \vec{j}, \vec{k}\}$.

The Earth-centered inertial frame with a set of basis vectors $\{\vec{I}, \vec{J}, \vec{K}\}$ has its origin at the Earth center as illustrated in Figure 2.2. The z-axis is normal to the equatorial plane and the x- and y-axes are in the equatorial plane. The x-axis is along the vernal equinox direction. Because the Earth's orbital motion around the sun is negligible in the trajectory analysis of launch vehicles, this frame is often considered as an inertial reference frame.

The position vector $\vec{r}$ of a launch vehicle is then described as

$$\vec{r} = x\vec{I} + y\vec{J} + z\vec{K} \tag{2.1}$$

The inertial velocity and the inertial acceleration of a launch vehicle become, respectively,

$$\vec{V} = \dot{x}\vec{I} + \dot{y}\vec{J} + \dot{z}\vec{K} \tag{2.2}$$

$$\dot{\vec{V}} = \ddot{x}\vec{I} + \ddot{y}\vec{J} + \ddot{z}\vec{K} \tag{2.3}$$

Figure 2.3　Launch Complex 39B at Kennedy Space Center

For example, if the inertial position vector of the Ares-I at liftoff from Launch Complex 39B (Figure 2.3) at Kennedy Space Center (with longitude 80.6208 deg west and latitude 28.6272 deg north) is given by

$$\vec{r}(0) = x(0)\vec{I} + y(0)\vec{J} + z(0)\vec{K} = -8.7899E4\vec{I} - 1.8385E7\vec{J} + 9.9605E6\vec{K} \text{ (ft)} \tag{2.4}$$

then, the inertial velocity vector of the vehicle at liftoff is obtained as

$$\vec{V}(0) = \dot{x}(0)\vec{I} + \dot{y}(0)\vec{J} + \dot{z}(0)\vec{K} = \vec{\omega}_e \times \vec{r}(0) = 1340.65\vec{I} - 6.41\vec{J} \text{ (ft/sec)} \tag{2.5}$$

where $\vec{\omega}_e = \omega_e \vec{K}$ is the angular velocity vector of the Earth and $\omega_e = 7.2921 \times 10^{-5}$ rad/s, which corresponds to 360 deg per sidereal day of 23 h 56 min 4 s.

2.2.2　Earth-Fixed Equatorial Reference Frame

The geocentric equatorial rotating frame with a set of basis vectors $\{\vec{I}_e, \vec{J}_e, \vec{K}_e\}$, with its origin at the Earth center, is fixed to the Earth (Figure 2.2). Its Z-axis is normal to the

equatorial plane and its x- and y-axes are in the equatorial plane. However, its x-axis is along the Greenwich meridian. This Earth frame has an angular velocity $\vec{\Omega}_e$ which is the rotational velocity of the Earth.

2.2.3 Body-Fixed Reference Frame

The body-fixed frame with basis vectors $\{\vec{i}, \vec{j}, \vec{k}\}$ is fixed to the vehicle's body as illustrated in Figure 2.2. Its origin is the center of mass. The $\vec{i}$-axis is along the vehicle's longitudinal axis. The $\vec{k}$-axis perpendicular to the $\vec{i}$-axis points downward while the $\vec{j}$-axis points rightward.

The inertial velocity vector $\vec{V}$ is then expressed as

$$\vec{V} = u\vec{i} + v\vec{j} + w\vec{k} \tag{2.6}$$

The angular velocity vector $\vec{\omega}$ of the launch vehicle is also expressed as

$$\vec{\omega} = p\vec{i} + q\vec{j} + r\vec{k} \tag{2.7}$$

The inertial acceleration vector is then described as

$$\dot{\vec{V}} = (\dot{u}\vec{i} + \dot{v}\vec{j} + \dot{w}\vec{k}) + \vec{\omega} \times \vec{V} \tag{2.8}$$

2.2.4 Structural Reference Frame

A structural reference frame with basis vectors $\{\vec{i}_s, \vec{j}_s, \vec{k}_s\}$ and with its origin at the top of vehicle is also employed in the SAVANT program. The locations of center of gravity, gimbal attach point, aerodynamic reference point, and other mass properties, are defined using this structural frame. However, Euler's rotational equations of motion will be written in terms of the body-fixed frame with its origin at the center of gravity. Because $\vec{i}_s = -\vec{i}$, $\vec{j}_s = \vec{j}$, and $\vec{k}_s = -\vec{k}$, we have

$$\boldsymbol{C}^{B/S} = \begin{pmatrix} -1 & 0 & 0 \\ 0 & 1 & 0 \\ 0 & 0 & -1 \end{pmatrix} \tag{2.9}$$

where $\boldsymbol{C}^{B/S}$ is the direction cosine matrix of frame B with respect to frame S.

2.2.5   Earth-Fixed Launch Pad Reference Frame
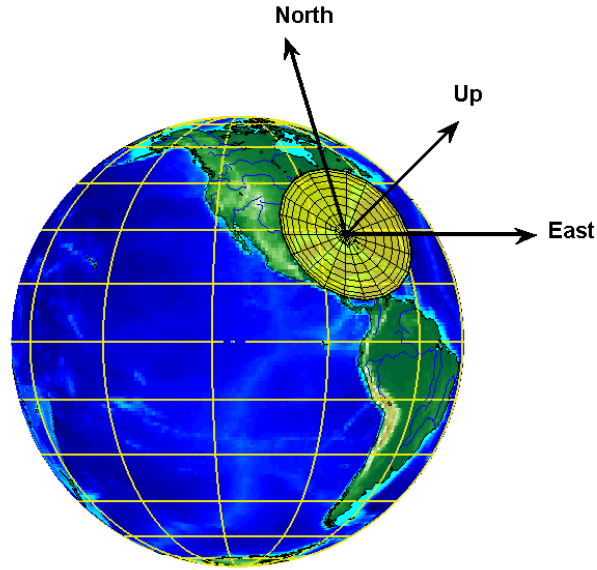
Figure 2.4   Earth-fixed launch pad reference frame with a local tangent
plan at Launch Complex 39B at Kennedy Space Center.

In order to visualize the ascent flight trajectory in an intuitive way, another reference frame, called the Earth-fixed launch pad (up, east, north) reference frame is introduced here. Its origin is at the Launch Complex 39B at NASA's Kennedy Space Center with the latitude 28.6272 deg and longitude -80.6208 deg as illustrated in Figures 2.4.

2.2.6   Euler Angles and Quaternions

The coordinate transformation to the body frame B from the inertial frame I is described by three Euler angles $(\theta_1, \theta_2, \theta_3)$. For a rotational sequence of $\boldsymbol{C}_1(\theta_1) \leftarrow \boldsymbol{C}_2(\theta_2) \leftarrow \boldsymbol{C}_3(\theta_3)$, we have

$$\boldsymbol{C}^{B/I} = \begin{pmatrix} \cos\theta_2\cos\theta_3 & \cos\theta_2\sin\theta_3 & -\sin\theta_2 \\ \sin\theta_1\sin\theta_2\cos\theta_3 - \cos\theta_1\sin\theta_3 & \sin\theta_1\sin\theta_2\sin\theta_3 + \cos\phi\cos\theta_3 & \sin\theta_1\cos\theta \\ \cos\theta_1\sin\theta_2\cos\theta_3 + \sin\theta_1\sin\theta_3 & \cos\theta_1\sin\theta_2\sin\theta_3 - \sin\phi\cos\theta_3 & \cos\theta_1\cos\theta \end{pmatrix}$$

(2.10)

which is the direction cosine matrix of the body frame B relative to the inertial frame I. However, the three Euler angles (θ_1, θ_2, θ_3) do not actually represent the vehicle's roll, pitch, and yaw attitude angles to be used for attitude feedback control.

The rotational kinematic equation for three Euler angles (θ_1, θ_2, θ_3) is given by

$$\begin{pmatrix} \dot{\theta}_1 \\ \dot{\theta}_2 \\ \dot{\theta}_3 \end{pmatrix} = \frac{1}{\cos\theta_2} \begin{pmatrix} \cos\theta_2 & \sin\theta_1\sin\theta_2 & \cos\theta_1\sin\theta_2 \\ 0 & \cos\theta_1\cos\theta_2 & -\sin\theta_1\cos\theta_2 \\ 0 & \sin\theta_1 & \cos\theta_1 \end{pmatrix} \begin{pmatrix} p \\ q \\ r \end{pmatrix} \tag{2.11}$$

The inherent singularity problem of Euler angles can be avoided by using quaternions [33]. The rotational kinematic equation in terms of quaternion (q_1, q_2, q_3, q_4) is given by

$$\begin{pmatrix} \dot{q}_1 \\ \dot{q}_2 \\ \dot{q}_3 \\ \dot{q}_4 \end{pmatrix} = \frac{1}{2} \begin{pmatrix} 0 & r & -q & p \\ -r & 0 & p & q \\ q & -p & 0 & r \\ -p & -q & -r & 0 \end{pmatrix} \begin{pmatrix} q_1 \\ q_2 \\ q_3 \\ q_4 \end{pmatrix} \tag{2.12}$$

where the quaterions are related to the three Euler angles as follows:

$$\begin{aligned} q_1 &= \sin(\theta_1/2)\cos(\theta_2/2)\cos(\theta_3/2) - \cos(\theta_1/2)\sin(\theta_2/2)\sin(\theta_3/2) \\ q_2 &= \cos(\theta_1/2)\sin(\theta_2/2)\cos(\theta_3/2) + \sin(\theta_1/2)\cos(\theta_2/2)\sin(\theta_3/2) \\ q_3 &= \cos(\theta_1/2)\cos(\theta_2/2)\sin(\theta_3/2) - \sin(\theta_1/2)\sin(\theta_2/2)\cos(\theta_3/2) \\ q_4 &= \cos(\theta_1/2)\cos(\theta_2/2)\cos(\theta_3/2) + \sin(\theta_1/2)\sin(\theta_2/2)\sin(\theta_3/2) \end{aligned} \tag{2.13}$$

The coordinate transformation matrix to the body frame from the inertial frame in terms of quaternions is

$$\mathbf{C}^{B/I} = \begin{pmatrix} 1-2(q_2^2+q_3^2) & 2(q_1q_2+q_3q_4) & 2(q_1q_3-q_2q_4) \\ 2(q_1q_2-q_3q_4) & 1-2(q_1^2+q_3^2) & 2(q_2q_3+q_1q_4) \\ 2(q_1q_3+q_2q_4) & 2(q_2q_3-q_1q_4) & 1-2(q_1^2+q_2^2) \end{pmatrix} \tag{2.14}$$

We also have

$$\mathbf{C}^{I/B} = [\mathbf{C}^{B/I}]^{-1} = [\mathbf{C}^{B/I}]^T = \begin{pmatrix} 1-2(q_2^2+q_3^2) & 2(q_1q_2-q_3q_4) & 2(q_1q_3+q_2q_4) \\ 2(q_1q_2+q_3q_4) & 1-2(q_1^2+q_3^2) & 2(q_2q_3-q_1q_4) \\ 2(q_1q_3-q_2q_4) & 2(q_2q_3+q_1q_4) & 1-2(q_1^2+q_2^2) \end{pmatrix} \tag{2.15}$$
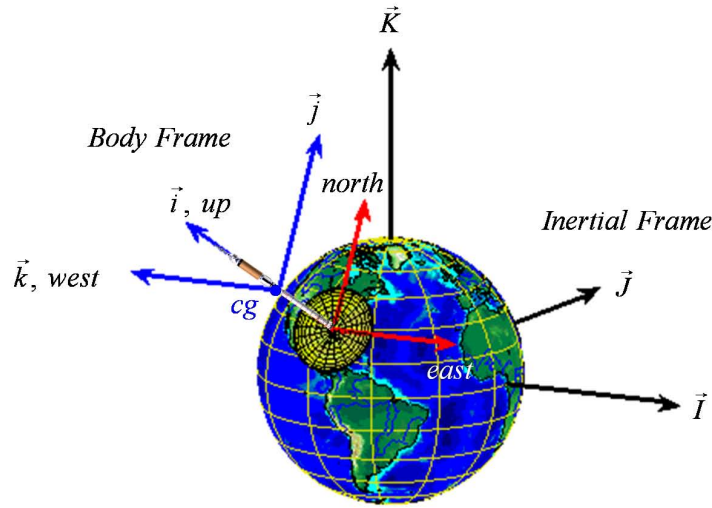
Figure 2.5   Illustration of the Earth-centered inertial reference frame with $\{\vec{I}, \vec{J}, \vec{K}\}$, the Earth-fixed launch pad (up, east, north) reference frame, and the Ares-I orientation with $\{\vec{i}, \vec{j}, \vec{k}\}$ on Launch Complex 39B.

2.2.7   Initial Position of Ares-I CLV on the Launch Pad

In NASA's SAVANT program [28, 29], the inertial attitude quaternion of the Ares-I are computed with respect to the ECI frame. For the Ares-I orientation on the launch pad, the x-axis of body-fixed reference frame points up to the sky, the y-axis points northward, and the z-axis points westward, as illustrated in Figure 2.5. Consequently, the initial Euler angles $(\theta_1,\ \theta_2,\ \theta_3)$ at $t = 0$ are $(89.9881, -28.6090, -90.2739)$ deg for the rotational sequence of $\mathbf{C}_1(\theta_1) \leftarrow \mathbf{C}_2(\theta_2) \leftarrow \mathbf{C}_3(\theta_3)$ [16]. It is emphasized that these Euler angles are not the traditional (roll, pitch, yaw) attitude angles which describe the orientation of a launch vehicle with respect to the boost trajectory plane or the so-called pitch plane.

2.3   The 6-DOF Equations of Motion

The six-degrees-of-freedom (6-DOF) equations of motion of a launch vehicle consist of the translational and rotational equations. The translational equation of motion of the center of gravity of a launch vehicle is simply given by

$$m\dot{\vec{V}} = \vec{F} \tag{2.16}$$

where $\vec{F}$ is the total force acting on the vehicle. Using Equation. (2.3) and Equation. (2.8), we obtain the translational equation of motion of the form

$$\ddot{x}\vec{I} + \ddot{y}\vec{J} + \ddot{z}\vec{K} = \frac{\vec{F}}{m} \tag{2.17}$$

or

$$\dot{u}\vec{i} + \dot{v}\vec{j} + \dot{w}\vec{k} + \vec{\omega} \times \vec{V} = \frac{\vec{F}}{m} \tag{2.18}$$

The Euler's rotational equation of motion of a rigid vehicle is

$$\dot{\vec{H}} = \vec{T} \tag{2.19}$$

where $\vec{H}$ is the angular momentum vector and $\vec{T}$ is the total external torque about the center of gravity. The angular momentum vector is often expressed as

$$\vec{H} = \hat{I} \cdot \vec{\omega} \tag{2.20}$$

where $\vec{\omega} = p\vec{i} + q\vec{j} + r\vec{k}$ is the angular velocity vector and $\hat{I}$ is the vehicle's inertia dyadic about the center of gravity of the form [16]

$$\hat{I} = \left(\begin{array}{ccc} \vec{i} & \vec{j} & \vec{k} \end{array} \right) \left(\begin{array}{ccc} I_{xx} & I_{xy} & I_{xz} \\ I_{xy} & I_{yy} & I_{yz} \\ I_{xz} & I_{yz} & I_{zz} \end{array} \right) \left(\begin{array}{c} \vec{i} \\ \vec{j} \\ \vec{k} \end{array} \right) \tag{2.21}$$

The rotational equation of motion is then given by

$$\hat{I} \cdot \dot{\vec{\omega}} + \vec{\omega} \times \hat{I} \cdot \vec{\omega} = \vec{T} \tag{2.22}$$

where $\dot{\vec{\omega}} = \dot{p}\vec{i} + \dot{q}\vec{j} + \dot{r}\vec{k}$ is the angular acceleration vector.

2.3.1   Aerodynamic Forces and Moments

Aerodynamic forces and moments depend on the vehicle's velocity relative to the surrounding air mass, called the air speed. It is assumed that the air mass is static relative to the Earth. That is, the entire air mass rotates with the Earth without slippage and shearing. A hybrid approach of CFD and wind tunnel data have been developed for Ares-I [34]. The air stream velocity vector $\vec{V}_m$ is then described by

$$\vec{V}_m = \vec{V}_{rel} - \vec{V}_w = \vec{V} - \vec{\omega}_e \times \vec{r} - \vec{V}_w \tag{2.23}$$

where $\vec{V}_{rel}$ is the vehicle's velocity vector relative to the Earth-fixed reference frame, $\vec{V}_w$ is the local disturbance wind velocity, $\vec{V}$ is the inertial velocity of the vehicle, $\vec{\omega}_e$ is the Earth's rotational angular velocity vector, and $\vec{r}$ is the vehicle's position vector from the Earth center.

The matrix form of Eq. (2.23) in the body frame is

$$\begin{pmatrix} V_{m.xb} \\ V_{m.yb} \\ V_{m.zb} \end{pmatrix} = \begin{pmatrix} u \\ v \\ w \end{pmatrix} - \mathbf{C}^{B/I} \begin{pmatrix} 0 & -\omega_e & 0 \\ \omega_e & 0 & 0 \\ 0 & 0 & 0 \end{pmatrix} \begin{pmatrix} x \\ y \\ z \end{pmatrix} - \begin{pmatrix} V_{w.xb} \\ V_{w.yb} \\ V_{w.zb} \end{pmatrix} \tag{2.24}$$

where $(V_{m.xb},\ V_{m.yb},\ V_{m.zb})$ are the body-axis components of the vehicle's air stream velocity vector. Note that $\vec{r} = x\vec{I} + y\vec{J} + z\vec{K}$ and $\vec{\omega}_e = \omega_e \vec{K}$.

The aerodynamic forces are expressed in the body-axis frame as

$$D = C_A QS - F_{base} \tag{2.25a}$$

$$C = C_{Y\beta}\beta QS \tag{2.25b}$$

$$N = (C_{N0} + C_{N\alpha}\alpha)QS \tag{2.25c}$$

where the base force F_{base} is a function of the altitude, the aerodynamic force coefficients are functions of Mach number, and

$$M = \frac{V_m}{a} = \text{Mach number} \tag{2.26}$$

$$Q = \frac{1}{2}\rho V_m^2 = \text{dynamic pressure} \tag{2.27}$$

$$\alpha = \arctan\left\{\frac{V_{m.zb}}{V_{m.xb}}\right\} = \text{angle of attack} \tag{2.28}$$

$$\beta = \arcsin\left\{\frac{V_{m.yb}}{V_m}\right\} = \text{sideslip angle} \tag{2.29}$$

The speed of sound a and the air density ρ are functions of the altitude h.

Furthermore, we have

$$F_{aero.xb} = -D \tag{2.30a}$$

$$F_{aero.yb} = C \tag{2.30b}$$

$$F_{aero.zb} = -N \tag{2.30c}$$

The aerodynamic moments about the center of gravity are also expressed in the body-axis frame as

$$\begin{pmatrix} T_{aero.xb} \\ T_{aero.yb} \\ T_{aero.zb} \end{pmatrix} = \begin{pmatrix} 0 & c_z & -c_y \\ -c_z & 0 & -X_a + c_x \\ c_y & X_a - c_x & 0 \end{pmatrix} \begin{pmatrix} F_{aero.xb} \\ F_{aero.yb} \\ F_{aero.zb} \end{pmatrix} + \begin{pmatrix} C_{Mr\beta}QSb \\ (C_{Mp0} + C_{Mp\alpha}\alpha)QSb \\ C_{My\beta}\beta QSb \end{pmatrix} \tag{2.31}$$

where $X_a = 275.6$ ft is the aerodynamic reference point in the structure frame, $(c_x,\ c_y,\ c_z)$ is the center of gravity location in the structure reference frame with its origin at the top of vehicle. At $t = 0$, we have $(c_x,\ c_y,\ c_z) = (220.31, 0.02, 0.01)$ ft. The aerodynamic moment coefficients are functions of Mach number.

2.3.2 Gravity Model

The J4 gravity model used in the SAVANT program is given as

$$C_1 = -1 + \frac{R_e^2}{r^2}\left[3J_2\left(\frac{3}{2}\sin^2\phi - \frac{1}{2}\right) + 4J_3\frac{R_e}{r}\left(\frac{5}{2}\sin^3\phi - \frac{3}{2}\sin\phi\right)\right.$$
$$\left. + 5J_4\frac{R_e^2}{r^2}\left(\frac{35}{8}\sin^4\phi - \frac{15}{4}\sin^2\phi + \frac{3}{8}\right)\right] \tag{2.32}$$

where ϕ is the Earth's geocentric latitude.

$$C_2 = J_2(3\sin\phi) + \frac{R_e}{r}J_3\left(\frac{15}{2}\sin^2\phi - \frac{3}{2}\right) + \frac{R_e^2}{r^2}J_4\left(\frac{35}{2}\sin^3\phi - \frac{15}{2}\sin\phi\right) \tag{2.33}$$

The inertial components of the gravitational acceleration are

$$
\begin{pmatrix} g_x \\ g_y \\ g_z \end{pmatrix} = \frac{\mu}{r^2} \left[C_1 \begin{pmatrix} x/r \\ y/r \\ z/r \end{pmatrix} - C_2 \begin{pmatrix} 0 & -z/r & y/r \\ z/r & 0 & -x/r \\ -y/r & x/r & 0 \end{pmatrix} \begin{pmatrix} -y/r \\ x/r \\ 0 \end{pmatrix} \right] \tag{2.34}
$$

The mathematical models used in the SAVANT program for computing the vehicle's altitude h are summarized as

$$
f = \frac{R_e - R_p}{R_e} = \frac{1}{298.257} \tag{2.35}
$$

$$
\tan \Phi = \frac{\tan \phi}{(1-f)^2} \tag{2.36}
$$

$$
A = \left(\frac{\cos \Phi}{R_e} \right)^2 + \left(\frac{\sin \Phi}{R_p} \right)^2 \tag{2.37}
$$

$$
B = -\frac{\sqrt{x^2 + y^2} \cos \Phi}{R_e^2} - \frac{z \sin \Phi}{R_p^2} \tag{2.38}
$$

$$
C = \left(\frac{z}{R_p} \right)^2 + \frac{x^2 + y^2}{R_p^2} - 1 \tag{2.39}
$$

$$
h = -\frac{B}{A} - \sqrt{\left(\frac{B}{A} \right)^2 - \frac{C}{A}} \tag{2.40}
$$

where f is the Earth's flatness parameter, ϕ is the geocentric latitude, and Φ is the geodetic latitude (which is commonly employed on geographical maps).

2.3.3   Rocket Propulsion Model

The rocket thrust is simply modeled as

$$
T = T_0 + (p_e - p_0) A_e \tag{2.41}
$$

where T is the total thrust force, $T_0 = |\dot{m}| V_e$ the jet thrust, p_e the nozzle exit pressure, p_0 the local atmospheric pressure (a function of the altitude), $\dot{m}$ the propellant mass flow rate, V_e the exit velocity, and A_e the nozzle exit area ($= 122.137$ ft^2).

If the thrust in the vacuum of space above the atmosphere is called T_∞, then the thrust at any lower level in the atmosphere is [8]

$$T = T_\infty - p_0 A_e \tag{2.42}$$

where $T_\infty = T_0 + p_e A_e$.

The body-axis components of the thrust force are

$$\begin{pmatrix} F_{rkt.xb} \\ F_{rkt.yb} \\ F_{rkt.zb} \end{pmatrix} = \begin{pmatrix} T \\ -T\delta_z \\ T\delta_y \end{pmatrix} \tag{2.43}$$

where δ_y and δ_z are the pitch and yaw gimbal deflection angles, respectively. Gimbal deflection angles are assumed to be small (with $\delta_{max} = \pm 10$ deg).

The body-axis components of the rocket thrust-generated torque are

$$\begin{pmatrix} T_{rkt.xb} \\ T_{rkt.yb} \\ T_{rkt.zb} \end{pmatrix} = \begin{pmatrix} 0 & c_z & -c_y \\ -c_z & 0 & -X_g + c_x \\ c_y & X_g - c_z & 0 \end{pmatrix} \begin{pmatrix} F_{rkt.xb} \\ F_{rkt.yb} \\ F_{rkt.zb} \end{pmatrix} \tag{2.44}$$

where $X_g = 296$ft is the gimbal attach point location in the structural frame.

The body-axis components of the roll control torque from the RCS are

$$\begin{pmatrix} T_{rcs.xb} \\ T_{rcs.yb} \\ T_{rcs.zb} \end{pmatrix} = \begin{pmatrix} T_{rcs} \\ 0 \\ 0 \end{pmatrix} \tag{2.45}$$

2.3.4 Guidance and Control

The commanded quaternion (q_{1c}, q_{2c}, q_{3c}, q_{4c}) computed by the guidance system are used to generate the attitude-error quaternion (q_{1e}, q_{2e}, q_{3e}, q_{4e}) as follows [16]:

$$\begin{pmatrix} q_{1e} \\ q_{2e} \\ q_{3e} \\ q_{4e} \end{pmatrix} = \begin{pmatrix} q_{4c} & q_{3c} & -q_{2c} & -q_{1c} \\ -q_{3c} & q_{4c} & q_{1c} & -q_{2c} \\ q_{2c} & -q_{1c} & q_{4c} & -q_{3c} \\ q_{1c} & q_{2c} & q_{3c} & q_{4c} \end{pmatrix} \begin{pmatrix} q_1 \\ q_2 \\ q_3 \\ q_4 \end{pmatrix} \tag{2.46}$$

where the attitude quaternion (q_1, q_2, q_3, q_4) are computed by numerically integrating the kinematic differential equation, Equation. (2.12).

The guidance command used in the simulation is for the ISS mission at an orbital inclination of 51.6 deg [7].

The simplified control laws of the ascent flight control system are then described as

$$T_{rcs} = -K_{px}(2q_{1e}) - K_{dx}p \tag{2.47a}$$

$$\delta_y = -K_{py}(2q_{2e}) - K_{iy}\int (2q_{2e})dt - K_{dy}q \tag{2.47b}$$

$$\delta_z = -K_{pz}(2q_{3e}) - K_{dz}r \tag{2.47c}$$

An integral control is added to the pitch control channel. The terms ($2q_{1e}$, $2q_{2e}$, $2q_{3e}$) are the roll, pitch, and yaw attitude errors, respectively. This quaternion-error feedback control is in general applicable for arbitrarily large angular motion of vehicles [16, 17, 18, 19]. Feedback of Euler-angle errors ($\theta_1 - \theta_{1c}$, $\theta_2 - \theta_{2c}$, $\theta_3 - \theta_{3c}$) is not applicable here because the Euler angles employed in this paper (also used in the SAVANT program) are defined with respect to the Earth-centered inertial reference frame, not with respect to the so-called pitch plane or a navigation reference frame of launch vehicles [10, 16, 30, 31, 32, 35].

2.3.5   Flexible-Body Modes

For the purposes of ascent flight control system stability analysis, the lateral vibration modes are important, since this motion is sensed by the IMU [10]. Usually, a forced vibration of a free-free beam model can be expressed mathematically by Euler-Bernoulli beam model, neglecting shear distortion and rotational inertia, as follows:

$$m(l)\frac{\partial^2\xi(l,t)}{\partial t^2} + \frac{\partial^2}{\partial l^2}[EI(l)\frac{\partial^2\xi(l,t)}{\partial l^2}] = T(t)\delta \tag{2.48}$$

where m is mass per unit length, EI is bending stiffness and ξ is beam deflection. Note that for the case of free vibration, the term on the right side of the equal sign in Equation. (2.48) is zero.

For the free-free case where the shear $\frac{\partial^2 \xi}{\partial l^2}$ and bending moment $\frac{\partial^3 \xi}{\partial l^3}$ at the ends of the beam are zero, the boundary conditions are given by

$$\frac{\partial^2 \xi(0,t)}{\partial l^2} = \frac{\partial^2 \xi(L,t)}{\partial l^2} = 0 \tag{2.49}$$

$$\frac{\partial^3 \xi(0,t)}{\partial l^3} = \frac{\partial^3 \xi(L,t)}{\partial l^3} = 0 \tag{2.50}$$

Assuming that there is one solution of the free vibration, it can be written in the form

$$\xi(l,t) = \phi(l)\eta(t) \tag{2.51}$$

where $\phi(l)$ presents the shape of a natural vibration mode and $\eta(t)$ is the modal coordinate of this mode.

Substituting Equation. (2.51) in Equation. (2.48) leads to

$$-\frac{1}{\eta(t)}\frac{d^2\eta(t)}{dt^2} = \frac{d^2}{dl^2}[EI(l)\frac{d^2\phi(l)}{dl^2}] \tag{2.52}$$

The left side is a function of time t only, and the right side is a function of l. This equation is valid only if the function on either side is equal to some constant, say ω^2. Thus the partial differential equation Equation. (2.48) becomes two ordinary differential equations as follows:

$$\frac{d^2\eta(t)}{dt^2} + \omega^2\eta(t) = 0 \tag{2.53}$$

$$\frac{d^2}{dl^2}[EI(l)\frac{d^2\phi(l)}{dl^2}] - \omega^2 m(l)\phi(l) = 0 \tag{2.54}$$

where ω is the vibration frequency corresponding to the mode $\phi(l)$. Here, for Equation. (2.54), numerical methods must be used to calculate the natural frequencies and mode shapes corresponding to specific boundary conditions. Once these are known, the complete solution in the case of free vibrations may be written as

$$\xi(l,t) = \sum_{i=1}^{\infty} \phi_i(x)\eta_i(t) \tag{2.55}$$

where $\phi_i(t)$ is the ith normal mode shape, $\eta_i(t)$ is the ith modal coordinate. It is very straightforward to express the forced motion in these terms and to take account of structural damping.

Detailed derivations for the Euler-Bernoulli model and forced vibrations of nonuniform beam can be found in text books [10, 16, 36]. Structural dynamics of Ares-I were modeled as linear second order systems with a damping ratio of 0.5%. The value 0.5% used for flight control analysis is considered conservative. A Finite Element Model (NASTRAN/PATRAN) was used to obtain bending mode frequencies and shapes [34].

A flexible-body model of Ares-I is expressed as

$$\ddot{\boldsymbol{\eta}} + 2\zeta\boldsymbol{\Omega}\dot{\boldsymbol{\eta}} + \boldsymbol{\Omega}^2\boldsymbol{\eta} = \boldsymbol{\Phi}^T\boldsymbol{F}_{rkt} \tag{2.56}$$

where $\boldsymbol{F}_{rkt} = (F_{rkt.xb}, \ F_{rkt.yb}, \ F_{rkt.zb})^T$ and $\boldsymbol{\Phi}$ is the flexible mode influence matrix at the gimbal attach point.

Sensor measurements including the effects of the flexible bending modes are modeled as

$$\boldsymbol{e}_{attitude} = \begin{pmatrix} 2q_{1e} \\ 2q_{2e} \\ 2q_{3e} \end{pmatrix} + \boldsymbol{\Psi}\boldsymbol{\eta} \tag{2.57}$$

$$\boldsymbol{e}_{rate} = \begin{pmatrix} p \\ q \\ r \end{pmatrix} + \boldsymbol{\Psi}\dot{\boldsymbol{\eta}} \tag{2.58}$$

where $\boldsymbol{\Psi}$ is the flex-mode influence matrix at the instrument unit location (Figure 1.3).

A summary of the 6-DOF equations of motion can be found in Appendix A.

2.4 Simulation Results of the Rigid Body Ares-I Crew Launch Vehicle

A set of initial conditions for the Ares-I is provided in Table 2.1. The corresponding the initial Euler angles $(\theta_1, \ \theta_2, \ \theta_3)$ at $t = 0$ are $(89.9881, -28.6090, -90.2739)$ deg. The inertia matrix about the body frame with its origin at the center of gravity at $t = 0$ is

$$\begin{pmatrix} I_{xx} & I_{xy} & I_{xz} \\ I_{xy} & I_{yy} & I_{yz} \\ I_{xz} & I_{yz} & I_{zz} \end{pmatrix} = \begin{pmatrix} 1.2634E6 & -1.5925E3 & 5.5250E4 \\ -1.5925E3 & 2.8797E8 & -1.5263E3 \\ 5.5250E4 & -1.5263E3 & 2.8798E8 \end{pmatrix} \text{ slug-ft}^2 \tag{2.59}$$

Table 2.1   Initial conditions at liftoff

State variables	Initial values	Units
$\dot{x}$	1340.65	ft/s
$\dot{y}$	-6.41	ft/s
$\dot{z}$	0	ft/s
x	-8.7899×10^4	ft
y	-1.8385×10^7	ft
z	9.9605×10^6	ft
p	3.4916×10^{-5}	rad/s
q	6.4018×10^{-5}	rad/s
r	0	rad/s
q_1	0.3594	
q_2	-0.6089	
q_3	-0.3625	
q_4	0.6072	

Flexible-body mode shape matrices (with 6 flexible modes) are

$$\mathbf{\Phi} = \begin{pmatrix} 0.000000272367963 & 0.000000174392026 & -0.000000347086527 \\ -0.000364943105155 & 0.006281028219530 & 0.000491932740239 \\ 0.006281175443849 & 0.000364891432306 & -0.006260333099131 \\ -0.000000266173427 & 0.000000329288262 & -0.000000369058169 \\ -0.006259406451949 & -0.000542750533582 & -0.007673360355205 \\ -0.000491798506301 & 0.007676195145027 & -0.000542218216634 \end{pmatrix} \tag{2.60}$$

$$\mathbf{\Psi} = \begin{pmatrix} 0.002287263504447 & -0.003936428406260 & -0.002315093057592 \\ -0.193164818571118 & -0.011222878633268 & -0.253963647069578 \\ -0.011222390194941 & 0.193169876159476 & -0.019955470041040 \\ 0.003866041325542 & 0.002898204936058 & 0.005033045198158 \\ -0.019956097043432 & -0.130518411476224 & 0.009224310239736 \\ 0.253971718426341 & -0.009226496087855 & -0.130493158175449 \end{pmatrix} \times 10^{-3} \tag{2.61}$$

The first three bending mode frequencies are: 6 rad/s, 14 rad/s, and 27 rad/s. The damping ratio is assumed as $\zeta = 0.005$.

The simulation results of a test case for a Matlab-based simulation program are shown in Figures 2.9- 2.23. These results are identical to those obtained using the SAVANT program for the same test case. However, these simulation results were for a preliminary reference model of the Ares-I available to the public, not for the most recent model of the Ares-I with properly updated, ascent flight guidance and control algorithms. The purpose of this chapter was to develop a Matlab-based simulation tool for an independent validation of the performance and stability of NASA's ascent flight control system baseline design for the Ares-I rigid body model.

The center of pressure (cp) location shown in Figure 2.10 was computed as

$$X_{cp} = X_a - \frac{(C_{Mp0} + C_{Mp\alpha}\alpha)b}{C_{N0} + C_{N\alpha}\alpha} \tag{2.62}$$

where X_{cp} is the distance to the cp location from the top of vehicle and X_a is the distance to the aerodynamic reference point from the top of vehicle (i.e., the origin of the structure reference frame).

A nominal ascent flight trajectory of the Ares-I obtained using the Matlab-based program is shown in Figure 2.6. The nominal ascent trajectory on the pitch plane is shown in Figure 2.7. The launch azimuth can be seen to be about 42 deg. The launch azimuth is defined as the angle between the vertical trajectory plane (or pitch plane) and a vector pointing from the launch pad toward the North Pole. Time histories of a different set of Euler angles of the Ares-I CLV, often called (roll, pitch, yaw) attitude angles, with respect to the vertical pitch plane, are shown in Figure 2.8. A 48 deg roll maneuver, prior to the start of the gravity turn pitch maneuver, can be seen in this figure. Because the crew are oriented with their heads pointing east on the launch pad, the 48 deg roll maneuver is designed to maintain the required heads-down orientation of the crew [5]. Because the International Space Station mission has a higher inclination (51.6 deg) than the lunar mission (28.5 deg), the larger roll angle maneuver has been the primary focus in the roll control system design for Ares-I CLV [7].

Additional figures from the simulation of the Ares-I can be found in Appendix B.
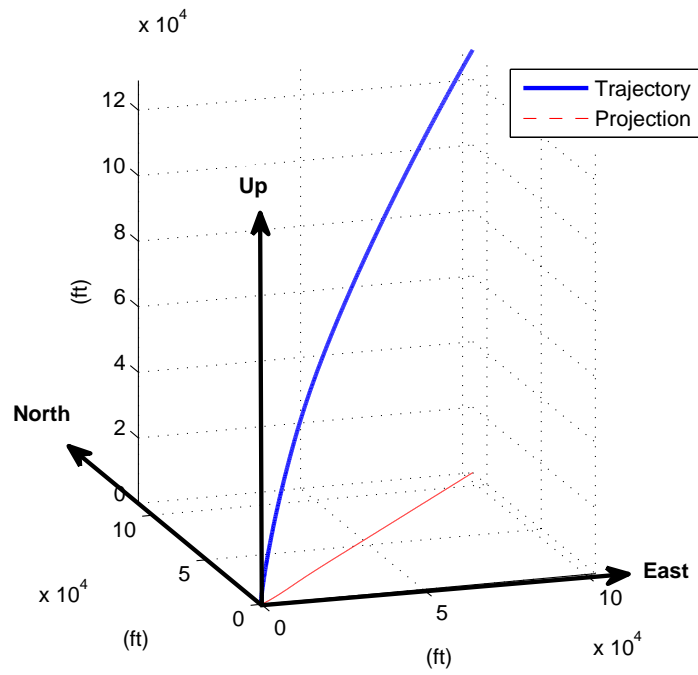
Figure 2.6   A nominal ascent trajectory of Ares-I in the Earth-fixed launch
             pad reference frame.
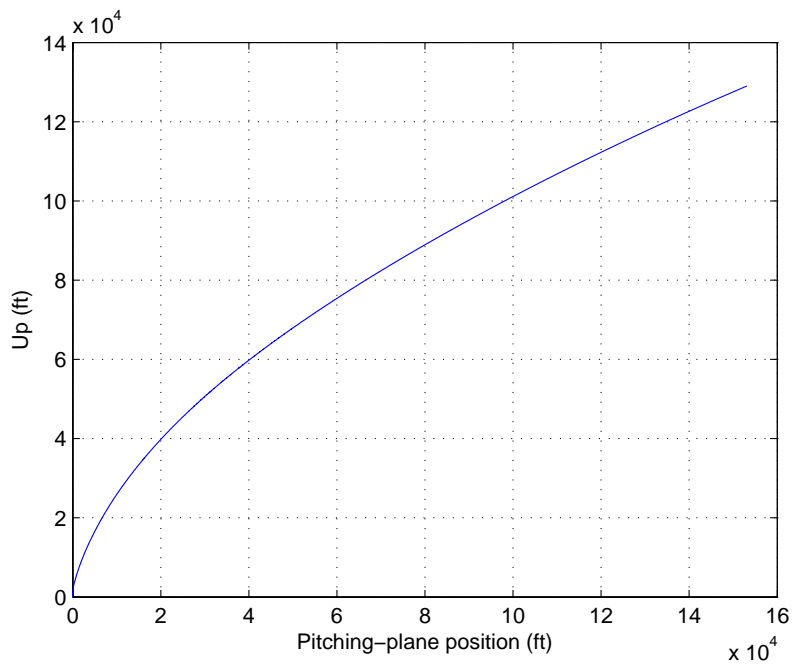
Figure 2.7   A nominal ascent trajectory of Ares-I in the pitch plane.
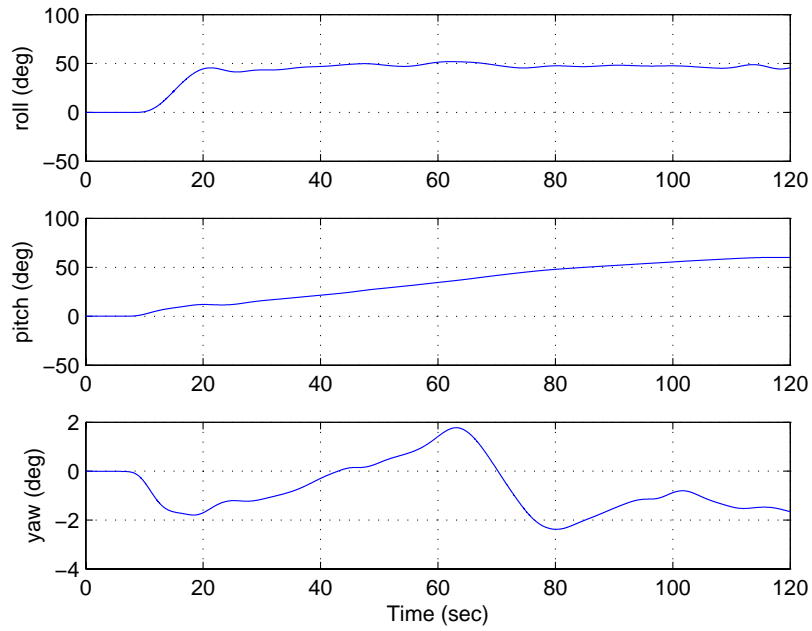
Figure 2.8   Time histories of conventional roll, pitch, and yaw angles, (ϕ, θ, ψ), of the Ares-I CLV.
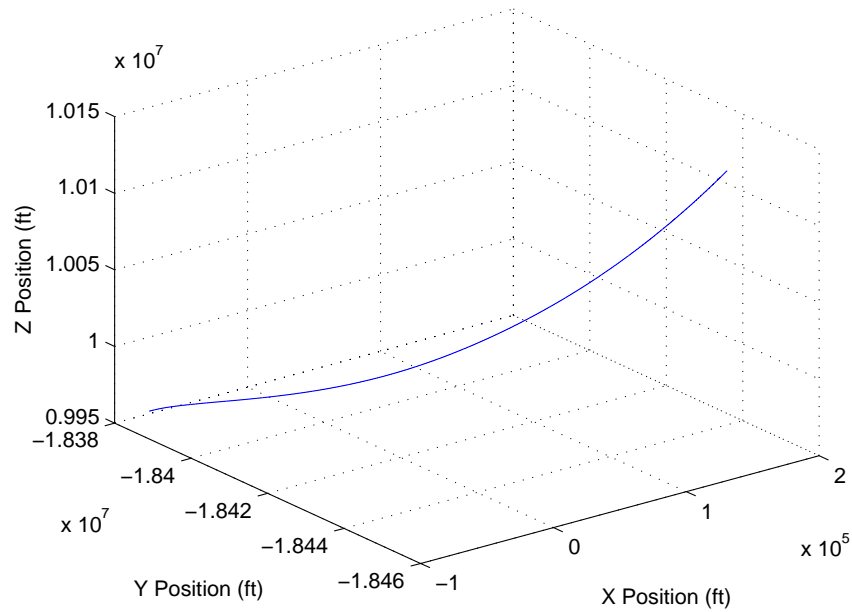
Figure 2.9   Trajectory in ECI.
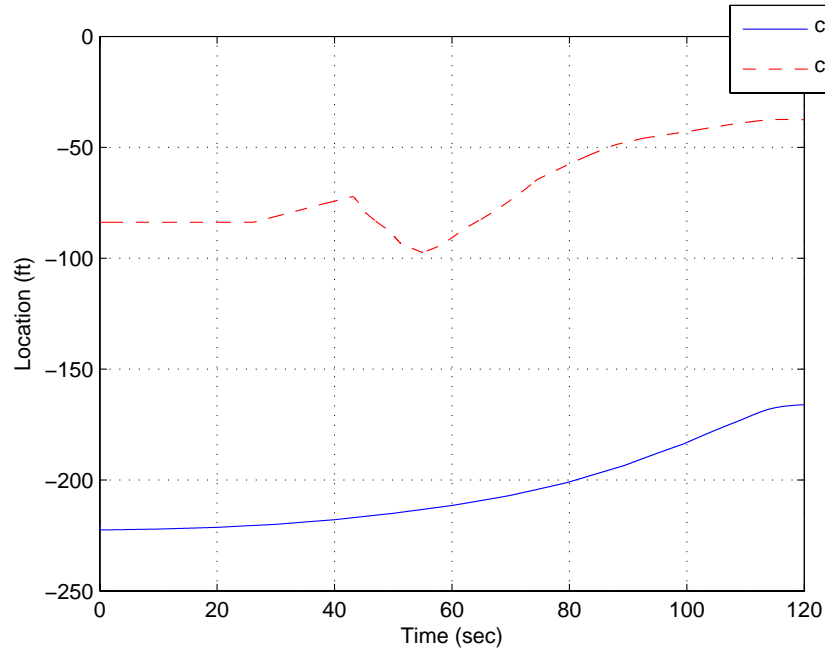
Figure 2.10   Center of pressure and center of gravity.
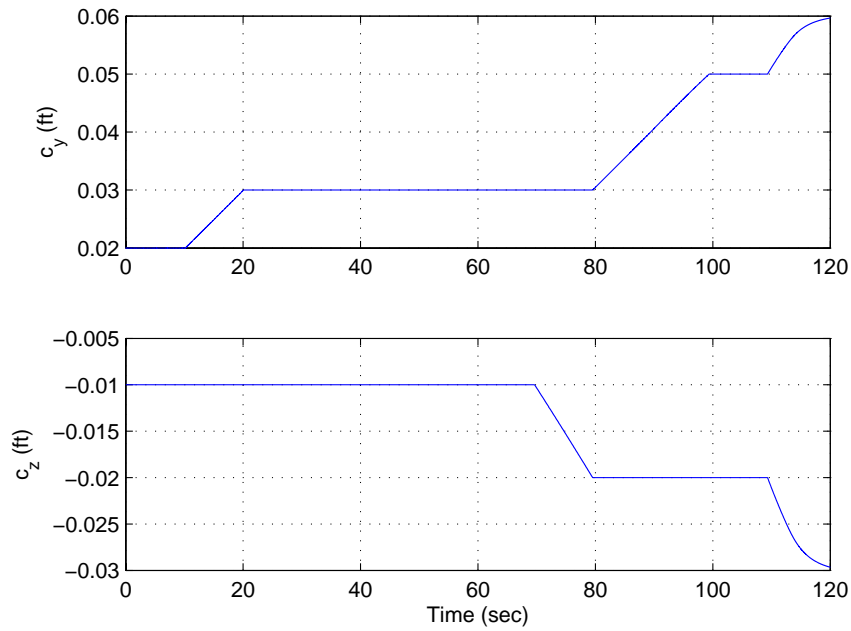
Figure 2.11   Center of gravity offset.
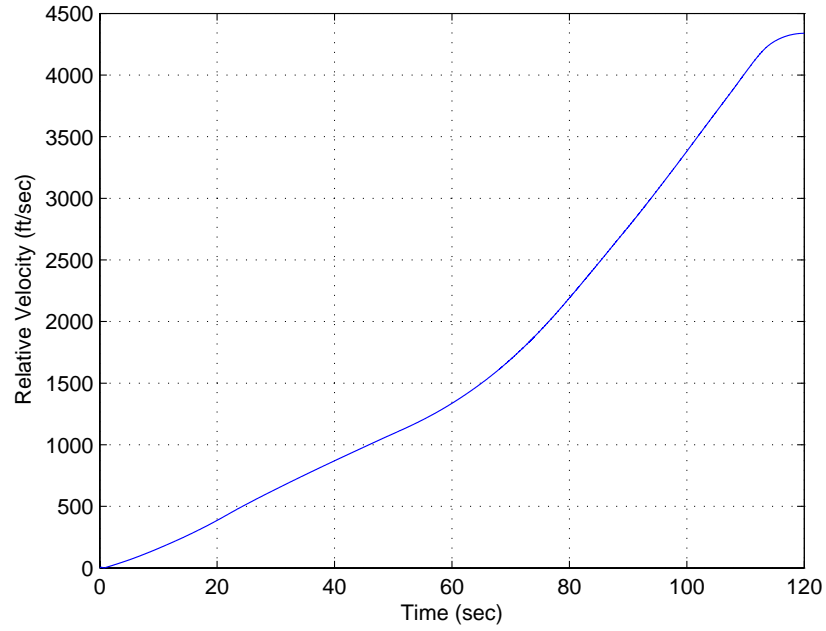
Figure 2.12   Relative velocity.
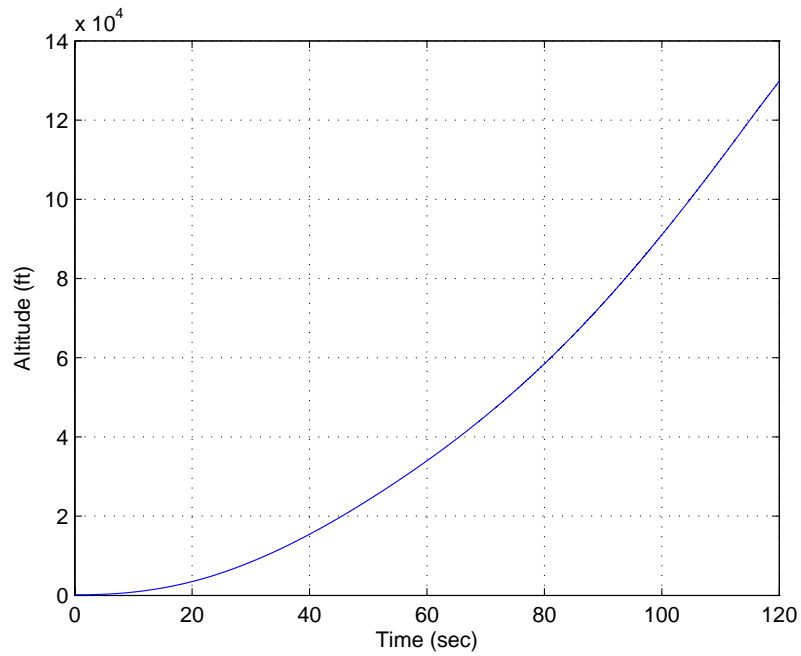
Figure 2.13   Altitude.
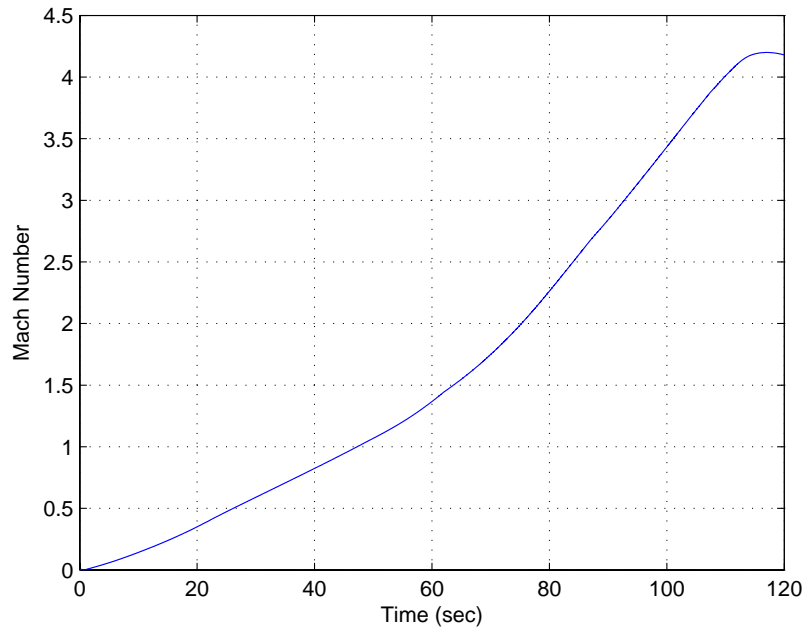
Figure 2.14   Mach number.
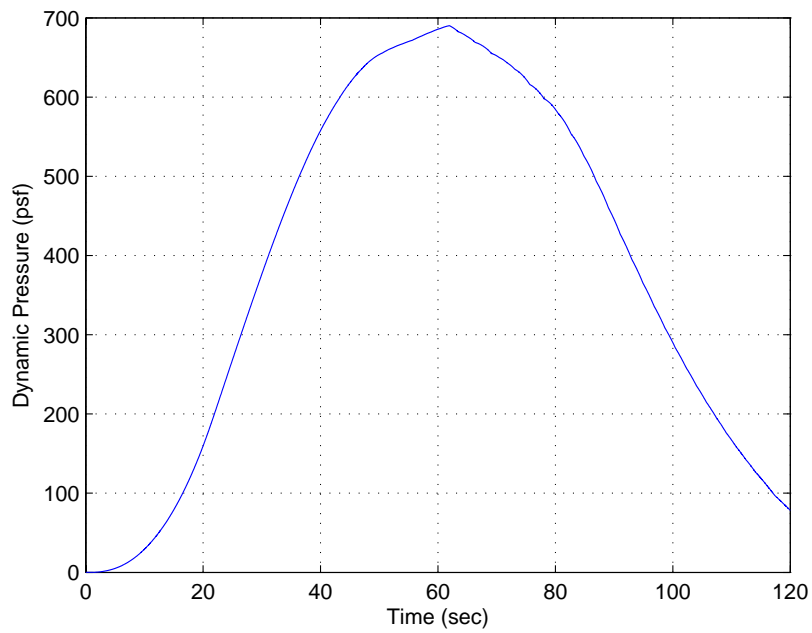
Figure 2.15   Dynamic pressure.
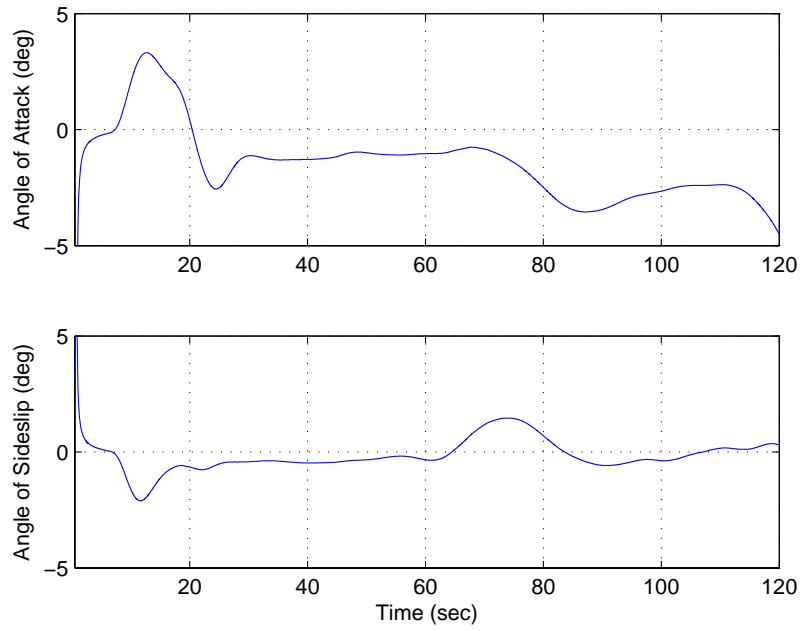
Figure 2.16   Angle of attack and angle of sideslip.
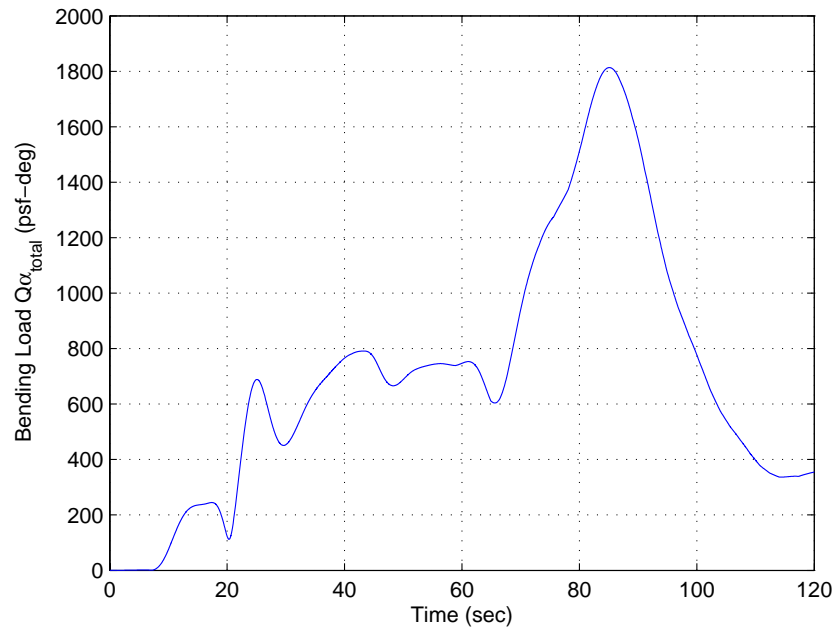
Figure 2.17   Bending load $Q\alpha_{total}$.
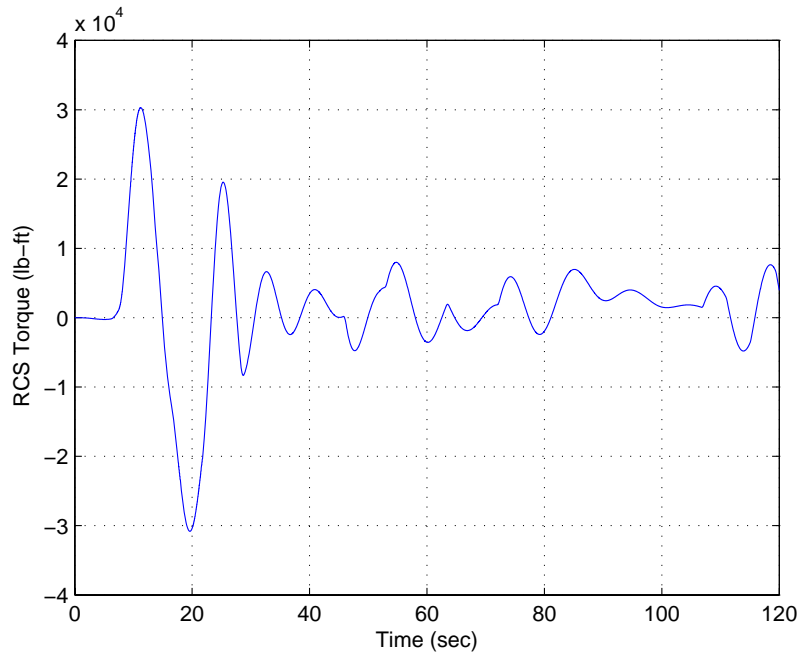
Figure 2.18   RCS torque.
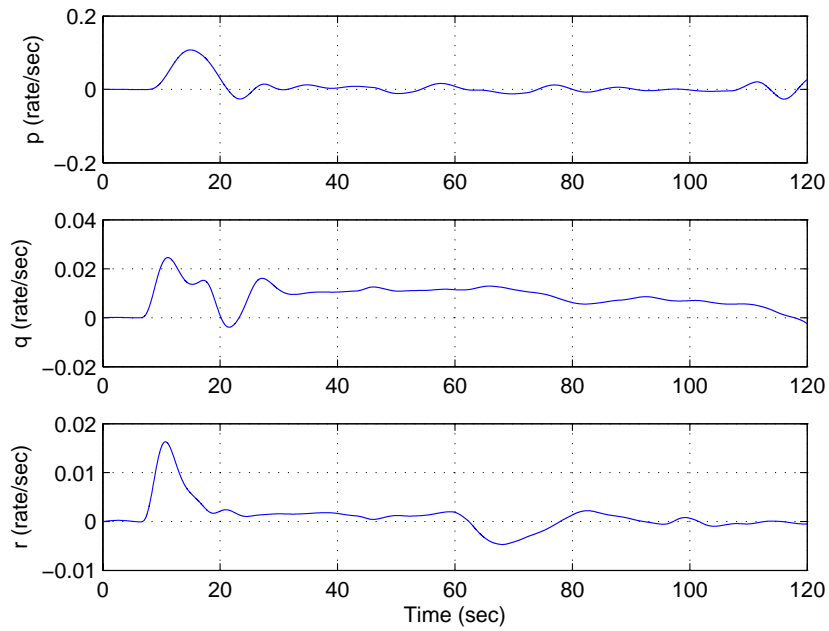
Figure 2.19   Angular velocity.
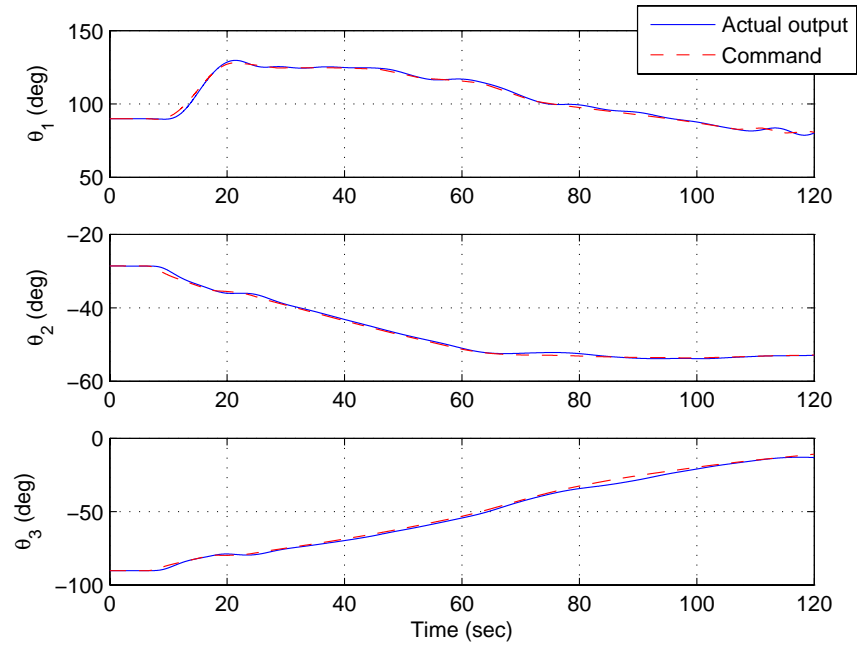
Figure 2.20   Euler angles.
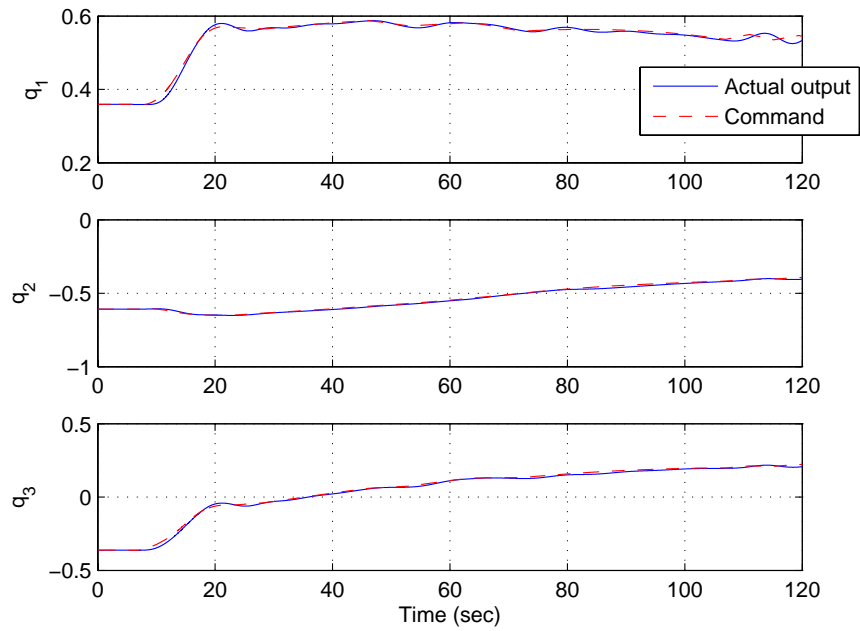
Figure 2.21   Attitude quaternion.
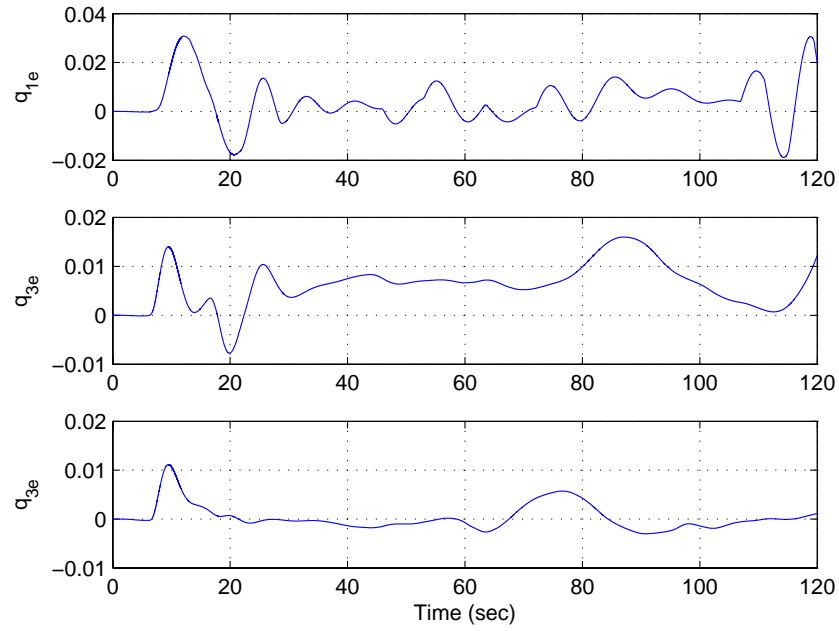
Figure 2.22   Attitude-error quaternion.
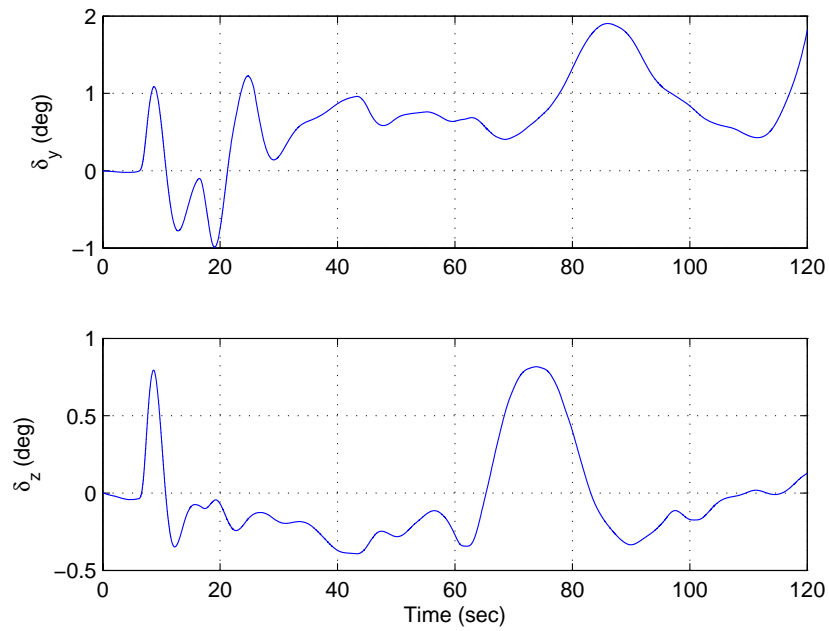
Figure 2.23   Gimbal angles.

CHAPTER 3.   ANALYSIS AND DESIGN OF ASCENT FLIGHT CONTROL SYSTEMS

3.1   Introduction

In analyzing and designing the attitude control system, the short period dynamics of the launch vehicle is used for expressing the rigid-body and flexible-body motion. It is assumed that the motion of the launch vehicle consists of small deviations from a reference trajectory. Another important assumption is that time varying mass, inertial, and other physical properties are changing slowly during the flight. As a result, all parameters of the launch vehicle can be "frozen" over a short period of time. In this way, analysis and design techniques for Linear Time-Invariant (LTI) systems can be exploited most fully.

In this section, a Matlab-based program is used to generate the reference trajectory of the Ares-I CLV. In this program, the Ares-I is considered to achieve attitude quaternion command perfectly and data for the reference trajectory is calculated in the ECI frame. Another Matlab-based program is developed to compute an LTI model at any operation point as shown in Figure 3.1. Linearization results in the ECI and linear state-space equations of both rigid-body and flex-body model can be found in Appendix C.
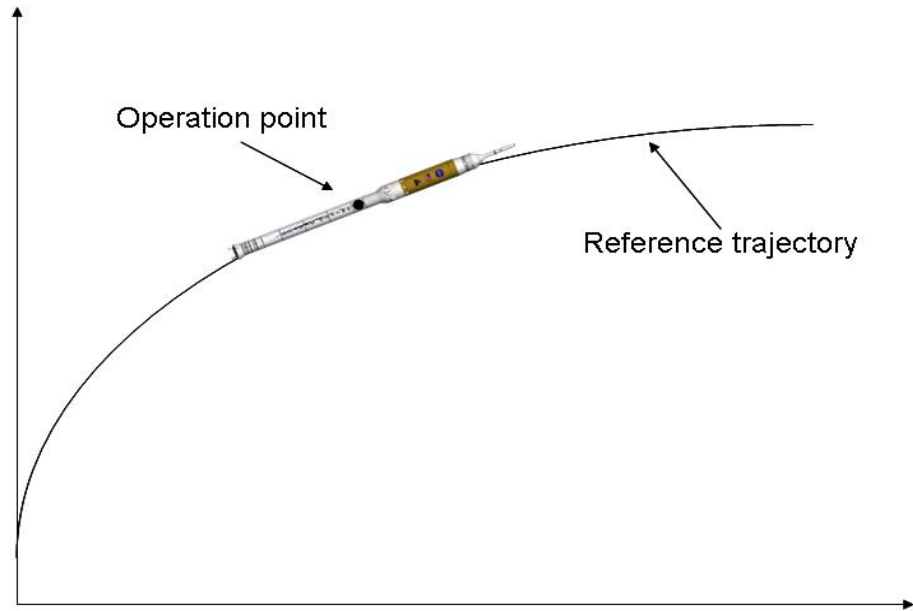
Figure 3.1   Reference trajectory and an operation point of Ares-I CLV in
the pitch plane.

3.2   Pitch Control Analysis of Rigid Launch Vehicles

For the preliminary analysis and design of a pitch-axis flight control system of a launch vehicle as illustrated in Figure 3.2, an inertial reference frame $(X,\ Y,\ Z)$ with its origin at the vehicle's center of gravity is assumed with its X-axis along the vertical axis and its Z-axis along the horizontal direction. Body-fixed $(x,\ y,\ z)$ axes with origin at the center of gravity are also shown in Figure 3.2.

A set of simplified pitch-axis dynamical models with small angular motions can be found as [10]

$$m\dot{V} = (F - D) - mg \tag{3.1}$$

$$m\ddot{Z} = -(F - D)\theta - N_\alpha\alpha + T_c\delta \tag{3.2}$$

$$\ddot{\theta} = M_\alpha\alpha + M_\delta\delta \tag{3.3}$$

$$\alpha = \theta + \gamma + \alpha_w\ =\text{effective angle of attack} \tag{3.4}$$

$$\gamma = \dot{Z}/V = \text{flight-path (drift) angle} \tag{3.5}$$

$$F = T_0 + T_c = \text{total thrust force} \tag{3.6}$$
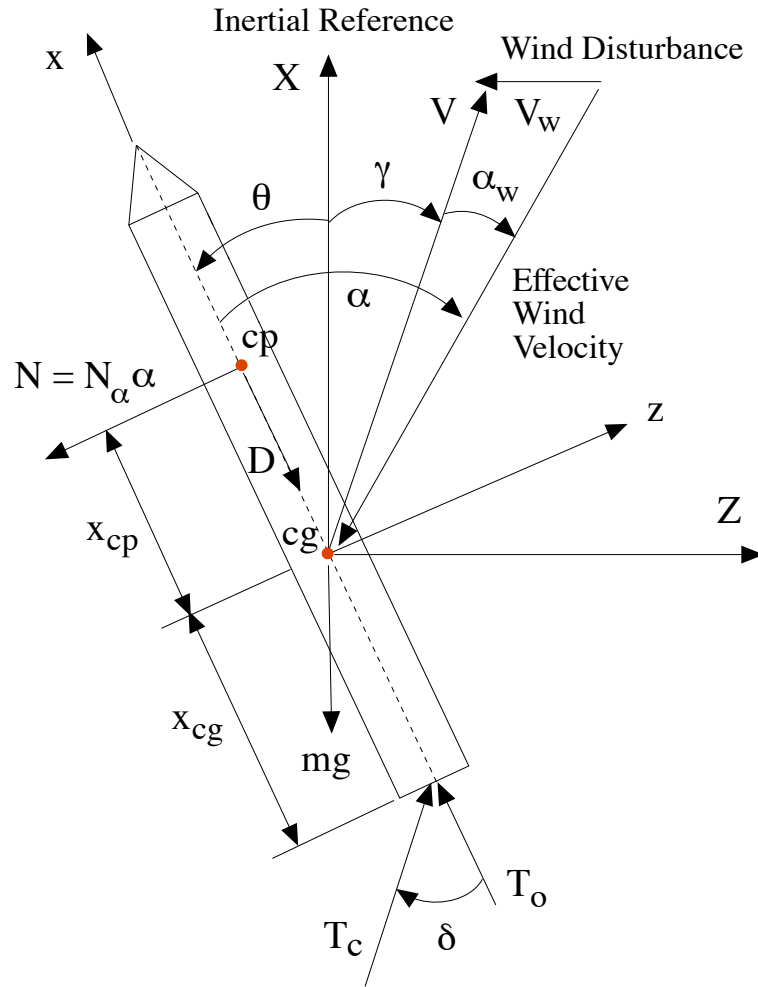
Figure 3.2   A simplified dynamic model of a launch vehicle for preliminary
pitch control design. All angles are assumed to be small.

where m is the vehicle mass, V is the vehicle velocity, g is the local gravitational acceleration, T_0 is the ungimballed sustainer thrust, T_c is the gimbaled control thrust, D is the aerodynamic axial (drag) force, Z is the inertial Z-axis drift position of the center-of-mass, $\dot{Z}$ is the inertial drift velocity, $N = N_\alpha \alpha$ is the aerodynamic normal (lift) force acting on the center-of-pressure, δ is the gimbal deflection angle, θ is the small pitch attitude from a vertical inertial reference axis X, $\alpha_w = V_w/V$ is the wind-induced angle of attack, V_w is the wind disturbance velocity. We also have

$$M_\alpha = x_{cp} N_\alpha / I_y \tag{3.7}$$

$$M_\delta = x_{cg} T_c / I_y \tag{3.8}$$

$$N_\alpha = \frac{1}{2}\rho V^2 S C_{N_\alpha} \tag{3.9}$$

where I_y is the pitch moment of inertia. For effective thrust vector control of a launch vehicle, we need

$$M_\delta \delta_{\max} > M_\alpha \alpha_{\max} \tag{3.10}$$

where $\delta_{\max}$ is the gimbal angle constraint and $\alpha_{\max}$ is the maximum wind-induced angle of attack.

Combining Equations. (3.2), (3.3), and (3.4), we obtain a state-space model of the form

$$\frac{d}{dt}\begin{pmatrix} \theta \\ \dot\theta \\ \dot Z \end{pmatrix} = \begin{pmatrix} 0 & 1 & 0 \\ M_\alpha & 0 & M_\alpha/V \\ -(F-D+N_\alpha)/m & 0 & -N_\alpha/(mV) \end{pmatrix}\begin{pmatrix} \theta \\ \dot\theta \\ \dot Z \end{pmatrix} + \begin{pmatrix} 0 \\ M_\delta \\ T_c/m \end{pmatrix}\delta + \begin{pmatrix} 0 \\ M_\alpha \\ -N_\alpha/m \end{pmatrix}\alpha_w \tag{3.11}$$

and $\alpha = \theta + \dot Z/V + \alpha_w$. Assuming all constant coefficients in the state-space model, we obtain the open-loop transfer functions from the control input $\delta(s)$ as

$$\frac{\theta(s)}{\delta(s)} = \frac{1}{\Delta(s)}\left(M_\delta\left(s + \frac{N_\alpha}{mV}\right) + \frac{M_\alpha T_c}{mV}\right) \tag{3.12}$$

$$\frac{\dot Z(s)}{\delta(s)} = \frac{1}{\Delta(s)}\left(\frac{T_c}{m}(s^2 - M_\alpha) - \frac{M_\delta(F-D+N_\alpha)}{m}\right) \tag{3.13}$$

$$\frac{\alpha(s)}{\delta(s)} = \frac{1}{\Delta(s)}\left(\frac{T_c}{mV}s^2 + M_\delta s - \frac{M_\delta(F-D)}{mV}\right) \tag{3.14}$$

where

$$\Delta(s) = s^3 + \frac{N_\alpha}{mV}s^2 - M_\alpha s + \frac{M_\alpha(F-D)}{mV} \tag{3.15}$$

In 1959, Hoelkner [37] introduced the "drift-minimum" and "load-minimum" control concepts as applied to a launch vehicle flight control system. The concepts have been further investigated in [10, 12, 13, 31, 38, 39, 40, 41, 42]. Basically, Hoelkner's controller utilizes a full-state feedback control of the form

$$\delta = -K_1\theta - K_2\dot\theta - K_3\alpha \quad \text{where} \quad \alpha = \theta + \dot Z/V + \alpha_w \tag{3.16}$$

The feedback gains are to be properly selected to minimize either lateral drift velocity $\dot{Z}$ or the bending moment caused by the angle of attack.

Substituting Equation. (3.16) into Equations. (3.2)-(3.3), we obtain the closed-loop transfer function from the wind disturbance $\alpha_w(s)$ to the drift velocity $\dot{Z}(s)$ as

$$\frac{\dot{Z}(s)}{V\alpha_w(s)} = -\frac{A_2 s^2 + A_1 s + A_o}{s^3 + B_2 s^2 + B_1 s + B_o} \tag{3.17}$$

where

$$B_2 = M_\delta K_2 + \frac{T_c}{mV}\left(K_3 + \frac{N_\alpha}{T_c}\right) \tag{3.18}$$

$$B_1 = M_\delta(K_1 + K_3) - M_\alpha + \frac{K_2 T_c}{mV}\left(M_\alpha + \frac{M_\delta N_\alpha}{T_c}\right) \tag{3.19}$$

$$B_o = \frac{T_c K_1}{mV}\left(M_\alpha + \frac{M_\delta N_\alpha}{T_c}\right) - \frac{F-D}{mV}\left(M_\delta K_3 - M_\alpha\right) \tag{3.20}$$

$$A_2 = \frac{T_c}{mV}\left(K_3 + \frac{N_\alpha}{T_c}\right) \tag{3.21}$$

$$A_1 = \frac{K_2 T_c}{mV}\left(M_\alpha + \frac{M_\delta N_\alpha}{T_c}\right) \tag{3.22}$$

$$A_o = B_o \tag{3.23}$$

For a step wind disturbance with a magnitude of V_w, the steady-state value of $\dot{Z}$ can be found as

$$\frac{\dot{Z}_{ss}}{V_w} = \lim_{s\to 0} \frac{-(A_2 s^2 + A_1 s + A_o)}{s^3 + B_2 s^2 + B_1 s + B_o} = \frac{-A_o}{B_o} = -1 \tag{3.24}$$

The launch vehicle drifts along the wind direction with $\dot{Z}_{ss} = -V_w$ and with $\theta = \dot{\theta} = \alpha = \delta = 0$ as $t \to \infty$. It is interesting to notice that the steady-state drift velocity (or the flight path angle) is independent of feedback gains for an asymptotically stable closed-loop system with $B_o \neq 0$.

If we choose the control gains such that $B_o = 0$ (i.e., one of the closed-loop system roots is placed at $s = 0$), the steady-state value of $\dot{Z}$ becomes

$$\frac{\dot{Z}_{ss}}{V_w} = \lim_{s \to 0} \frac{-(A_2 s + A_1)}{s^2 + B_2 s + B_1} = \frac{-A_1}{B_1} = \frac{-1}{1 + C} \tag{3.25}$$

where

$$C = \frac{mV[M_\delta(K_1 + K_3) - M_\alpha]}{M_\alpha K_2 T_c + M_\delta N_\alpha / T_c} \tag{3.26}$$

For a stable closed-loop system with $M_\delta(K_1 + K_3) - M_\alpha > 0$, we have $C > 1$ and

$$|\dot{Z}_{ss}| < V_w \tag{3.27}$$

when $B_o = 0$. The drift-minimum condition, $B_o = 0$, can be rewritten as

$$\frac{M_\delta K_3 - M_\alpha}{M_\delta K_1} = \frac{N_\alpha}{F - D}\left(1 + \frac{x_{cp}}{x_{cg}}\right) \tag{3.28}$$

Consider the following closed-loop transfer functions:

$$\frac{\alpha(s)}{\alpha_w(s)} = -\frac{s(s^2 + M_\delta K_2 s + M_\delta K_1)}{s^3 + B_2 s^2 + B_1 s + B_o} \tag{3.29}$$

$$\frac{\delta}{\alpha_w} = -\frac{s(K_3 s^2 + M_\alpha K_2 s + M_\alpha K_1)}{s^3 + B_2 s^2 + B_1 s + B_o} \tag{3.30}$$

For a unit-step wind disturbance of $\alpha_w(s) = 1/s$, we have $\alpha = \delta = 0$ as $t \to \infty$. However, for a unit-ramp wind disturbance of $\alpha_w(s) = 1/s^2$, we have

$$\lim_{t \to \infty} \alpha(t) = M_\delta K_1 \tag{3.31}$$

$$\lim_{t \to \infty} \delta(t) = M_\alpha K_1 \tag{3.32}$$

Consequently, the bending moment induced by α and δ can be minimized by choosing $K_1 = 0$, which is the "load-minimum" condition introduced by Hoelkner [37]. The closed-loop system with $K_1 = 0$ is unstable because

$$B_o = -\frac{F - D}{mV}(M_\delta K_3 - M_\alpha) < 0 \tag{3.33}$$

However, the load-minimum control for short durations has been known to be acceptable provided a deviation from the nominal flight trajectory is permissible.

A set of full-state feedback control gains, (K_1, K_2, K_3), can be found by using a pole-placement approach or the linear-quadratic-regulator (LQR) control method, as follows:

$$\min_{\delta} \int_0^{\infty} (x^T Q x + \delta^2) dt \tag{3.34}$$

subject to $\dot{x} = Ax + B\delta$ and $\delta = -Kx$ where $x = [\theta \ \dot{\theta} \ \alpha]^T$ and $K = [K_1 \ K_2 \ K_3]$. Some simulation results and comparisons of those designs can be found in [43].

3.3 Pitch Control of a Rigid-Body Model of the Ares-I CLV

Table 3.1   Ares-I reference parameters at $t = 60$ sec

Parameters	Values	Unit
I_y	2.186×10^8	slug-ft^2
m	$38,901$	slug
T_c	2.361×10^6	lb
V	1347	ft/s
C_{N_α}	0.1465	
g	26.10	ft/s^2
N_α	$686,819$	lb/rad
M_α	0.3807	s^{-2}
M_δ	0.5726	s^{-2}
x_{cg}	53.19	ft
x_{cp}	121.2	ft

$$\frac{\theta(s)}{\delta(s)} = \frac{0.5726(s + 0.04309)}{(s + 0.6330)(s - 0.01942)(s - 0.6005)} \tag{3.35}$$

Pole–Zero Map
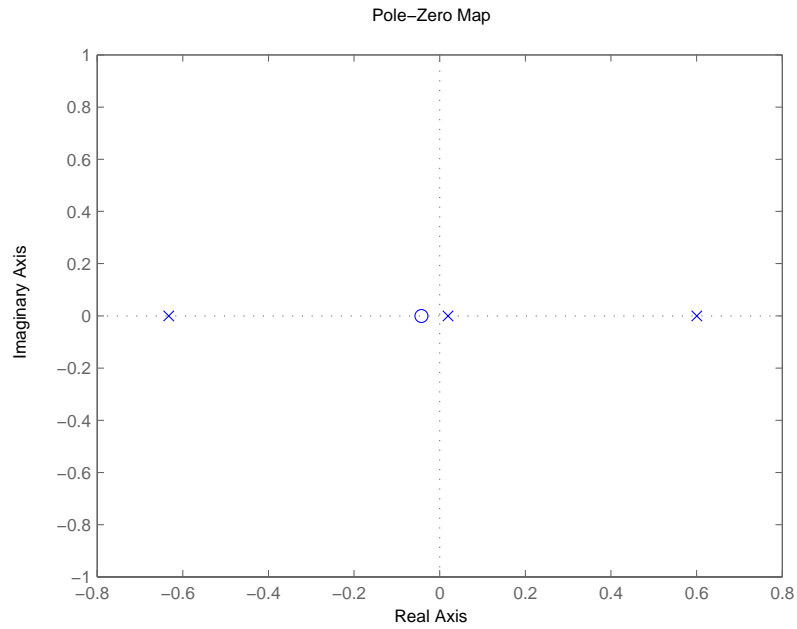
Figure 3.3   Poles and zeros of Ares-I CLV rigid-body model transfer function.
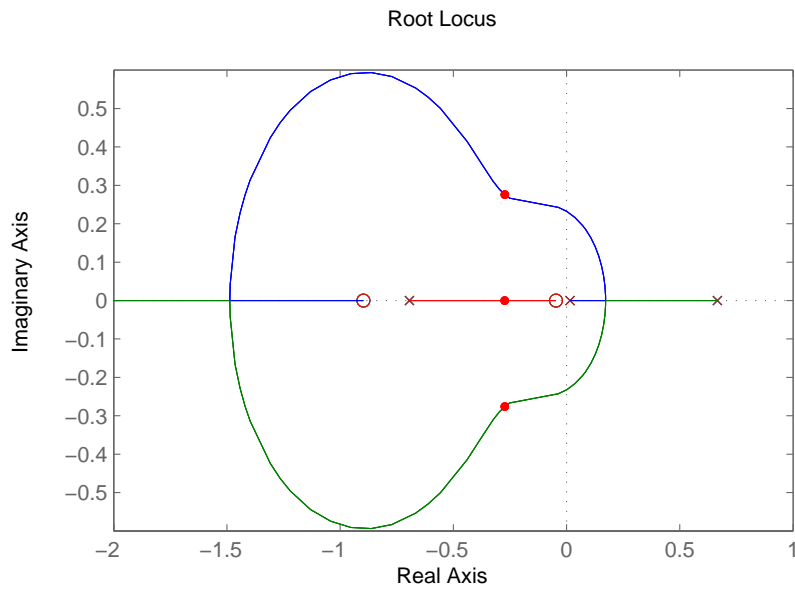
Root Locus

Figure 3.4   Root locus vs overall loop gain K of the pitch control system of a rigid Ares-I model.

3.4 Flexible-Body Control of an Ares-I Reference Model

Now we consider the flexible-body control of the Ares-I CLV. Its flexible mode shapes and sensor locations are shown in Figure 1.3. For the Ares-I having a high degree of axial symmetry, there is negligible coupling between the pitch and yaw lateral modes. This statement can be verified by inspecting Equation. (2.60) and Equation. (2.61). After neglecting relatively small values in $\mathbf{\Phi}$ and $\mathbf{\Psi}$, we obtain

$$\mathbf{\Phi} = \begin{pmatrix} 0 & 0 & 0 & 0 & 0 & 0 \\ 0 & 0.006281 & 0 & 0.006259 & 0 & -0.007673 \\ 0.006281 & 0 & -0.006260 & 0 & 0.007676 & 0 \end{pmatrix} \quad (3.36)$$

$$\mathbf{\Psi} = \begin{pmatrix} 0 & 0 & 0 & 0 & 0 & 0 \\ -0.1932 & 0 & -0.2540 & 0 & -0.1305 & 0 \\ 0 & 0.1932 & 0 & 0.2540 & 0 & -0.1305 \end{pmatrix} \times 10^{-3} \quad (3.37)$$

The pitch and yaw lateral modes are decoupled in Equation. (2.56). The first three bending modes data of the pitch and yaw lateral modes are given in Table 3.2 and Table 3.3 respectively.

Table 3.2   Ares-I structural bending modes for the pitch axis

Mode number	ω_i, rad/sec	Φ_i	Ψ_i
1	6.0469	0.006281	-0.1932×10^{-3}
2	14.2206	-0.006260	-0.2540×10^{-3}
3	27.1667	0.007676	-0.1305×10^{-3}

Table 3.3   Ares-I structural bending modes for the yaw axis

Mode number	ω_i, rad/sec	Φ_i	Ψ_i
1	6.0470	0.006281	0.1932×10^{-3}
2	14.2213	0.006259	0.2540×10^{-3}
3	27.1712	-0.007673	0.1305×10^{-3}

Thus the over all Ares-I reference model can be divided into two parts (Figure 3.5), the

rigid-body part and the flexible-body part,

$$\frac{\theta(s)}{\delta(s)} = G_{rigid}(s) + G_{flex}(s) \tag{3.38}$$

where $G_{rigid}(s)$ is expressed in Equation. (3.35).
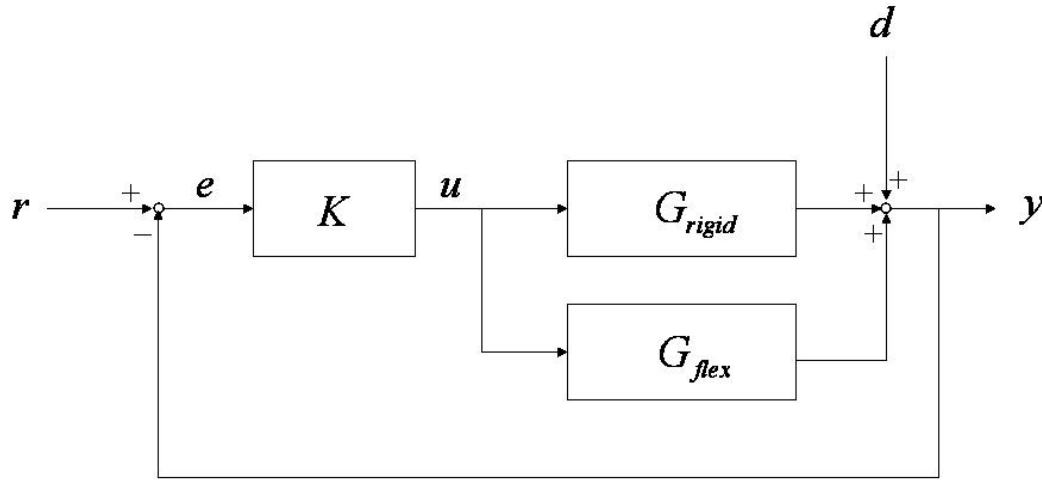
Figure 3.5 Block diagram of attitude control loop with flexible-body dynamics.

The flexible-body part of the pitch transfer function model as shown in Figure 3.7 is

$$G_{flex}(s) = \frac{\theta_b(s)}{\delta(s)} = \sum_{i=1}^{3} G_i(s) = \sum_{i=1}^{3} \frac{\Psi_i \Phi_i T}{s^2 + 2\zeta\omega_i + \omega_i^2} \tag{3.39}$$

where θ_b is the additional angle due to the bending vibration measured by the IMU (Figure 3.6).

For the ith bending mode

$$G_i(s) = \frac{\Psi_i \Phi_i T}{s^2 + 2\zeta\omega_i + \omega_i^2} \tag{3.40}$$

The pitch transfer function model of the Ares-I CLV can be written as

$$\frac{\theta(s)}{\delta(s)} = \frac{-0.9036(s+0.041)(s+3.68)(s-3.75)(s^2-35s+510)(s^2+35s+512)}{(s+0.63)(s-0.019)(s-0.60)(s^2+0.06s+36.56)(s^2+0.14s+202.2)(s^2+0.27s+738)} \tag{3.41}$$

where θ is the pitch attitude error measured by the instrument unit (Figure 1.3) and δ is the

pitch gimbal angle.
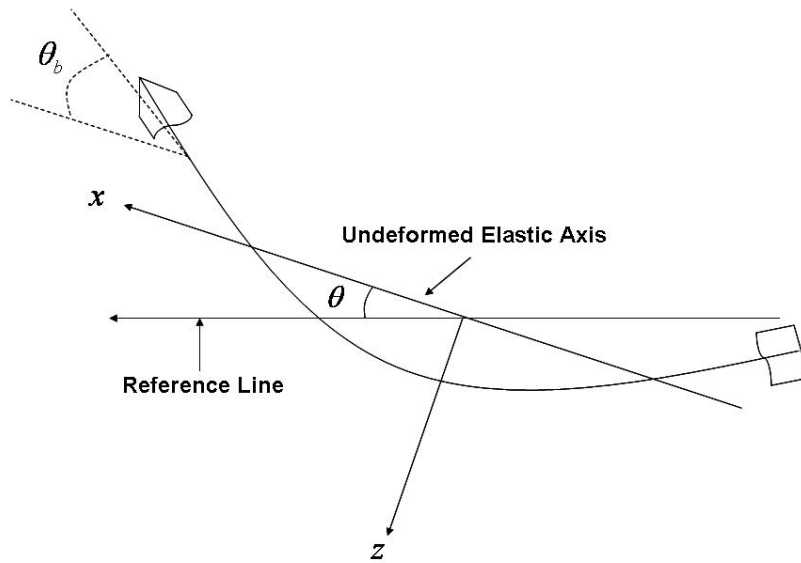
Figure 3.6   Flexible structure in the pitch plane.

The poles and zeros of this pitch transfer function are illustrated in Figure 3.8. Such a pole-zero pattern is typical for flexible vehicles with non-collocated actuator and sensor.

The root locus vs overall loop gain K of a simple PD control system is shown in Figure 3.9. The instability of the first and third bending modes, caused by unstable interactions with the rigid-body control, is evident from the root locus.
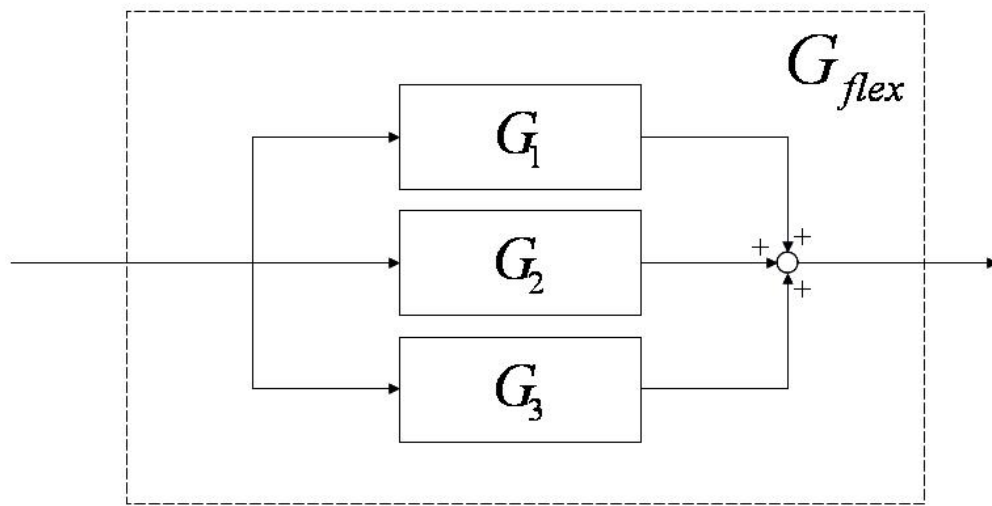
Figure 3.7   Block diagram of the flexible-body part of the pitch transfer
function.
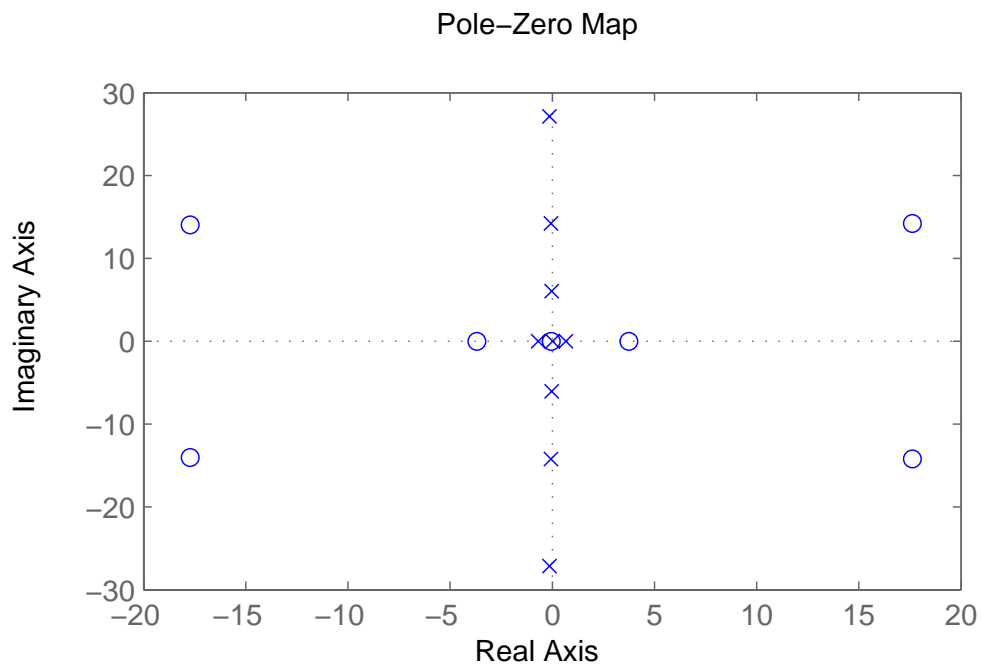
Figure 3.8   Pitch transfer function model of a reference model of the Ares-I
CLV.
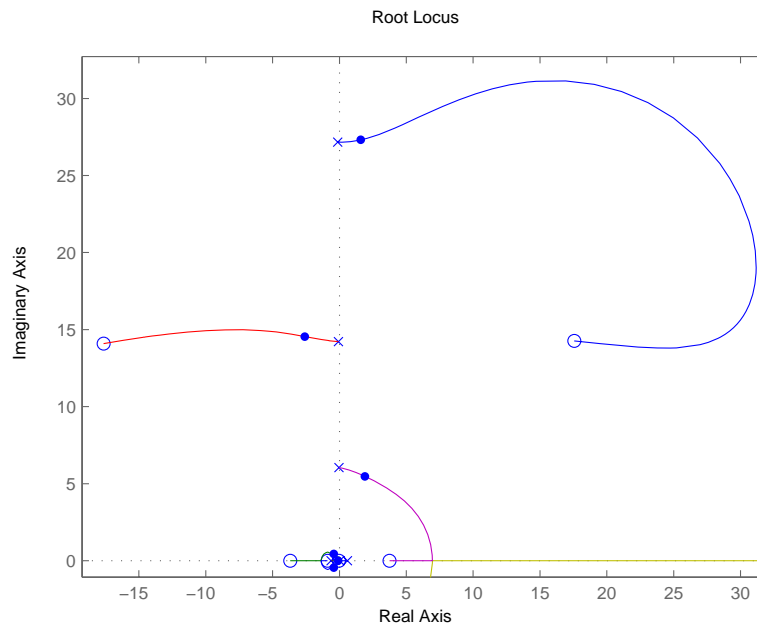
Figure 3.9   Root locus of the pitch control system without structural filters.

3.5 NMP Structural Filter Design

The root locus, shown in Figure 3.9, clearly indicates that those two unstably interacting bending modes can be effectively stabilized by using two NMP filters. Detailed discussions of the classical gain-phase stabilization approach using NMP filters can be found in [16, 20, 21]. It is important to notice that nowadays, one can easily perform an inherently iterative, classical control design using the interactive root locus tool of the SISO Design Toolbox of Matlab. After several design iterations, the structural filter for the first bending mode is found as

$$F_1(s) = \frac{1.0036(s^2 - 4.295s + 48.76)}{s^2 + 11.9s + 48.94} \tag{3.42}$$

and the structural filter for the third bending mode is

$$F_3(s) = \frac{0.91123(s^2 - 19.48s + 708.7)}{s^2 + 17.93s + 645.8} \tag{3.43}$$

The impulse responses provided in Figures 3.11 and 3.12 also indicate that the bending modes are more actively controlled by using such NMP filters although standard roll-off and notch filters [12, 13, 14] can also be employed to stabilize such unstably interacting bending modes. This design has met the standard rigid-body stability margin requirements (± 6 dB gain margin and 30 deg phase margin). Nonlinear coupled dynamic simulation results of validating the stability of the NMP filters as well as the baseline attitude-error quaternion feedback control scheme for the Ares-I are the similar to Figures 2.19-2.23.
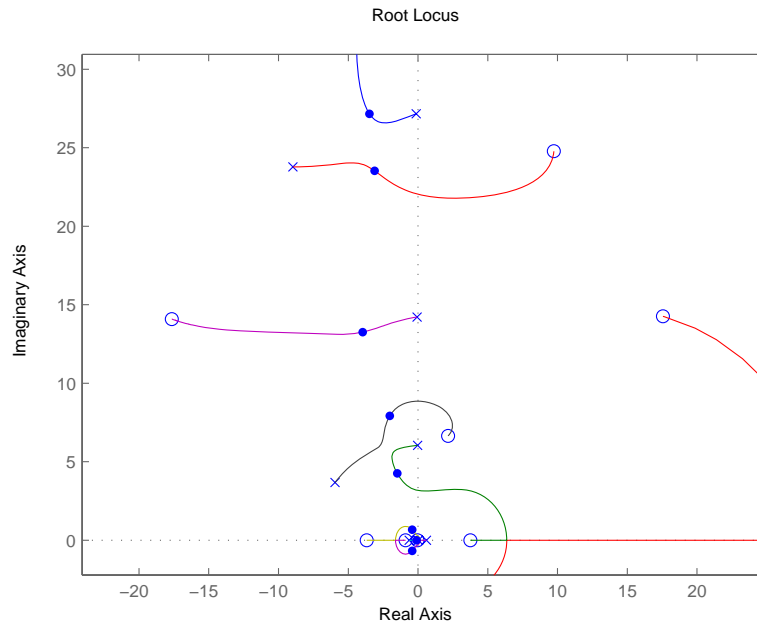
Figure 3.10   Root locus of the pitch control system with two NMP structural filters.
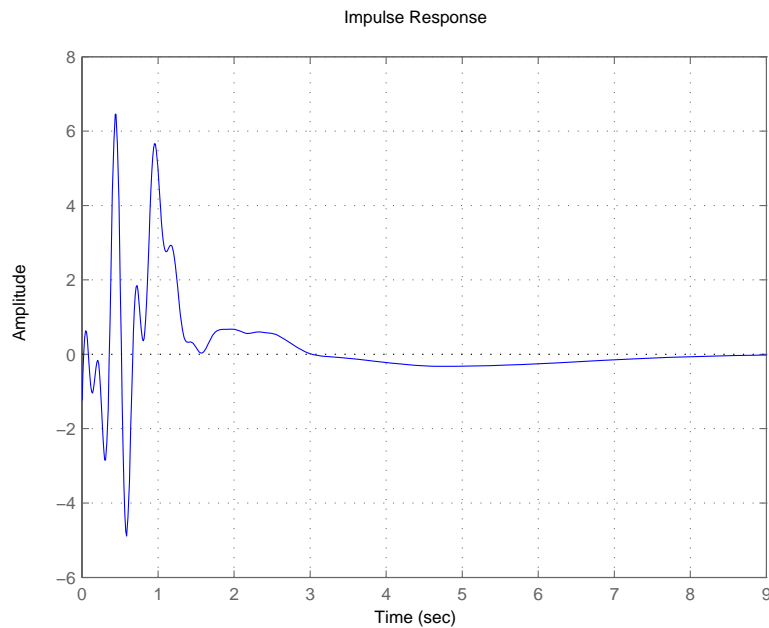
Figure 3.11   Impulse responses for the pitch attitude θ (in degrees) of the flexible Ares-I.
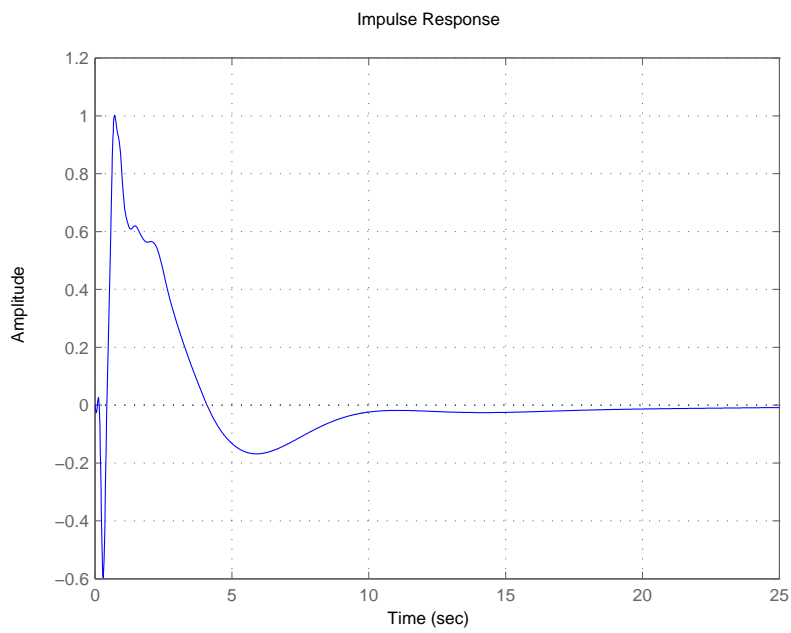
Figure 3.12   Impulse responses for the pitch gimbal angle δ (in degrees) of the flexible Ares-I.

3.6 Robust Analysis for Structural Filters Design

In this section, the robustness of the ascent flight control system will be analyzed based on the structured singular value μ. A general configuration which includes all the different systems resulting from variations in the form and location of the controller and the system uncertainty is illustrated in Figure 3.13. P is called the generalized plant and includes the nominal plant together with dynamics associated with the weighting transfer functions used to model system uncertainty. K is the generalized controller. In this dissertation, it is a PD-type baseline controller with NMP structural filters designed in the last section. Δ is an unknown but norm-bounded uncertainty. The signal w is called the exogenous input. Typically, it includes external disturbances, measurement noise and command signals. The signal z is exogenous output. Usually, it is the "error" signal to be minimized. The signal u is called the actuator input to P. For a launch vehicle, u could be gimbal angle command. The signal y is controller input and is composed of all the measured plant output which are available for feedback.

For the problem of analyzing the robustness of a given controller K, we can rearrange the system into the M-Δ structure of Figure 3.14 where M is the transfer function from the output to the input of the perturbations. We need to determine whether the system remains stable for all the uncertainty set. The basic conceptions and framework of linear robust control theory, especially the μ-condition for robust stability, can be found in [44, 45, 46]. MATLAB Robust Control Toolbox (μ-Analysis) is used in this section.

3.6.1 Uncertainty Description of Rigid-Body Model

Typical rigid-body parametric uncertainties for a launch vehicle can be found in Table 3.4. The parametric uncertainties are quantified by a ratio. Although the sources of uncertainties are known, it is hard to represent perturbed plants by a structured set with a finite number of scalar parameters. For this case, dynamic (frequency-dependent) uncertainty is particularly well-suited. This leads to a normalized complex perturbations $\|\Delta\|_\infty \leq 1$.

Let the set of possible plants be

$$G_p(s) = G_{rigid}(s)(1 + W_I(s)\Delta_I(s)); \quad |\Delta_I(j\omega)| \leq 1 \forall \omega \tag{3.44}$$

50
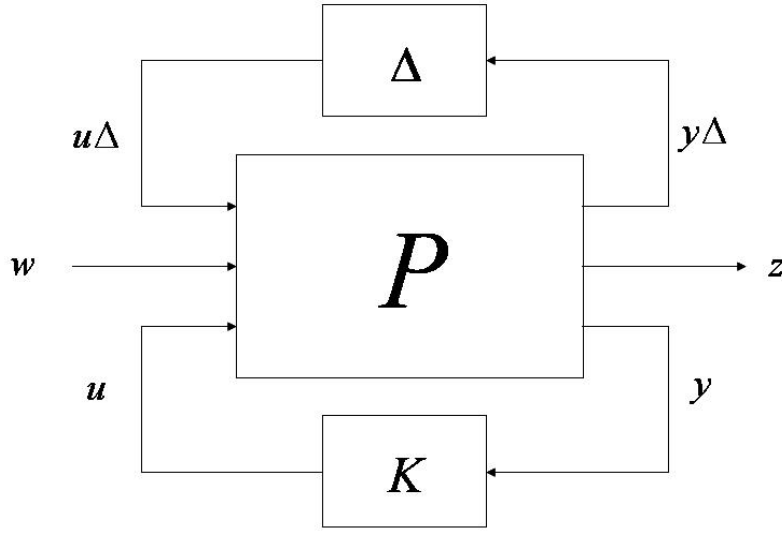
Figure 3.13   General control configuration.

Table 3.4   Ares-I rigid-body parametric uncertainty

Parameters	Nominal values (Unit)	Relative uncertainties
I_y	2.186×10^8 (slug-ft^2)	$\pm 5\%$
T_c	2.361×10^6 (lb)	$\pm 5\%$
C_{N_α}	0.1465	$\pm 6\%$
x_{cg}	53.19 (ft)	$\pm 10\%$
x_{cp}	121.2 (ft)	$\pm 10\%$

where $G_p(s)$ is a perturbed plant model, which may be represented by the block diagram in Figure 3.15. $\Delta_I(s)$ is any stable transfer function which at each frequency is less than or equal in magnitude to 1. The subscript I denotes "input", but for SISO systems it is not important that whether the perturbation is considered at the input or output of the plant.

The multiplicative weight are calculated by the Robust Toolbox for 50 samples of the rigid-body model with parametric uncertainty,

$$W_I(s) = \frac{0.11745(s + 9.741)(s + 0.5113)(s + 0.01471)(s^2 + 2.52s + 3.645)}{(s + 9.463)(s + 0.2936)(s + 0.04434)(s^2 + 2.837s + 3.447)} \quad (3.45)$$

As seen from the blue solid line and red dashed line in Figure 3.16, the perturbed plant model $G_p(s)$ can cover a range of 50 samples of the nominal plant $G_{rigid}(s)$ with parametric
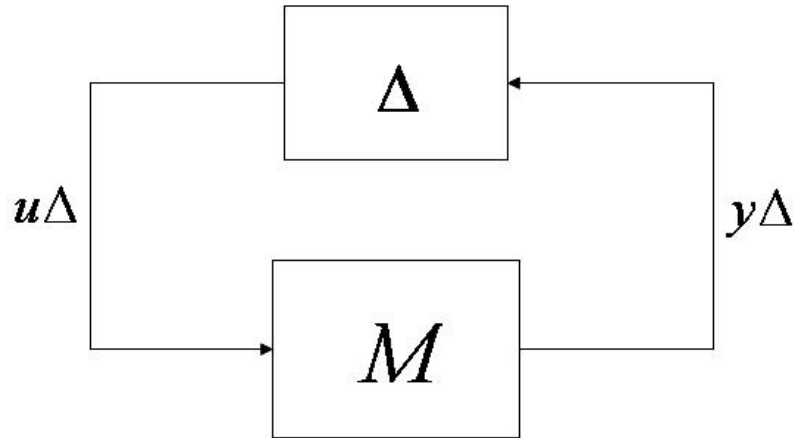
Figure 3.14   M-Δ structure for robust stability analysis.
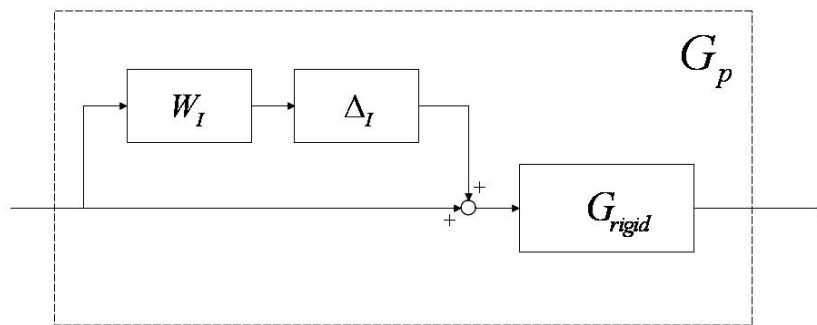
Figure 3.15   Plant with multiplcative uncertainty.

uncertainties in Table 3.4. Furthermore, Figure 3.17 shows that the upper and lower bounds of $G_p(s)$ cover the gain uncertainty of those samples.

3.6.2   Uncertainty Description of Flexible-Body Model

Another significant uncertainty source is the structural flexibility of the launch vehicle. Based on [47], vibration frequencies should be accurate to within $\pm 5\%$ for the first bending mode and $\pm 10\%$ for the second through the fourth or fifth bending modes. One important requirement of the Ares-I ascent FCS is that the resulting control system is stable with $\pm 10\%$
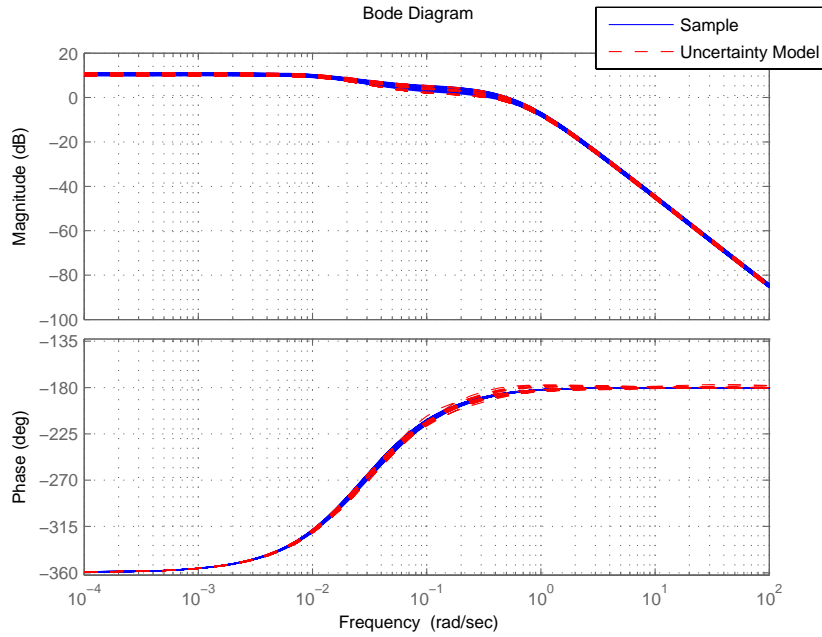
Figure 3.16   Bode plot of parameter uncertainty plant and perturbed plant samples.

natural frequency uncertainty of first three bending modes throughout the first stage flight.

Uncertainty modeling of the flexible structure is critical to evaluate robustness of a controller design. Usually, norm-bounded additive or multiplicative perturbations of a nominal model in the frequency domain are used to account for uncertainty in the model frequencies, damping ratios and mode shape matrix of the model [48, 49, 50]. Such approaches to uncertainty modeling in large flexible launch vehicles do not handle natural frequencies shift very well. Slight variation in the mode frequencies usually causes the associated dynamic perturbations to be large in the ∞-norm sense. This will make the uncertainty model too conservative for robust stability analysis. In this section, structured uncertainty is adopted to model real parameter uncertainty.

The nominal values of flex frequency are given in Table 3.2. The uncertainty model of flex frequency can be rewritten as

$$\omega_i = \overline{\omega}_i(1 + r_\omega \Delta_i) \tag{3.46}$$

where $\overline{\omega}_i$ is the nominal value of ith bending mode natural frequency, $r_\omega = 10\%$ is the relative
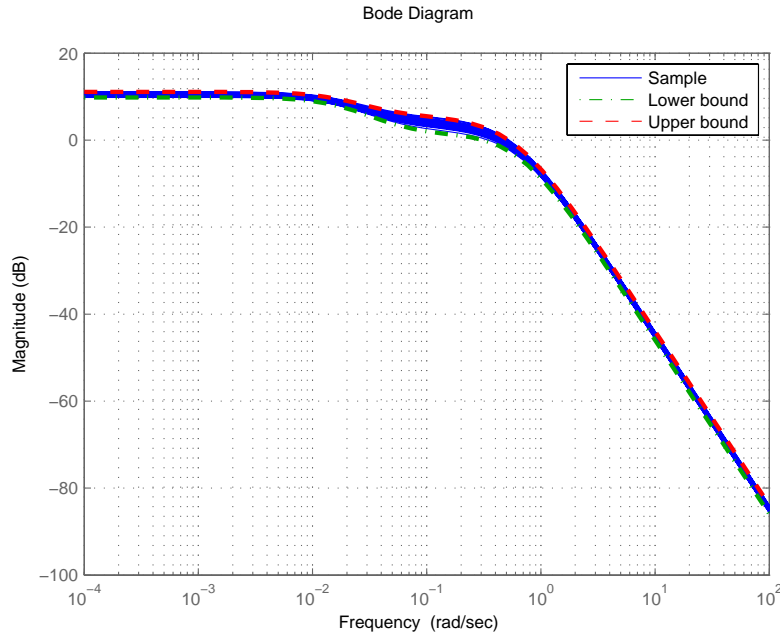
Figure 3.17   Bode plot magnitude.

uncertainty in the parameter, and Δ_i is any real scalar satisfying $|\Delta_i| \leq 1$.

For the ith bending mode, the perturbed transfer function can be written as

$$G_{pi}(s) = \frac{\Psi_i \Phi_i T}{s^2 + 2\zeta\omega_i + \omega_i^2} = \frac{\Psi_i \Phi_i T}{s^2 + 2\zeta\overline{\omega}_i(1 + r_\omega \Delta_i) + \overline{\omega}_i^2(1 + r_\omega \Delta_i)^2} \tag{3.47}$$

where $|\Delta_i| \leq 1$ and thus $|\Delta_i^2| \leq |\Delta_i|$. We could use a larger uncertainty Δ_i to replace $|\Delta_i^2|$.

After replacing Δ_i^2 by Δi in the denominator of $G_{pi}(s)$, we get

$$G_{pi} = \frac{\Psi_i \Phi_i T}{s^2 + 2\zeta\overline{\omega}_i + \overline{\omega}_i^2 + \Delta_i[2\zeta\overline{\omega}_i r_\omega s + \overline{\omega}_i(2r_\omega + r_\omega^2)]} \tag{3.48}$$

Define the weight function for the ith bending mode as

$$W_i(s) = \frac{2\zeta\overline{\omega}_i r_\omega}{\Psi_i \Phi_i T} s + \frac{\overline{\omega}_i(2r_\omega + r_\omega^2)}{\Psi_i \Phi_i T} \tag{3.49}$$

then we obtain

$$G_{pi}(s) = \frac{G_i(s)}{1 + G_i(s)W_i(s)\Delta_i}; \quad |\Delta_i| \leq 1 \tag{3.50}$$

This may be represented by the block diagram in Figure 3.18.
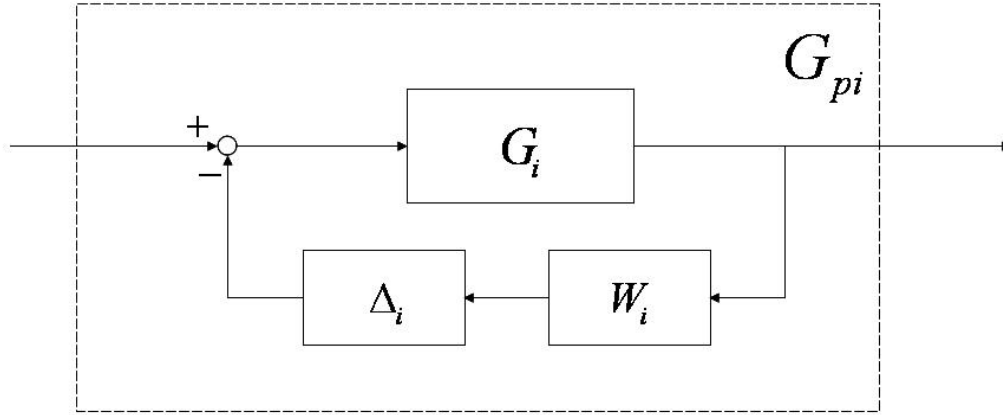
Figure 3.18   Block diagram of perturbed transfer function $G_{pi}(s)$.

The weight functions can be found as

$$W_1(s) = -0.002111s - 2.681 \tag{3.51a}$$

$$W_2(s) = 0.003789s + 11.31 \tag{3.51b}$$

$$W_3(s) = -0.01149s - 65.53 \tag{3.51c}$$

As seen in Figure 3.19, perturbed models could represent frequency uncertainty of $G_{flex}(s)$ very well. It covers the whole range of the frequency shift.

3.6.3   Robust Stability Analysis

The overall structure of the uncertainty model of Ares-I is shown in Figure 3.20.

The structure of uncertainty perturbation is written as a block-diagonal matrix.

$$\Delta = \text{diag}\{\Delta_I, \Delta_1, \Delta_2, \Delta_3\} = \begin{pmatrix} \Delta_I & 0 & 0 & 0 \\ 0 & \Delta_1 & 0 & 0 \\ 0 & 0 & \Delta_2 & 0 \\ 0 & 0 & 0 & \Delta_3 \end{pmatrix} \tag{3.52}$$

The M-Δ system in Figure 3.14 is stable for all allowed perturbations with $\overline{\sigma}(\Delta) \leq 1, \forall \omega$, if and only if

$$\mu_\Delta(M(j\omega)) \leq 1, \ \forall \omega \tag{3.53}$$
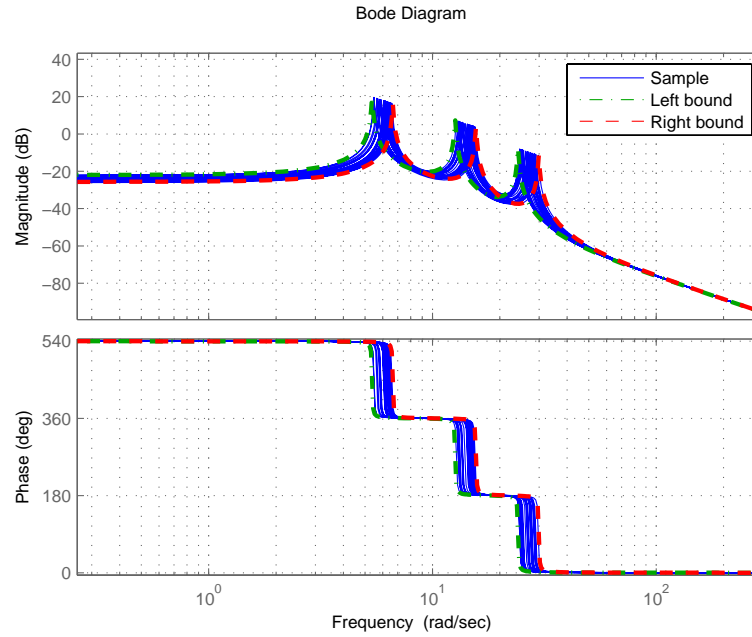
Figure 3.19   Bode plot samples of $G_{flex}(s)$ with frequencies uncertainty and
the boundary of perturbed models $\sum_{i=1}^{3} G_{pi}(s)$.

$\mu_{\Delta}(M)$ can be calculated by the MATLAB Robust Control Toolbox. Figure 3.21 clearly shows that the upper bound of $\mu_{\Delta}(M)$ is smaller than 1. The maximum value of $\mu_{\Delta}(M)$ is 0.8858. It means that the flight control system is stable with respect to the rigid-body parameter uncertainties in Table 3.4 and $\pm 10\%$ bending mode frequency uncertainties of all three modes.
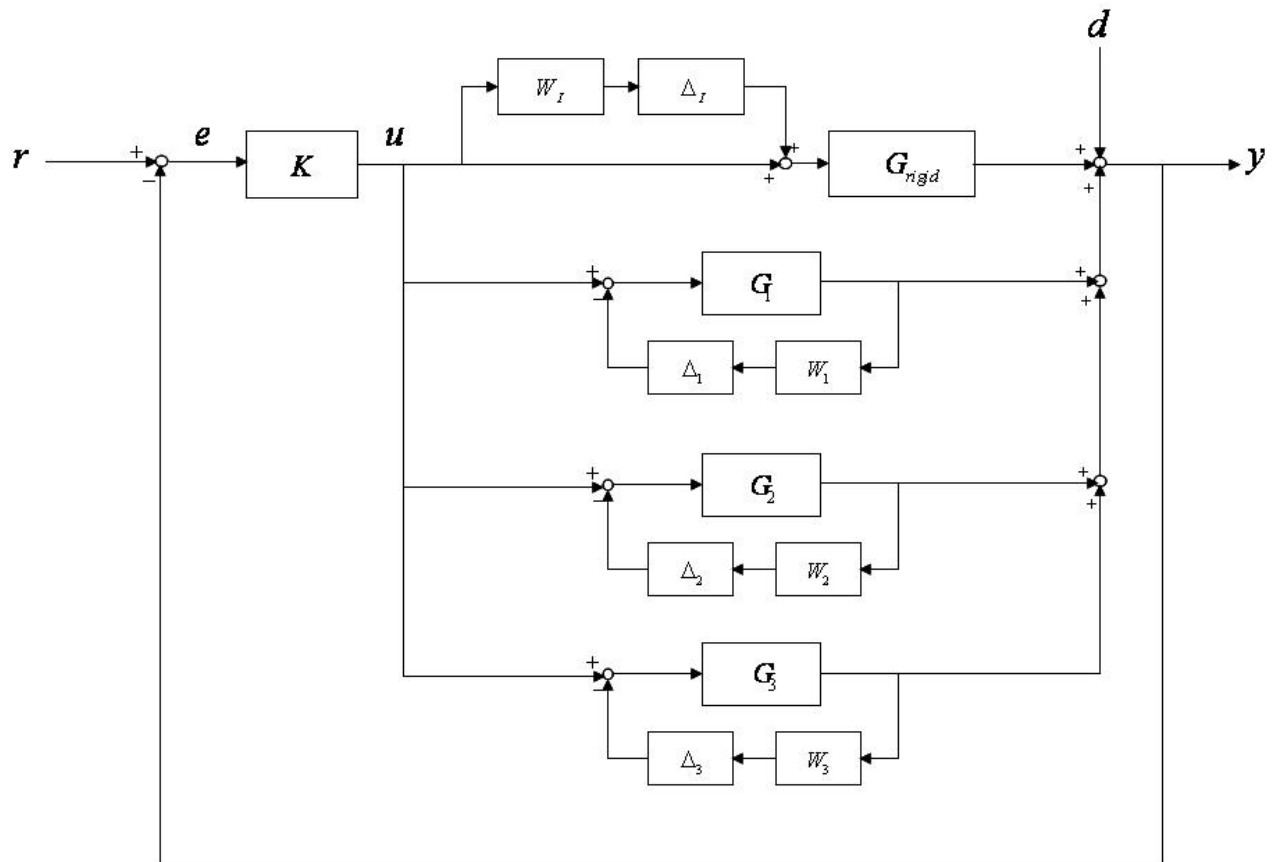
Figure 3.20   Block diagram of perturbed attitude control system.
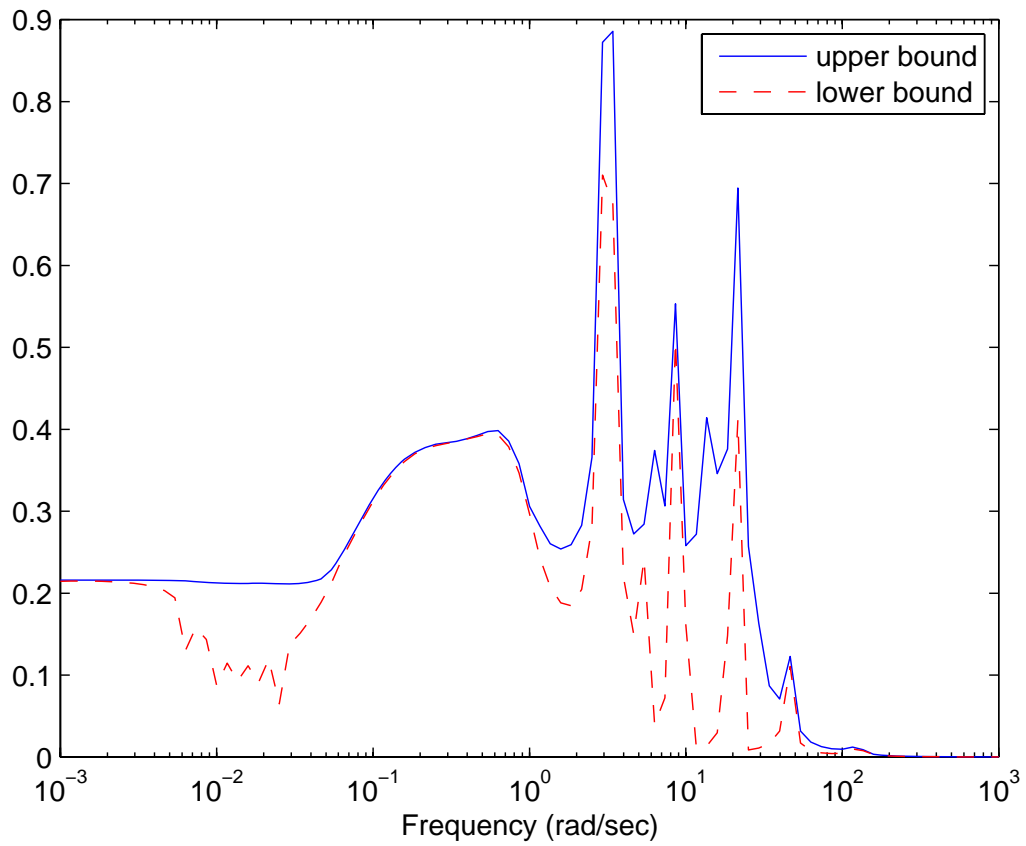
Figure 3.21 μ-plot for RS of structural filters design.

CHAPTER 4.   UNCONTROLLED ROLL DRIFT

4.1   Introduction

The roll motion of Ares-I CLV under nominal flight conditions is actively stabilized by its RCS equipped with thrusters. However, in this chapter, we examine the feasibility of maintaining the pitch/yaw attitude stability as well as the ascent flight performance of Ares-I CLV during its ascent phase but in the event of disabled or failed roll control. This situation can occur when the roll-axis disturbance torque unexpectedly exceeds the control authority of the RCS of a slender launch vehicle.

A simple pitch/yaw control logic will be proposed for such a technically challenging problem by exploiting the inherent versatility of a quaternion-based attitude control system. The proposed pitch/yaw control logic only requires the desired inertial attitude quaternion to be re-computed using the actual uncontrolled roll angle information. This simple approach achieves an ascent flight trajectory identical to the nominal flight case with active roll control. Another approach that utilizes a simple adjustment of the proportional-derivative gains of the quaternion-based flight control system without active roll control is also presented in this chapter. This approach doesn't require the re-computation of desired inertial attitude quaternion. Linear stability criterion is developed for proper adjustments of attitude and rate gains. The linear stability analysis results are validated by nonlinear simulations of the ascent flight phase. However, the first approach, requiring a simple modification of the desired attitude quaternion, is recommended for the Ares-I as well as other launch vehicles in the event of no active roll control.

4.2 Pitch/Yaw Closed-Loop Instability Caused by Uncontrolled Roll Drift

Simulation results of a reference Ares-I CLV with a baseline ascent flight control system but in the event of uncontrolled roll drift are provided in Figures 4.1, 4.2, and 4.3. An M-file based nonlinear 6-DOF simulation program is used for simulation of this nominal case. As can be seen from these figures, the pitch/yaw flight control system becomes unstable slightly after $t = 60$ sec although it maintains closed-loop stability during the early ascent phase.
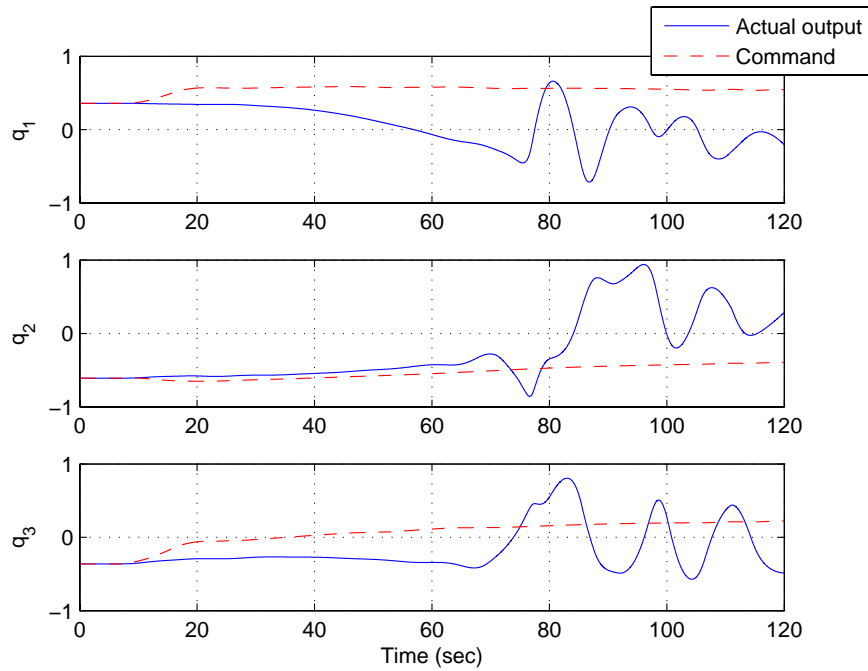
Figure 4.1   Attitude quaternion for an unstable closed-loop system caused by uncontrolled roll drift.
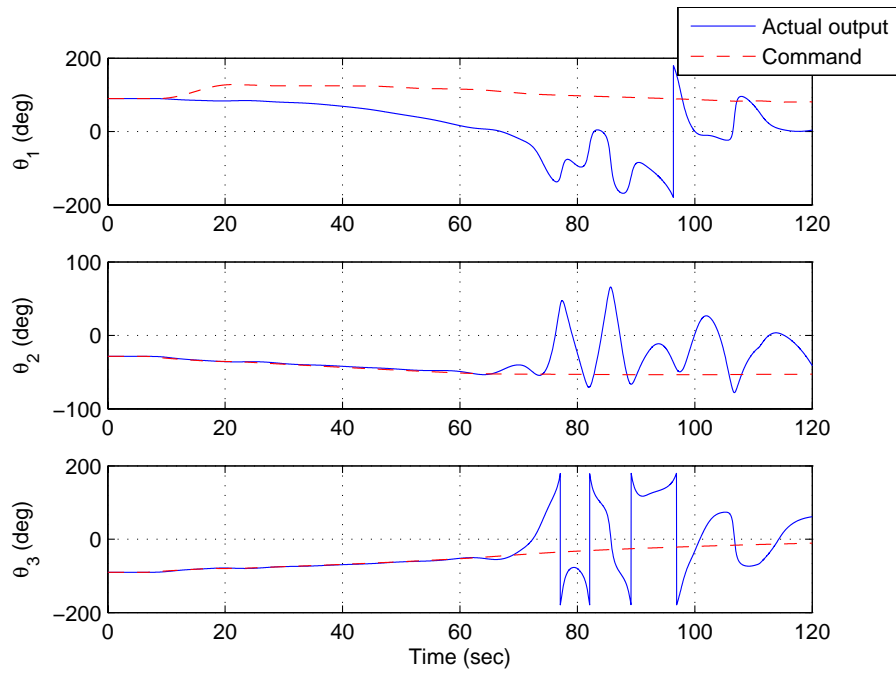
Figure 4.2   Euler angles for an unstable closed-loop system caused by un-
controlled roll drift.
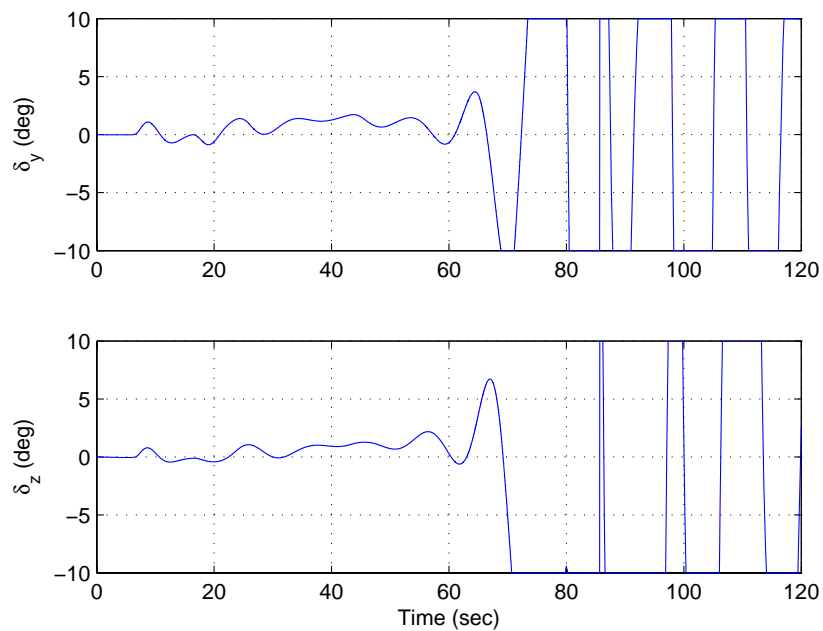
Figure 4.3   Gimbal angles for an unstable closed-loop system caused by
uncontrolled roll drift.

4.3 Stability Analysis

In this section we briefly describe the rotational equations of motion of the Ares-I CLV for its ascent flight control analysis and design. Details of the six-degrees-of-freedom (6-DOF) equations of motion of the Ares-I CLV can be found in Chapter 2. Also, detailed discussions of ascent flight control analysis and design for the Ares-I under nominal flight conditions can be found Chapter 2 and Chapter 3.

The angular velocity vector $\vec{\omega}$ of the vehicle is expressed as

$$\vec{\omega} = p\vec{i} + q\vec{k} + r\vec{k} \tag{4.1}$$

Rotational equations of motion of a reference Ares-I CLV are described by

$$
\begin{pmatrix} I_{xx} & I_{xy} & I_{xz} \\ I_{xy} & I_{yy} & I_{yz} \\ I_{xz} & I_{yz} & I_{zz} \end{pmatrix} \begin{pmatrix} \dot{p} \\ \dot{q} \\ \dot{r} \end{pmatrix} = - \begin{pmatrix} 0 & -r & q \\ r & 0 & -p \\ -q & p & 0 \end{pmatrix} \begin{pmatrix} I_{xx} & I_{xy} & I_{xz} \\ I_{xy} & I_{yy} & I_{yz} \\ I_{xz} & I_{yz} & I_{zz} \end{pmatrix} \begin{pmatrix} p \\ q \\ r \end{pmatrix}
$$
$$
+ \begin{pmatrix} T_{aero.x} \\ T_{aero.y} \\ T_{aero.z} \end{pmatrix} + \begin{pmatrix} T_{rkt.x} \\ T_{rkt.y} \\ T_{rkt.z} \end{pmatrix} + \begin{pmatrix} T_{rcs} \\ 0 \\ 0 \end{pmatrix} \tag{4.2}
$$

The rocket thrust is simply modeled as Equation. (2.41) and Equation. (2.42). The body-axis components of the rocket thrust-generated torque are expressed by Equation. (2.44). The commanded quaternion $(q_{1c}, q_{2c}, q_{3c}, q_{4c})$ from an ascent guidance system, are used to generate the attitude-error quaternion, are expressed by Equation. (2.46)

The classical proportional and derivative (PD) control laws of the ascent flight control system utilizing the quaternion-error feedback concept are described by

$$T_{rcs} = -2K_{px}q_{1e} - K_{dx}p \tag{4.3a}$$

$$\delta_y = -2K_{py}q_{2e} - K_{dy}q \tag{4.3b}$$

$$\delta_z = -2K_{pz}q_{3e} - K_{dz}r \tag{4.3c}$$

A simplified block diagram representation of the quaternion-based ascent flight control system of Ares-I CLV is provided in Figure 4.4. Detailed discussions of the advantages of the

Table 4.1 Reference Ares-I CLV parameters at t = 60 sec.

Parameters	Initial values	Units
I_{xx}	9.2356×10^5	slug-ft^2
I_{yy}	2.1860×10^8	slug-ft^2
I_{zz}	2.1860×10^8	slug-ft^2
T	2.3608×10^6	lb
ℓ	53	ft
K_{py}	1.3484	rad
K_{pz}	1.3484	rad
K_{dy}	1.5023	rad-sec
K_{dz}	1.5023	rad-sec

quaternion-feedback control system, especially with its large-angle control capability, can be found in [16].
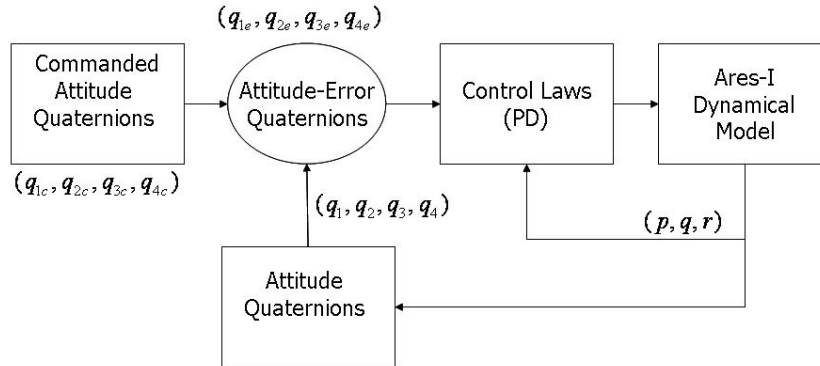
Figure 4.4 A simplified block diagram representation of the quaternion based ascent flight control system of Ares-I CLV.

A summary of the basic parameters of a reference Ares-I CLV is provided in Table 4.1.

4.3.1 Simplified Nonlinear Closed-Loop Pitch/Yaw Dynamics

Assuming uncontrolled, but slow, roll motion and controlled, fast pitch/yaw attitude dynamics of the Ares-I CLV, we consider the pitch/yaw attitude dynamics simply described by

$$\dot{q} \approx \frac{T\ell}{I_{yy}}\delta_y = \frac{T\ell}{I_{yy}}(-2K_{py}q_{2e} - K_{dy}q) \tag{4.4a}$$

$$\dot{r} \approx \frac{T\ell}{I_{zz}}\delta_z = \frac{T\ell}{I_{zz}}(-2K_{pz}q_{3e} - K_{dz}r) \tag{4.4b}$$

where T is the total thrust force and $\ell = -X_g + c_x$ is the thrust force arm. Furthermore, we also consider the quaternion-error differential equations given by

$$\begin{pmatrix} \dot{q}_{1e} \\ \dot{q}_{2e} \\ \dot{q}_{3e} \\ \dot{q}_{4e} \end{pmatrix} = \frac{1}{2} \begin{pmatrix} 0 & r & -q & p \\ -r & 0 & p & q \\ q & -p & 0 & r \\ -p & -q & -r & 0 \end{pmatrix} \begin{pmatrix} q_{1e} \\ q_{2e} \\ q_{3e} \\ q_{4e} \end{pmatrix} \tag{4.5}$$

Derivation of Equation. (4.5) is provided in Appendix D.

4.3.2 Linear Stability Analysis

For the Ares-I with $I_{yy} = I_{zz} = I$, $K_{dy} = K_{dz} = K_d$, $K_{py} = K_{pz} = K_p$ (see Table 4.1), and with controlled pitch/yaw motions, we have

$$\begin{pmatrix} \dot{q} \\ \dot{r} \\ \dot{q}_{2e} \\ \dot{q}_{3e} \end{pmatrix} = \begin{pmatrix} -\frac{T\ell}{I}K_d & 0 & -2\frac{T\ell}{I}K_p & 0 \\ 0 & -\frac{T\ell}{I}K_d & 0 & -2\frac{T\ell}{I}K_p \\ q_{4e}/2 & -q_{1e}/2 & 0 & 0 \\ q_{1e}/2 & q_{4e}/2 & 0 & 0 \end{pmatrix} \begin{pmatrix} q \\ r \\ q_{2e} \\ q_{3e} \end{pmatrix} \tag{4.6}$$

Note that for controlled pitch/yaw motions, q_{2e} and q_{3e} are small. Furthermore, q_{1e} and q_{4e} can be assumed to be slowly time varying if p is small. Also note that $q_{1e}^2 + q_{4e}^2 \approx 1$ for small q_{2e} and q_{3e}.

The characteristic equation of the linear system described by Equation. (4.6), which is assumed to have constant coefficients, can be found as

$$s^4 + (2KK_d)s^3 + (2q_{4e}KK_p + K^2K_d^2)s^2 + (2q_{4e}K^2K_pK_d)s + K^2K_p^2 = 0 \tag{4.7}$$

where $K = T\ell/I$.

Table 4.2   Routh arrays.

s^4	1	$2q_{4e}KK_p + K^2K_d^2$	$K^2K_p^2$
s^3	$2KK_d$	$2q_{4e}K^2K_pK_d$	0
s^2	$q_{4e}KK_p + K^2K_d^2$	$K^2K_p^2$	
s^1	$\dfrac{-2K^3K_dK_p^2 + 2q_{4e}K^3K_dK_p^2 + 2q_{4e}K^4K_d^3K_p}{q_{4e}KK_p + K^2K_d^2}$	0	
s^0	$K^2K_p^2$		

According to the Routh stability criterion [51] as illustrated in Table 4.2, if $q_{4e}KK_p + K^2K_d^2 > 0$ and also if

$$\frac{-2K^3K_dK_p^2 + 2q_{4e}K^3K_dK_p^2 + 2q_{4e}K^4K_d^3K_p}{q_{4e}KK_p + K^2K_d^2} > 0 \tag{4.8}$$

then we have a stable closed-loop system. Equation. (4.8) can be rewritten as

$$\frac{2K^3K_dK_p}{q_{4e}KK_p + K^2K_d^2}(-K_p + q_{4e}^2K_p + q_{4e}KK_d^2) > 0 \tag{4.9}$$

By defining $B = KK_d^2/K_p$, we obtain the linear stability criterion as

$$q_{4e}^2 + Bq_{4e} - 1 > 0 \tag{4.10}$$

which becomes

$$q_{4e} > \frac{-B}{2} + \frac{\sqrt{B^2 + 4}}{2} \tag{4.11}$$

or

$$q_{4e} < \frac{-B}{2} - \frac{\sqrt{B^2 + 4}}{2} \tag{4.12}$$

This result confirms that the pitch/yaw closed-loop system can become unstable for small q_{4e} (i.e., for large error q_{1e}), which can occur without active roll control. Equation. (4.10) shows that the critical parameter is B, which is determined by physical parameters of the Ares-I CLV and its control gains. Assuming that q_{4e} is positive, therefore the linear stability criterion becomes

$$B > \frac{1 - q_{4e}^2}{q_{4e}} \tag{4.13}$$

The plot of function $B = \frac{1 - q_{4e}^2}{q_{4e}}$ is provided in blue line (Figure 4.5). When the data point $(q_{4e},\ B)$ in the region above the blue line, the attitude control system is stable, otherwise it

is unstable. For example, at $t = 60$ sec, $B = 0.9595$, the corresponding value of q_{4e} is 0.6294, illustrated by the red dash line in Figure 4.5. In terms of Euler angle it is about 102 deg. It means that when the roll error is smaller than 102 deg ($q_{4e} > 0.6294$), the attitude control system is stable. If the roll error is larger than 102 deg ($q_{4e} < 0.6294$), the attitude control system becomes unstable.
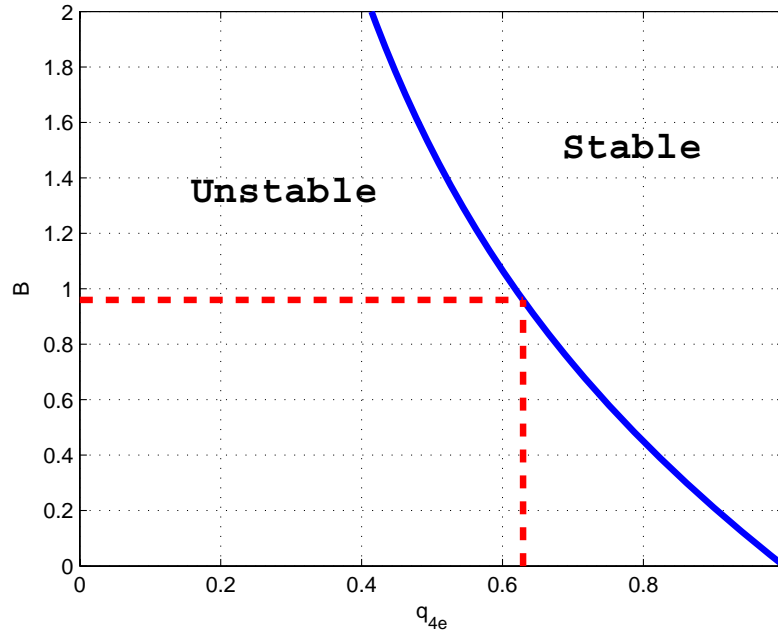
Figure 4.5   Plot of the function $B = \frac{1-q_{4e}^2}{q_{4e}}$.

In order to illustrate how the specific values of q_{1e} and q_{4e} affect closed-loop system stability, we consider three cases as described in Table 4.3. Figures 4.6 and 4.7 clearly show that closed-loop stability is affected by a large value of q_{1e}. As can be seen in Figure 4.8, the aerodynamic disturbance makes the case worse. The linear model of uncontrolled roll drift with aerodynamic disturbance can be found in Appendix E.

Table 4.3   Three cases for root locus stability analysis.

Case numbers	$(\theta_{1e}, \theta_{2e}, \theta_{3e})$ deg	q_{1e}	q_{4e}	Aerodynamic disturbance
1	(30, 0, 0)	0.2588	0.9659	No
2	(80, 0, 0)	0.6428	0.7660	No
3	(80, 0, 0)	0.6428	0.7660	Yes
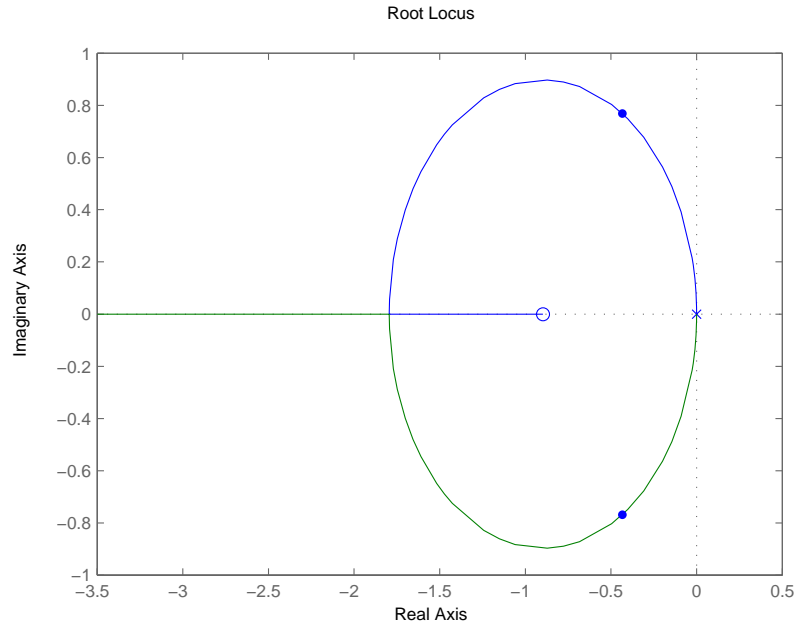
Figure 4.6   Root locus plot for Case 1.
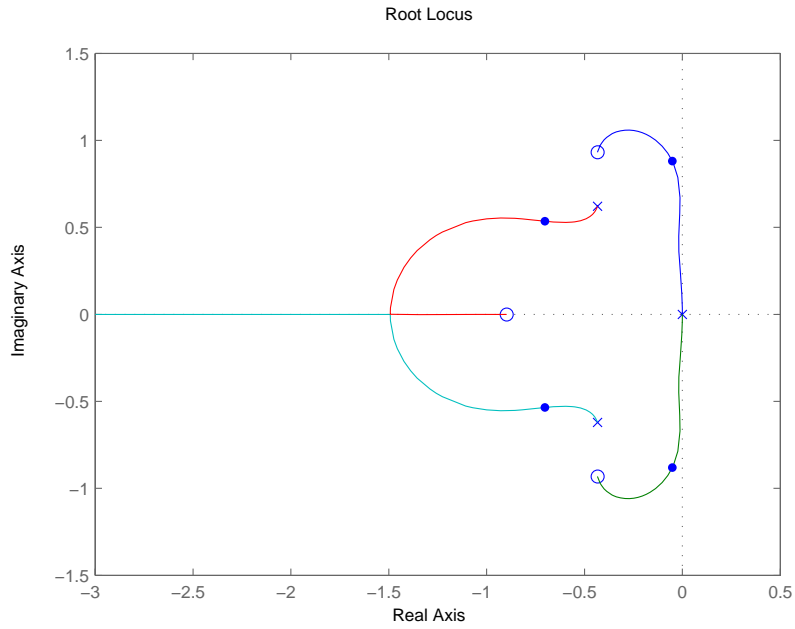
Figure 4.7   Root locus plot for Case 2.
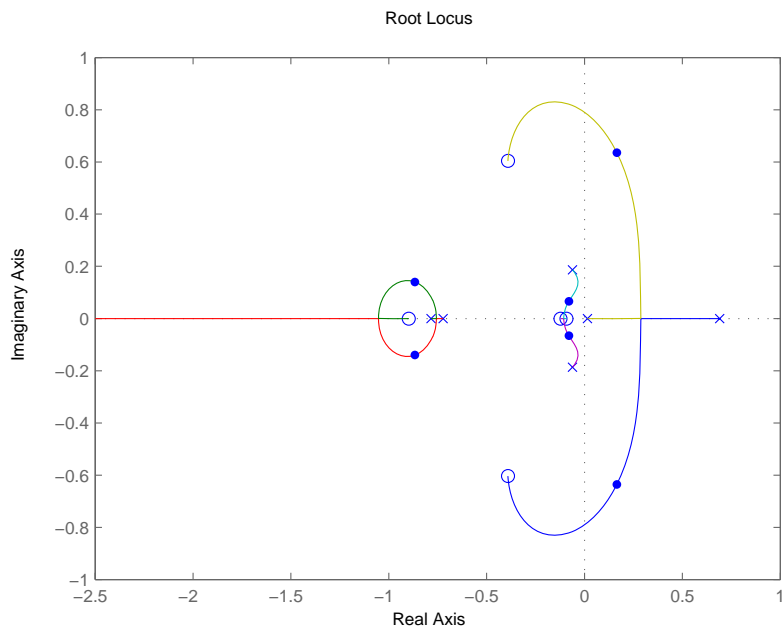
Figure 4.8   Root locus plot for Case 3, showing closed-loop instability with a nominal loop gain.

4.3.3   Nonlinear Stability Analysis

In general, when RCS fails, it becomes an underactuated control problem of an axisymmetric rigid body. Equation. (4.5) can help us to simplify the analysis of this problem by checking the dynamics of the attitude-error quaternion, which can be described as

$$
\begin{pmatrix} \dot{p} \\ \dot{q} \\ \dot{r} \end{pmatrix} = \begin{pmatrix} \frac{I_y - I_z}{I_x} qr \\ \frac{I_z - I_x}{I_y} rp \\ \frac{I_x - I_y}{I_z} pq \end{pmatrix} + \begin{pmatrix} 0 \\ \frac{T\ell}{I_y} \delta_y \\ \frac{T\ell}{I_z} \delta_z \end{pmatrix} + \begin{pmatrix} \frac{T_{rcs}}{I_x} \\ 0 \\ 0 \end{pmatrix}
\tag{4.14}
$$

$$
\begin{pmatrix} \dot{q}_{1e} \\ \dot{q}_{2e} \\ \dot{q}_{3e} \\ \dot{q}_{4e} \end{pmatrix} = \frac{1}{2} \begin{pmatrix} 0 & r & -q & p \\ -r & 0 & p & q \\ q & -p & 0 & r \\ -p & -q & -r & 0 \end{pmatrix} \begin{pmatrix} q_{1e} \\ q_{2e} \\ q_{3e} \\ q_{4e} \end{pmatrix}
\tag{4.15}
$$

$$
T_{rcs} = 0
\tag{4.16a}
$$

$$
\delta_y = -2K_{py}q_{2e} - K_{dy}q
\tag{4.16b}
$$

$$
\delta_z = -2K_{pz}q_{3e} - K_{dz}r
\tag{4.16c}
$$

The attitude-error quaternion feedback control law always tries to drive the attitude-error quaternion from any initial values to $(0,\ 0,\ 0,\ 1)$. In order to simplify the notation, $(q_1,\ q_2,\ q_3,\ q_4)$ will be used to replace $(q_{1e},\ q_{2e},\ q_{3e},\ q_{4e})$ in Equation.(4.15).

Since the body is axisymmetric, it is assumed $I_y = I_z$, and $p = 0$. The whole dynamical system becomes an autonomous system, $\dot{\mathbf{x}} = f(\mathbf{x})$, where $\mathbf{x} = (q,\ r,\ q_1,\ q_2,\ q_3,\ q_4)^T$

$$
\begin{pmatrix} \dot{q} \\ \dot{r} \\ \dot{q}_1 \\ \dot{q}_2 \\ \dot{q}_3 \\ \dot{q}_4 \end{pmatrix} = \begin{pmatrix} -\hat{K}_p q_2 - \hat{K}_d q \\ -\hat{K}_p q_3 - \hat{K}_d r \\ \frac{r}{2}q_2 - \frac{q}{2}q_3 \\ -\frac{r}{2}q_1 + \frac{q}{2}q_4 \\ \frac{q}{2}q_1 + \frac{r}{2}q_4 \\ -\frac{q}{2}q_2 - \frac{r}{2}q_3 \end{pmatrix}
\tag{4.17}
$$

where $\hat{K}_p = \frac{T\ell}{I_y}K_p$ and $\hat{K}_d = \frac{T\ell}{I_y}K_d$. Note that the notation of attitude-error quaternion is changed from $(q_{1e}, q_{2e}, q_{3e}, q_{4e})$ to (q_1, q_2, q_3, q_4), in order to keep expressions simple.

A Lyapunov function candidate can be taken as the energy-like function

$$V(\mathbf{x}) = \frac{1}{2\hat{K}_p}q^2 + \frac{1}{2\hat{K}_p}r^2 + q_1^2 + q_2^2 + q_3^2 + (1 - q_4)^2 \tag{4.18}$$

and $V(\mathbf{x}) = 0$ when $\mathbf{x} = (0, 0, 0, 0, 0, 1)^T$, otherwise $V(\mathbf{x}) > 0$.

Its derivative $\dot{V}(\mathbf{x})$ along any trajectory is

$$\dot{V}(\mathbf{x}) = -\frac{\hat{K}_d}{\hat{K}_p}(q^2 + r^2) \leq 0 \tag{4.19}$$

which is negative semidefinite.

Define a set M,

$$M = \{(q, r, q_1, q_2, q_3, q_4): q = r = 0, q_2 = q_3 = 0\} \tag{4.20}$$

The set M is a positive invariant set, since

$$\mathbf{x}(0) \in M \Rightarrow \mathbf{x}(t) \in M, \forall t \geq 0 \tag{4.21}$$

By LaSalle's theorem (Invariance Principle) [52], all trajectories approach M as $t \to \infty$.

In order to visualize the attitude quaternion a new variable z is defined as $z^2 = q_2^2 + q_3^2 = 1 - q_1^2 - q_4^2$ and z is a nonnegative real number. Therefore the time history of attitude quaternion is a trajectory on the spherical surface $q_1^2 + q_4^2 + z^2 = 1$ (Figure 4.9) or on the surface of the cone $z = \sqrt{q_2^2 + q_3^2}$. The set M is the circle in the $q_1 - q_4$ plane (Figure 4.10).

Simulation results are given below to verify both the linear and nonlinear stability analysis. The initial value of the simulation case can be found in Table 4.4. Note that by linear stability analysis, if $q_4 < 0.6294$ ($q_1 > 0.7771$), the linear system is unstable. The stable and unstable regions are shown in Figure 4.11.

For an axisymmetric rigid-body, if the uncontrolled principal axis is an axis of symmetry and the other two axes are controlled by an attitude quaternion feedback law, the dynamical system, Equation. (4.17), will converge to an invariant set or a subsystem, Equations. (4.20), globally. On the other hand, by the Hartman-Grobman theorem [53], the local behavior near
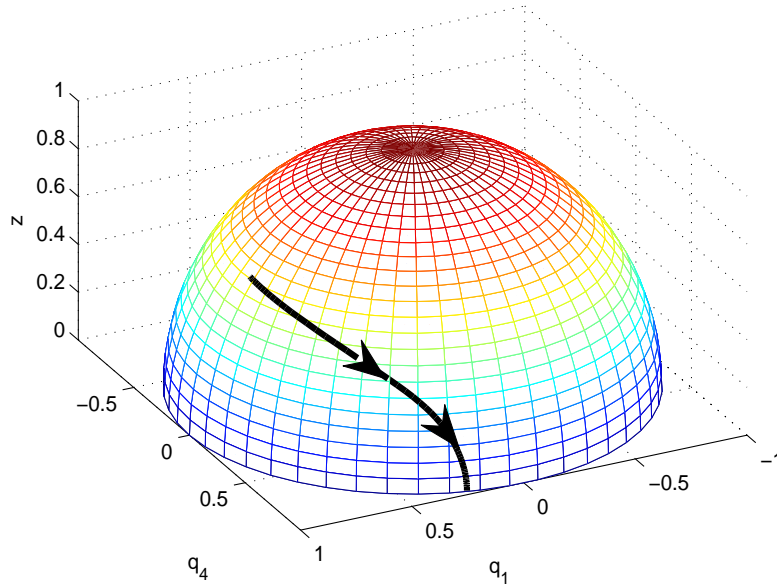
Figure 4.9　Trajectory on the spherical surface $q_1^2 + q_4^2 + z^2 = 1$.

Table 4.4　Three simulation cases for nonlinear stability analysis.

Case numbers	Initial values of quaternion $(q_1,\ q_2,\ q_3,\ q_4)$
1	$(0, 0.01, 0.01, 0.9999)$
2	$(0.5, 0.01, 0.01, 0.8659)$
3	$(0.85, 0.01, 0.01, 0.5266)$

the invariant set M is governed by the linear system Equation. (4.6). This is the reason why an oscillation phenomenon can be observed when q_{1e} is very large from Figure 4.20 to Figure 4.24.
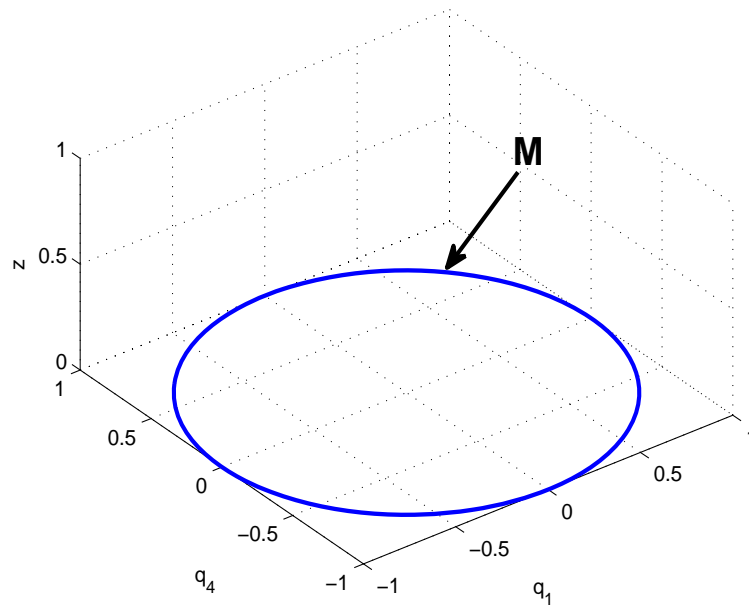
Figure 4.10 The positive invariant set M.
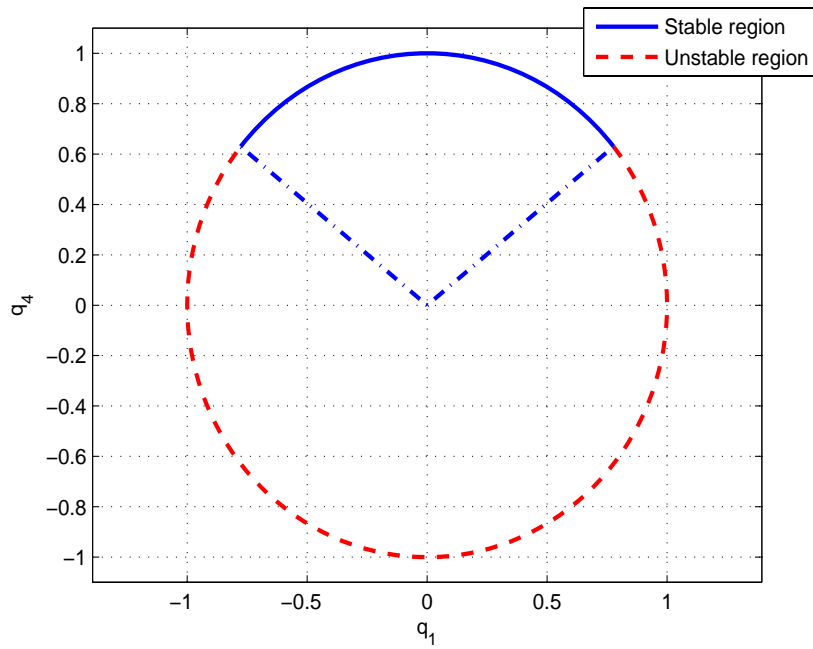
Figure 4.11 The stable and unstable regions in M.
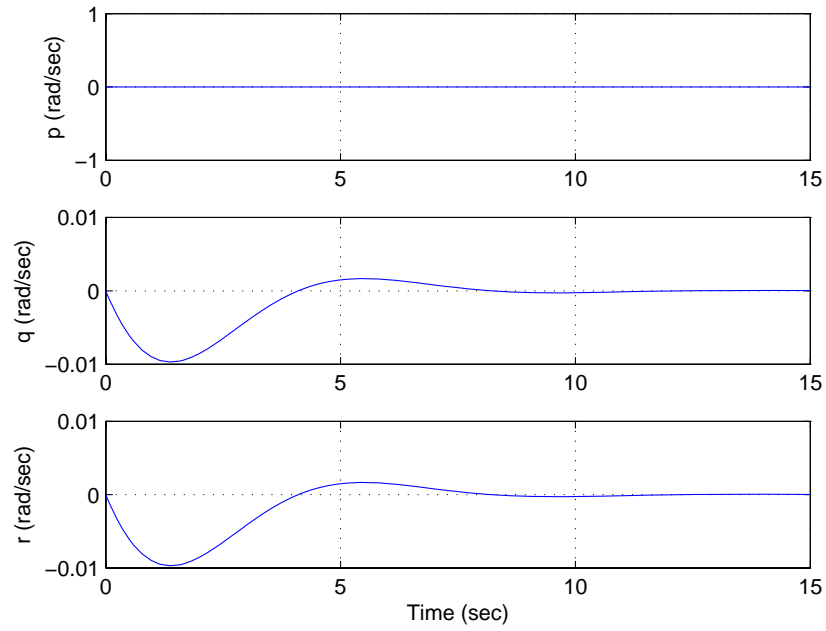
Figure 4.12   Angular velocity for Case 1.
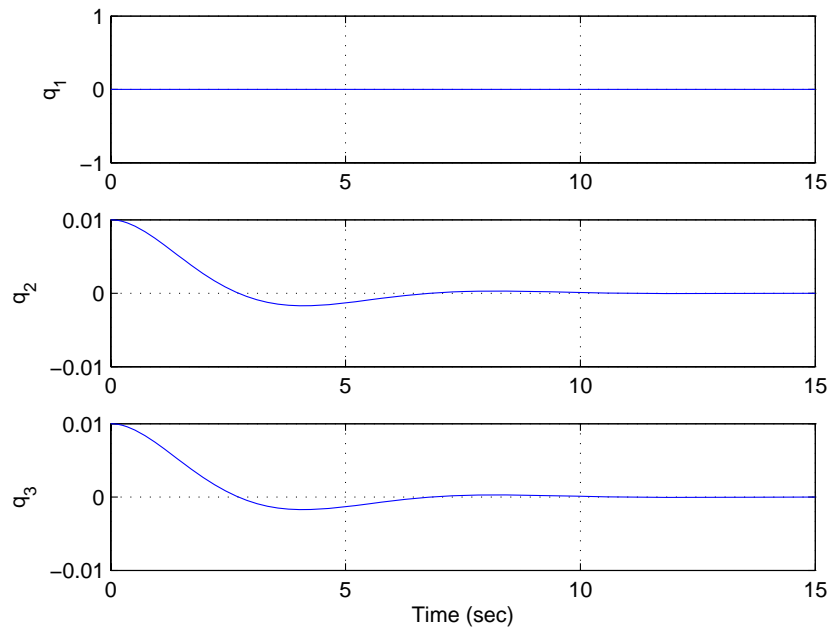
Figure 4.13   Attitude quaternion for Case 1.
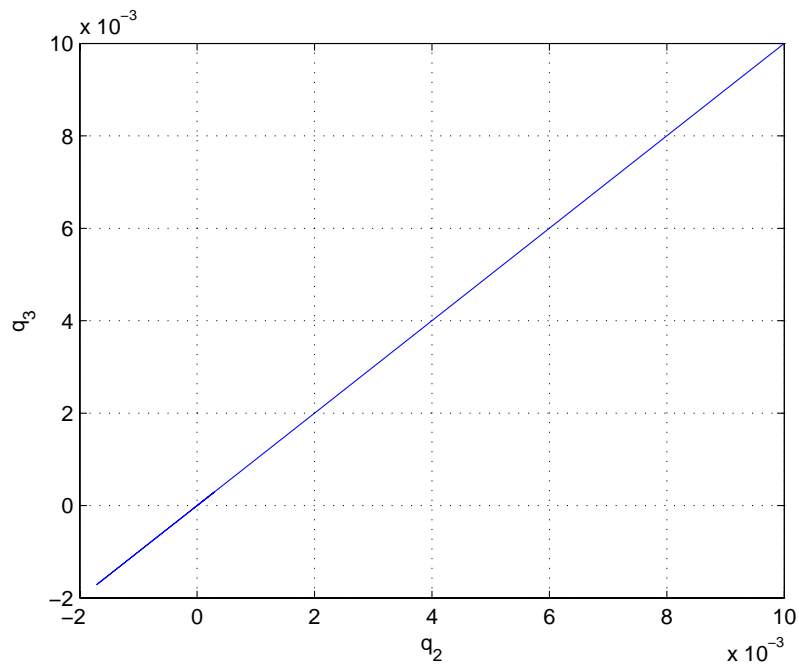
Figure 4.14   Phase portrait of q_2 and q_3 for Case 1.
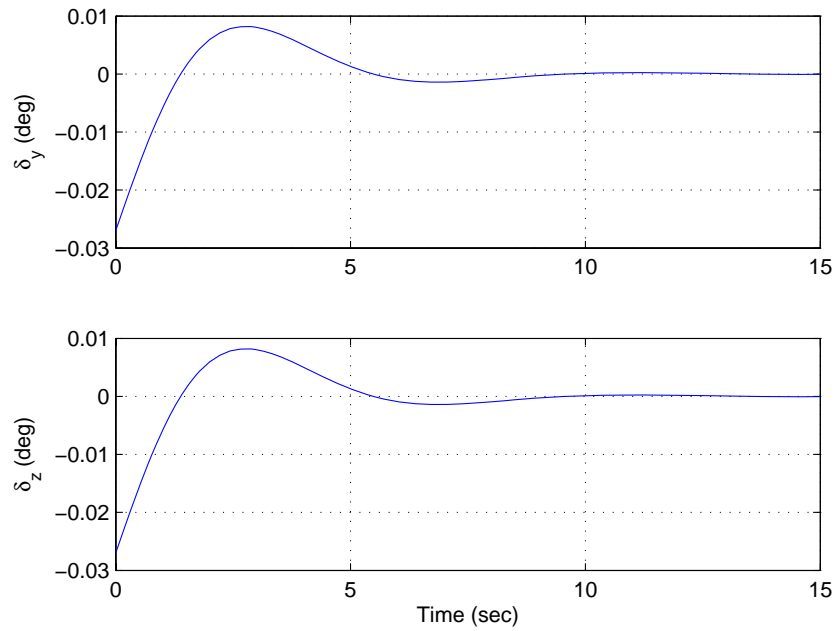
Figure 4.15   Control inputs for Case 1.
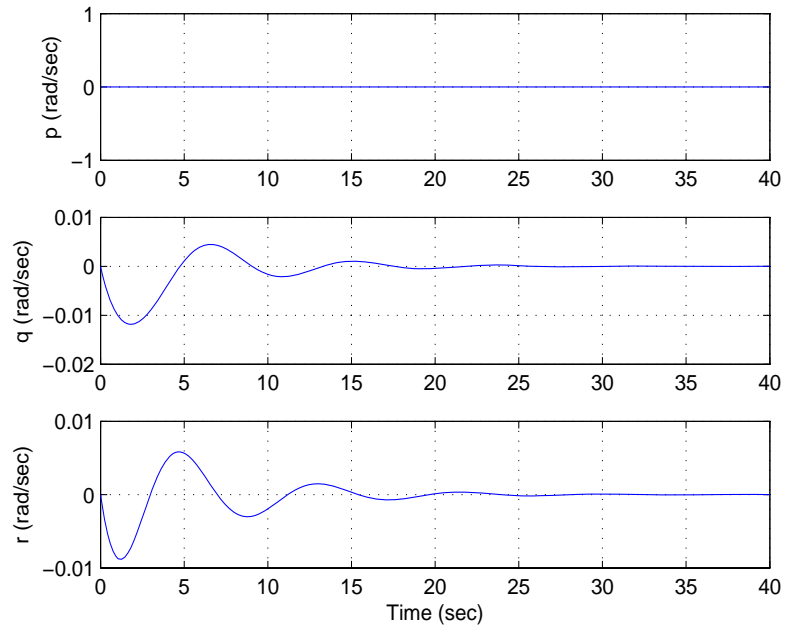
Figure 4.16   Angular velocity for Case 2.
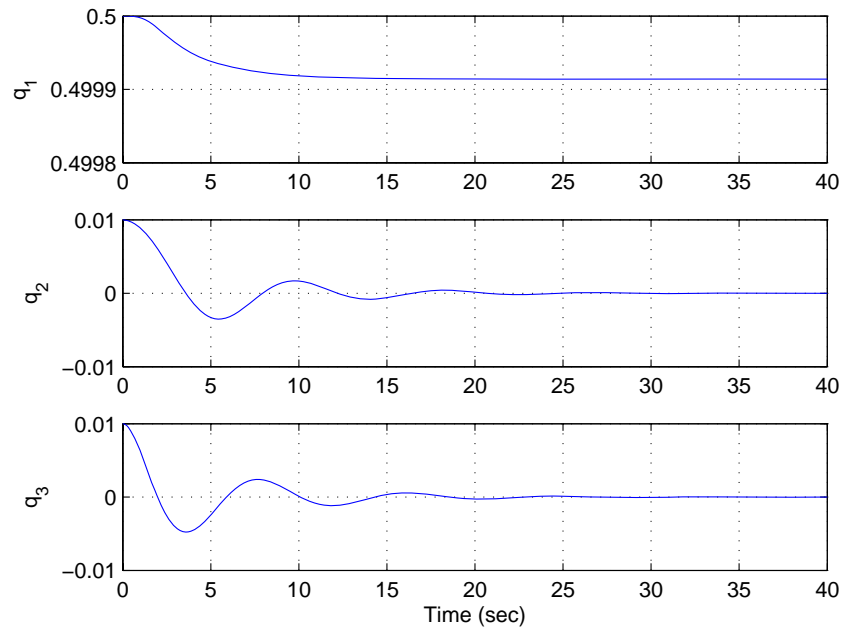
Figure 4.17   Attitude quaternion for Case 2.
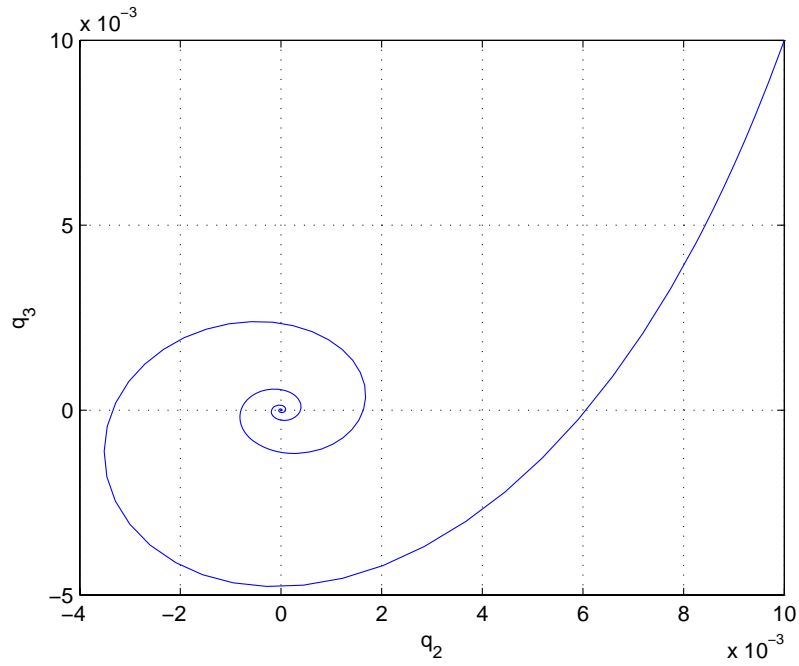
Figure 4.18   Phase portrait of q_2 and q_3 for Case 2.
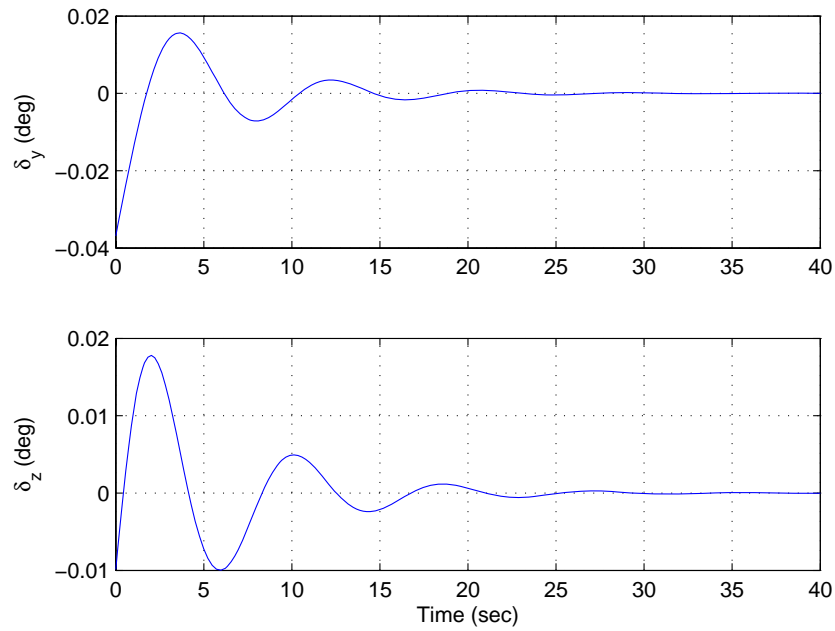
Figure 4.19   Control inputs for Case 2.
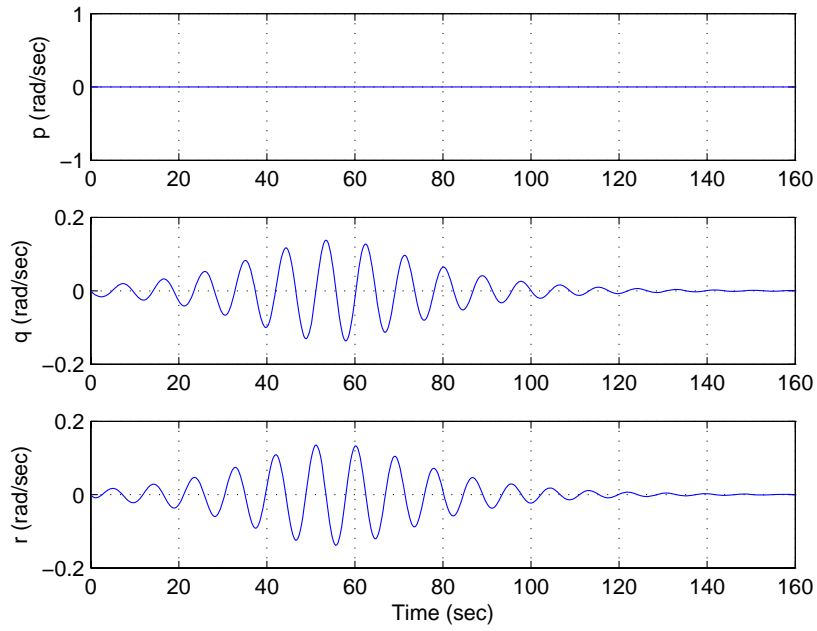
Figure 4.20   Angular velocity for Case 3.
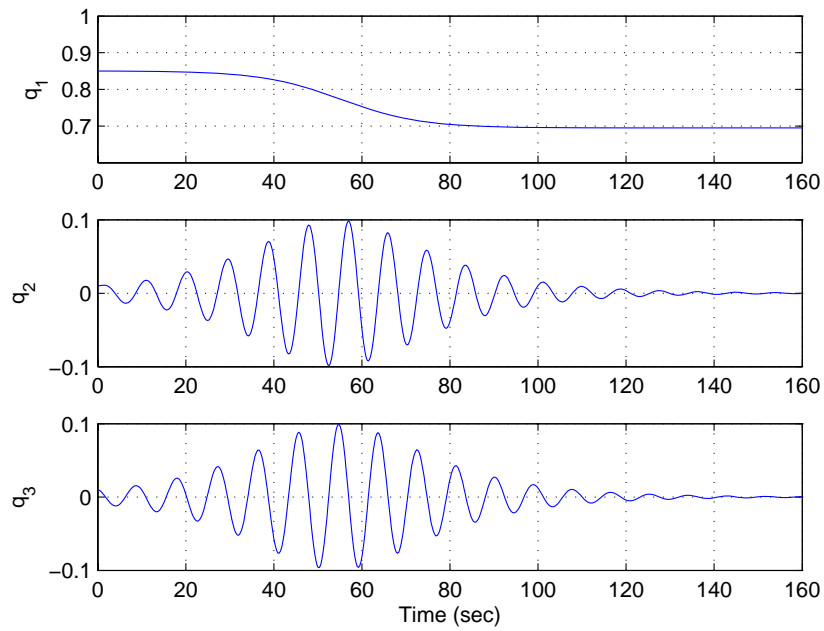
Figure 4.21   Attitude quaternion for Case 3.
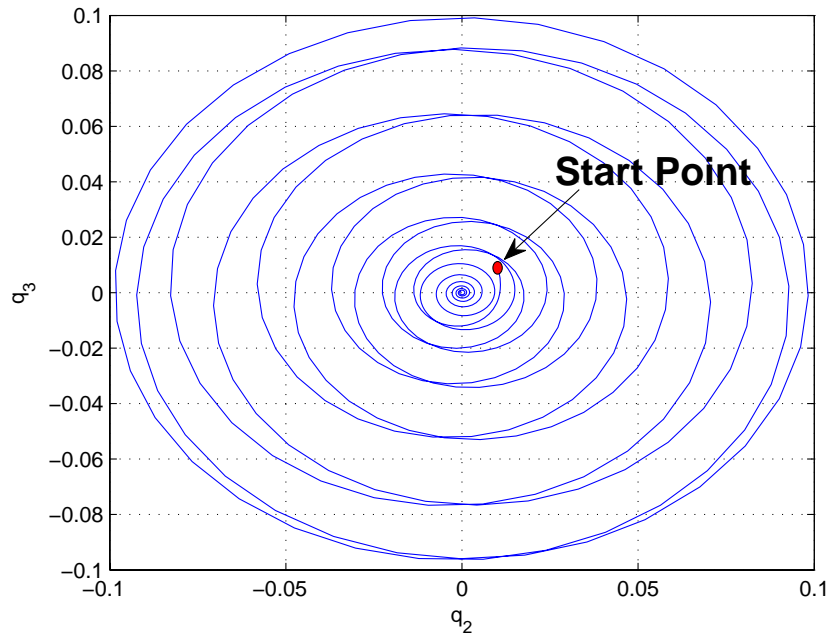
Figure 4.22   Phase portrait of q_2 and q_3 for Case 3.
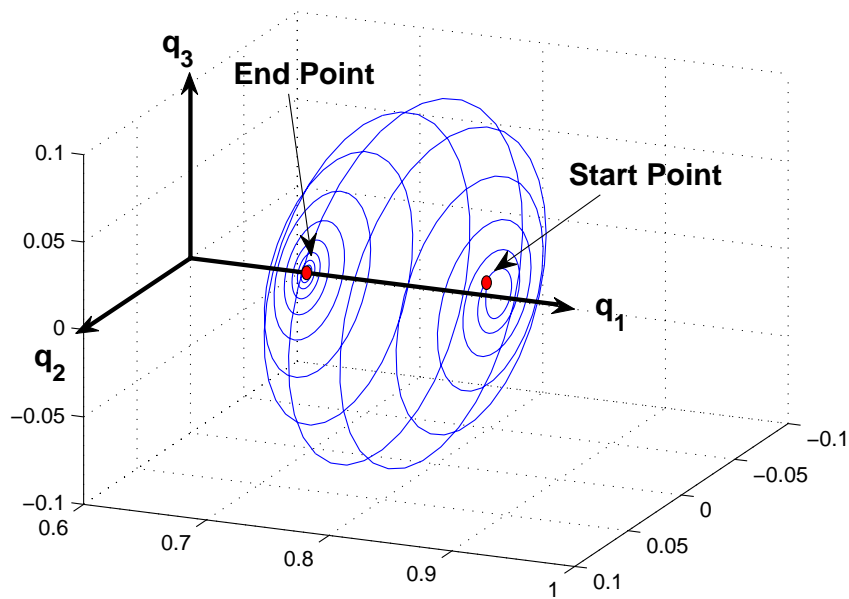
Figure 4.23 q_1-q_2-q_3 plot for Case 3.
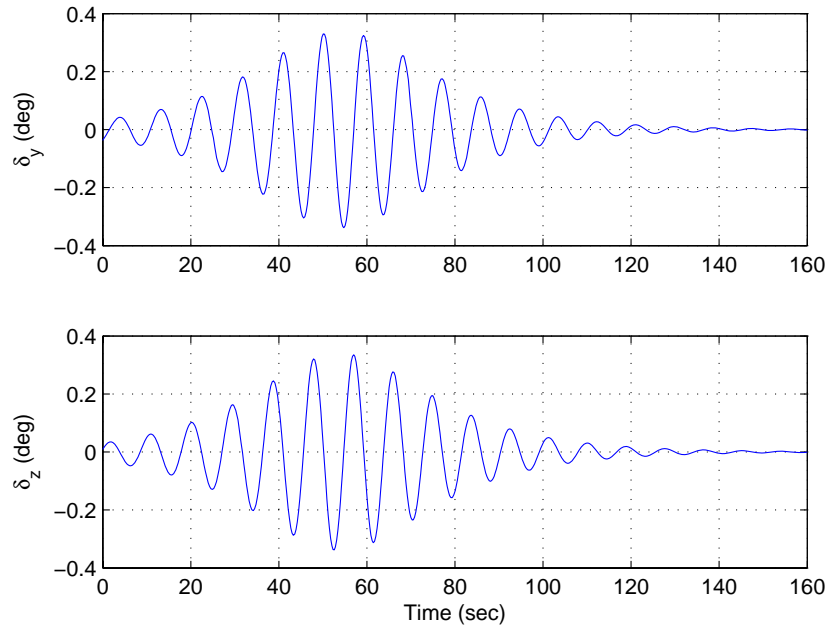
Figure 4.24   Control inputs for Case 3.
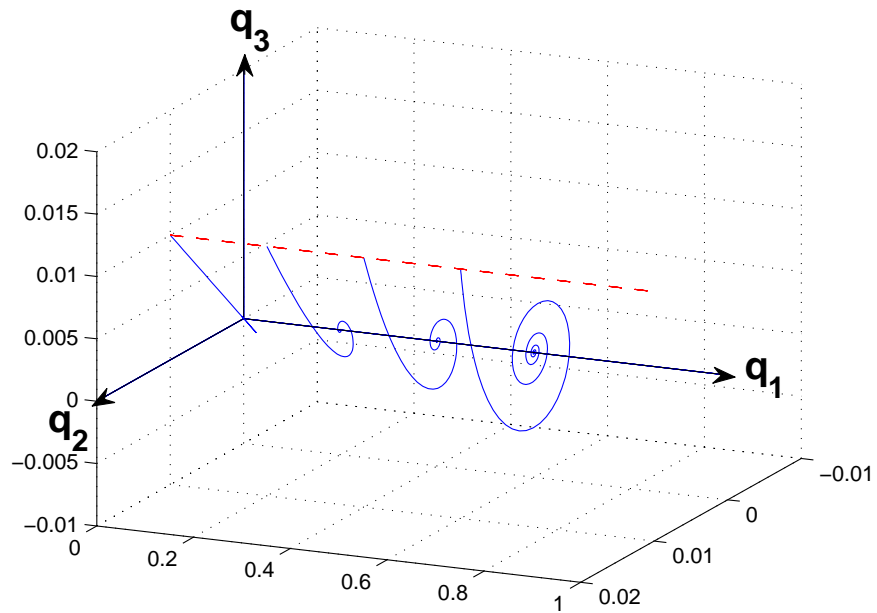
Figure 4.25 q_2-q_3 plot, from left to right $q_1 = 0$, $q_1 = 0.2$, $q_1 = 0.4$, $q_1 = 0.6$.

4.4 New Pitch/Yaw Control Logic with Modified Commanded Quaternions

In this section, we present an approach for maintaining the pitch/yaw closed-loop stability even in the event of uncontrolled roll drift. This approach utilizes the inherent versatility of the quaternion-based attitude control system [16]. This approach simply requires an on-board computation of the desired attitude quaternion using the actual uncontrolled roll angle information as illustrated in Figure 4.26.
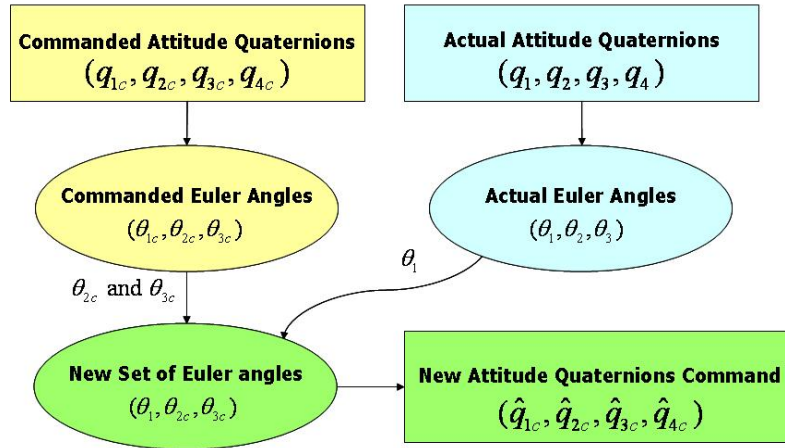
Figure 4.26   A block diagram representation of a proposed method for computing a new set of commanded attitude quaternion.

The attitude quaternion $(q_1, \; q_2, \; q_3, \; q_4)$ are computed by numerically integrating the kinematic differential equations Equation. (2.12).

The attitude quaternion $(q_1, \; q_2, \; q_3, \; q_4)$ for a rotational sequence of $\mathbf{C}_1(\theta_1) \leftarrow \mathbf{C}_2(\theta_2) \leftarrow \mathbf{C}_3(\theta_3)$ are related to Euler angles as follows [16]:

$$
\begin{aligned}
q_1 &= \sin(\theta_1/2)\cos(\theta_2/2)\cos(\theta_3/2) - \cos(\theta_1/2)\sin(\theta_2/2)\sin(\theta_3/2) \\
q_2 &= \cos(\theta_1/2)\sin(\theta_2/2)\cos(\theta_3/2) + \sin(\theta_1/2)\cos(\theta_2/2)\sin(\theta_3/2) \\
q_3 &= \cos(\theta_1/2)\cos(\theta_2/2)\sin(\theta_3/2) - \sin(\theta_1/2)\sin(\theta_2/2)\cos(\theta_3/2) \\
q_4 &= \cos(\theta_1/2)\cos(\theta_2/2)\cos(\theta_3/2) + \sin(\theta_1/2)\sin(\theta_2/2)\sin(\theta_3/2)
\end{aligned}
\tag{4.22}
$$

Also, we have the following direction cosine matrix relationship for the rotational sequence of $\mathbf{C}_1(\theta_1) \leftarrow \mathbf{C}_2(\theta_2) \leftarrow \mathbf{C}_3(\theta_3)$

$$
\begin{pmatrix}
\cos\theta_2\cos\theta_3 & \cos\theta_2\sin\theta_3 & -\sin\theta_2 \\
\sin\theta_1\sin\theta_2\cos\theta_3 - \cos\theta_1\sin\theta_3 & \sin\theta_1\sin\theta_2\sin\theta_3 + \cos\phi\cos\theta_3 & \sin\theta_1\cos\theta \\
\cos\theta_1\sin\theta_2\cos\theta_3 + \sin\theta_1\sin\theta_3 & \cos\theta_1\sin\theta_2\sin\theta_3 - \sin\phi\cos\theta_3 & \cos\theta_1\cos\theta
\end{pmatrix}
$$

$$
= \begin{pmatrix} C_{11} & C_{12} & C_{13} \\ C_{21} & C_{22} & C_{23} \\ C_{31} & C_{32} & C_{33} \end{pmatrix} = \begin{pmatrix} 1-2(q_2^2+q_3^2) & 2(q_1q_2+q_3q_4) & 2(q_1q_3-q_2q_4) \\ 2(q_1q_2-q_3q_4) & 1-2(q_1^2+q_3^2) & 2(q_2q_3+q_1q_4) \\ 2(q_1q_3+q_2q_4) & 2(q_2q_3-q_1q_4) & 1-2(q_1^2+q_2^2) \end{pmatrix}
$$

(4.23)

For this particular rotational sequence of Euler angles, the Euler angles (θ_2, θ_3) describe the inertial orientation of the longitudinal axis of the Ares-I CLV.

The actual Euler angle θ_1 of the Ares-I CLV can then be determined from the attitude quaternion (q_1, q_2, q_3, q_4) as follows:

$$
\theta_1 = \operatorname{sgn}\{C_{23}\}\cos^{-1}\left\{\frac{C_{33}}{\cos\theta_2}\right\} = \operatorname{sgn}\{2(q_2q_3+q_1q_4)\}\cos^{-1}\left\{\frac{1-2(q_1^2+q_2^2)}{\sqrt{1-4(q_1q_3-q_2q_4)^2}}\right\} \quad (4.24)
$$

when $|\theta_2| \neq \pi/2$.

Similarly, the commanded angles $(\theta_{2c}, \theta_{3c})$ of the Ares-I CLV can be determined from the desired attitude quaternion $(q_{1c}, q_{2c}, q_{3c}, q_{4c})$ commanded from an ascent guidance system as follows:

$$
\theta_{2c} = \sin^{-1}\{-2(q_{1c}q_{3c}-q_{2c}q_{4c})\} \quad (4.25)
$$

$$
\theta_{3c} = \operatorname{sgn}\{2(q_{1c}q_{2c}+q_{3c}q_{4c})\}\cos^{-1}\left\{\frac{1-2(q_{2c}^2+q_{3c}^2)}{\sqrt{1-4(q_{1c}q_{3c}-q_{2c}q_{4c})^2}}\right\} \quad (4.26)
$$

By using the actual Euler angle θ_1 and the commanded angles $(\theta_{2c}, \theta_{3c})$, we can obtain a modified set of desired attitude quaternion as follows:

$$
\begin{aligned}
\hat{q}_{1c} &= \sin(\theta_1/2)\cos(\theta_{2c}/2)\cos(\theta_{3c}/2) - \cos(\theta_1/2)\sin(\theta_{2c}/2)\sin(\theta_{3c}/2) \\
\hat{q}_{2c} &= \cos(\theta_1/2)\sin(\theta_{2c}/2)\cos(\theta_{3c}/2) + \sin(\theta_1/2)\cos(\theta_{2c}/2)\sin(\theta_{3c}/2) \\
\hat{q}_{3c} &= \cos(\theta_1/2)\cos(\theta_{2c}/2)\sin(\theta_{3c}/2) - \sin(\theta_1/2)\sin(\theta_{2c}/2)\cos(\theta_{3c}/2) \\
\hat{q}_{4c} &= \cos(\theta_1/2)\cos(\theta_{2c}/2)\cos(\theta_{3c}/2) + \sin(\theta_1/2)\sin(\theta_{2c}/2)\sin(\theta_{3c}/2)
\end{aligned} \quad (4.27)
$$
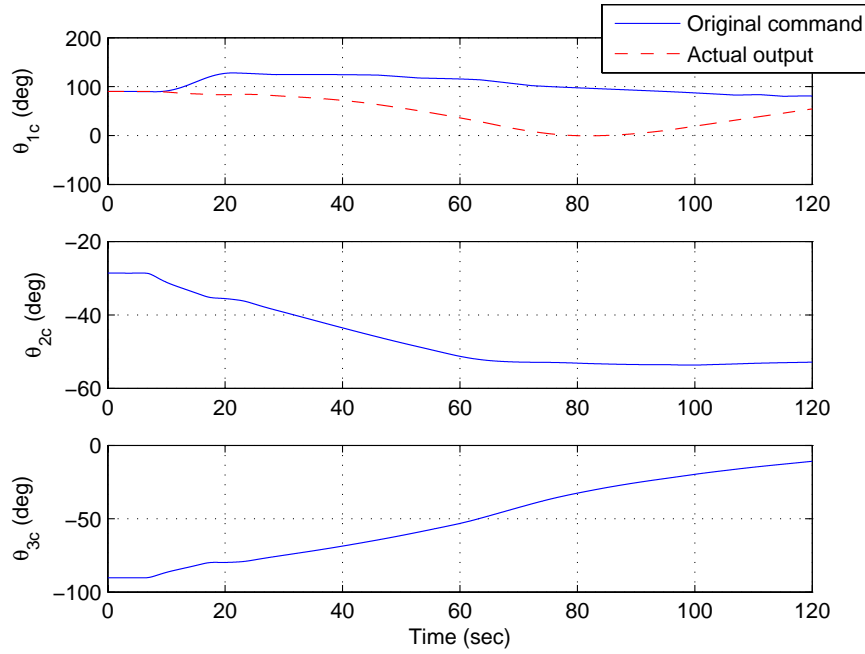
Figure 4.27   Comparison of new and original attitude Euler angles command.

These new commanded quaternion ($\hat{q}_{1c}$, $\hat{q}_{2c}$, $\hat{q}_{3c}$, $\hat{q}_{4c}$) are then used to determine the attitude-error quaternion (q_{1e}, q_{2e}, q_{3e}, q_{4e}) as follows:

$$
\begin{pmatrix} q_{1e} \\ q_{2e} \\ q_{3e} \\ q_{4e} \end{pmatrix} = \begin{pmatrix} \hat{q}_{4c} & \hat{q}_{3c} & -\hat{q}_{2c} & -\hat{q}_{1c} \\ -\hat{q}_{3c} & \hat{q}_{4c} & \hat{q}_{1c} & -\hat{q}_{2c} \\ \hat{q}_{2c} & -\hat{q}_{1c} & \hat{q}_{4c} & -\hat{q}_{3c} \\ \hat{q}_{1c} & \hat{q}_{2c} & \hat{q}_{3c} & \hat{q}_{4c} \end{pmatrix} \begin{pmatrix} q_1 \\ q_2 \\ q_3 \\ q_4 \end{pmatrix}
\tag{4.28}
$$

The pitch and yaw gimbal control laws are simply the same as the original ascent flight control laws described by

$$
\delta_y = -2K_{py}q_{2e} - K_{dy}q
\tag{4.29a}
$$

$$
\delta_z = -2K_{pz}q_{3e} - K_{dz}r
\tag{4.29b}
$$

No adjustment of the control gains of the original ascent flight control system is required for controlling the pitch and yaw motions without active roll control.
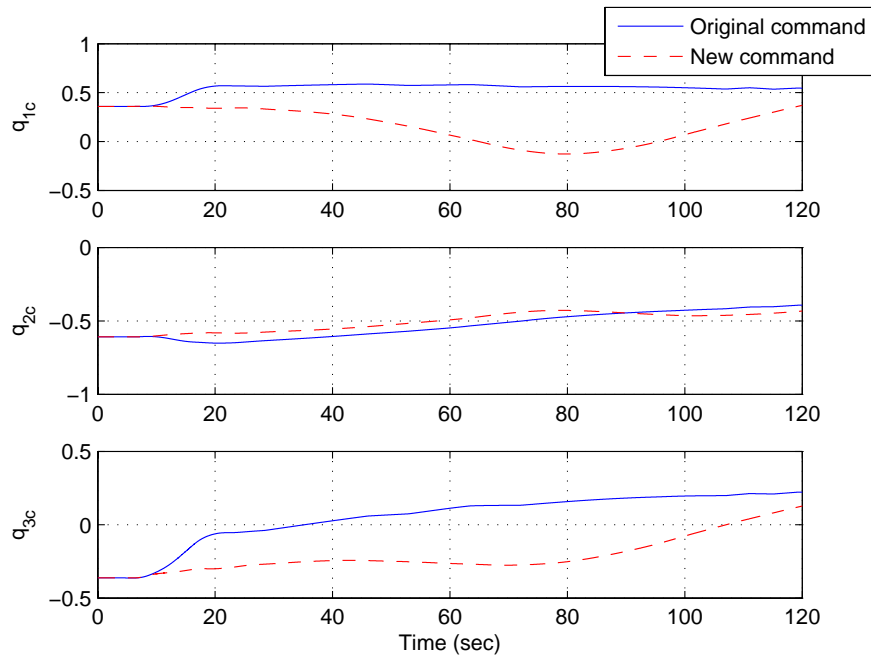
Figure 4.28   Comparison of new and original attitude quaternion command.

Stable closed-loop responses of the proposed approach with a modified set of desired quaternion can be seen from Figure 4.29 to Figure 4.32 in the event of uncontrolled roll drift. Furthermore, as can be seen in Figure 4.32, the proposed control approach achieves an identical ascent flight trajectory as the nominal ascent flight control system with active roll control.
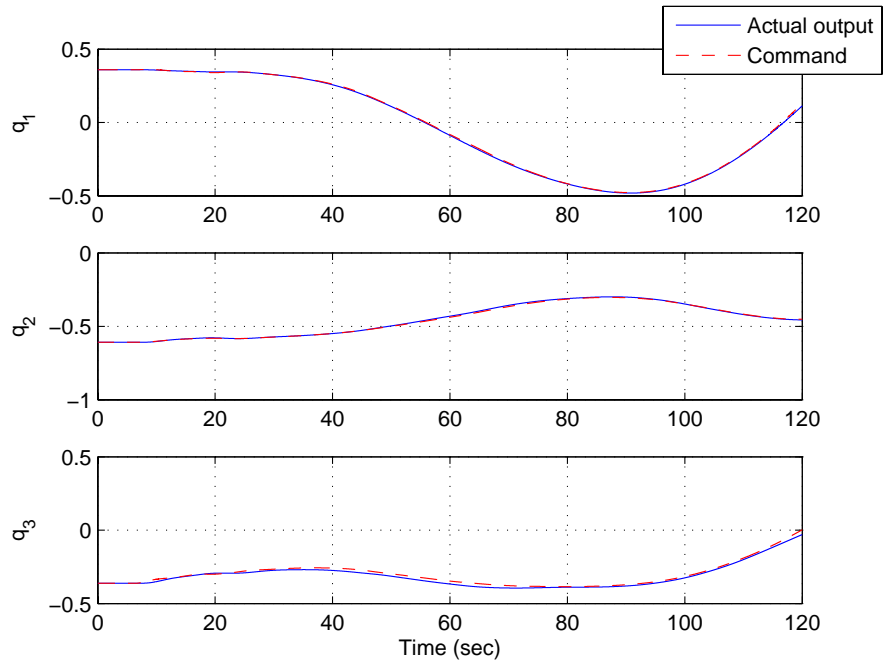
Figure 4.29   Quaternion for a closed-loop system stabilized by the proposed control logic employing modified commanded quaternion.
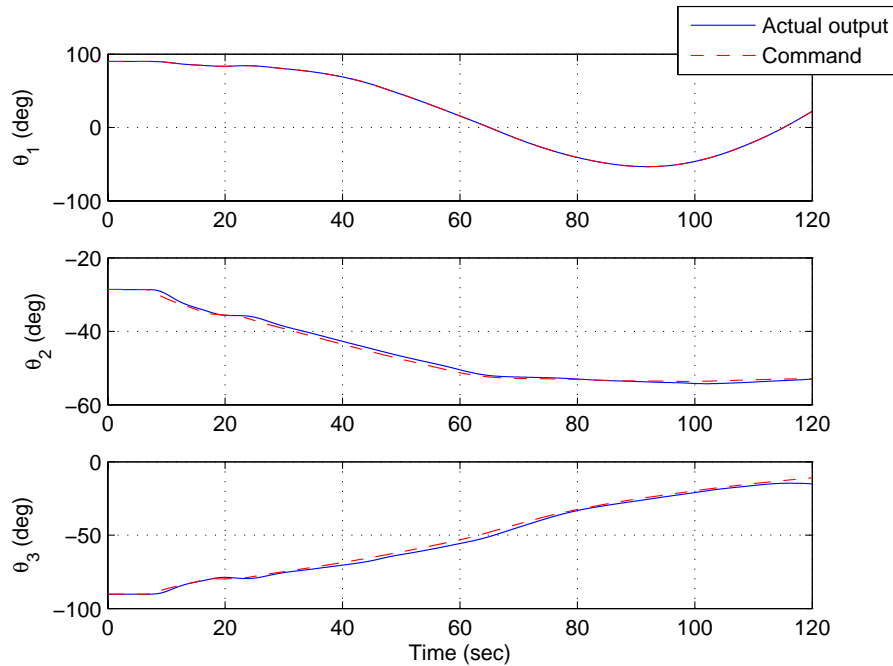
Figure 4.30   Euler angles for a closed-loop system stabilized by the proposed control logic employing modified commanded quaternion.

84
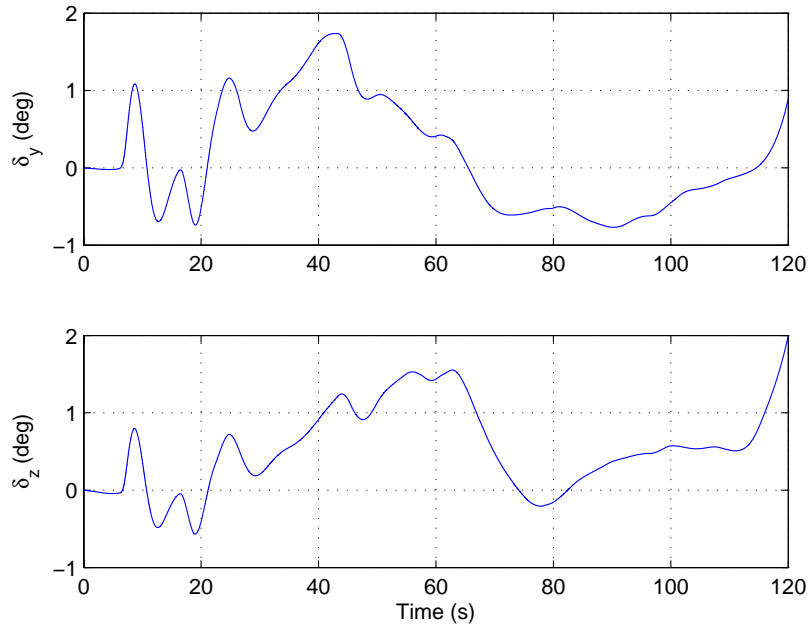
Figure 4.31   Gimbal angles for a closed-loop system stabilized by the pro-
posed control logic employing modified commanded quater-
nion.
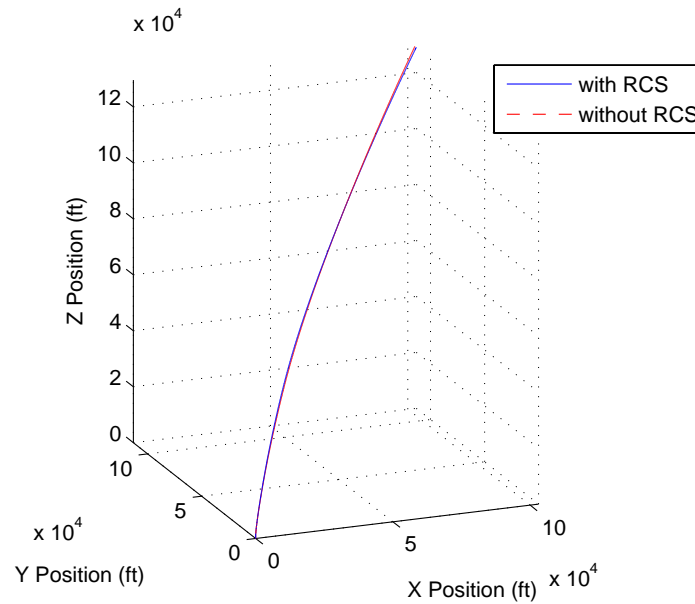
Figure 4.32   Comparison of ascent trajectories: with roll control system vs.
without roll control system.

4.5 Simple Adjustment of Control Gains

The approach presented in the preceding section provides the desired ascent flight performance despite the uncontrolled roll drift. However, it requires on-board computation of $(\theta_1, \theta_{2c}, \theta_{3c})$ to generate modified command quaternion $(\hat{q}_{1c}, \hat{q}_{2c}, \hat{q}_{3c}, \hat{q}_{4c})$.

In this section, we examine the feasibility of achieving pitch/yaw closed-loop stability by simply adjusting the PD control gains without such on-board computation of $(\theta_1, \theta_{2c}, \theta_{3c})$.

We introduce a new derivative gain as

$$\hat{K}_d = \gamma K_d \tag{4.30}$$

where γ is a scale factor to be properly chosen and K_d is the original derivative gain selected for the nominal flight conditions. And a simple PD control laws in the event of uncontrolled roll drift are proposed as

$$\delta_y = -2K_p \text{sgn}(q_{4e})q_{2e} - \hat{K}_d q \tag{4.31a}$$

$$\delta_z = -2K_p \text{sgn}(q_{4e})q_{3e} - \hat{K}_d r \tag{4.31b}$$

As discussed in [16], the term $\text{sgn}(q_{4e})$ is necessary for a quaternion-based feedback control logic for accommodating a short angular path. In particular, such a sign change term is necessary to avoid an undesirable 360 deg flip-over of the CLV. Some detailed analysis of this approach is presented in this section.

From Equation. (4.11), we notice that a larger value of $B = KK_d^2/K_p$ is necessary for stability when q_{4e} is small. The parameter $K = T\ell/I$ is determined by the physical parameters of the rocket. If K_p is decreased, then the overall loop gain of the control system is decreased, which is not desirable. A simple way to increase the parameter B is to increase the derivative gain K_d.

From Equation. (4.10), we have

$$B > \frac{1 - q_{4e}^2}{q_{4e}} \tag{4.32}$$

$$\frac{K\gamma^2 K_d^2}{K_p} > \frac{1 - q_{4e}^2}{q_{4e}} \tag{4.33}$$

or

$$\gamma > \frac{1}{K_d}\sqrt{\frac{(1 - q_{4e}^2)K_p}{q_{4e}K}} \tag{4.34}$$

A root locus plot of case 3 with a new derivative gain $\hat{K}_d = 4K_d$ only in the pitch channel is shown in Figure 4.33.
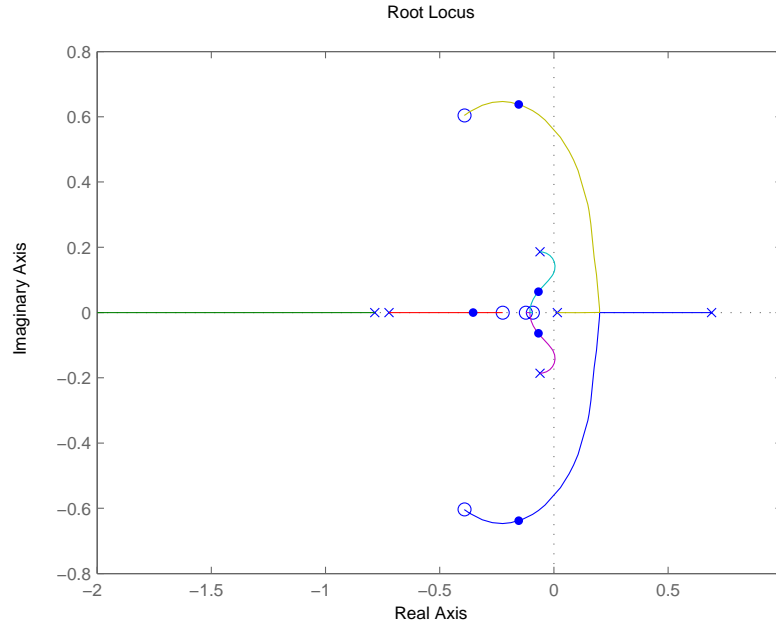
Figure 4.33   Root locus plot for Case 3 but with a new derivative gain with $\gamma = 4$ in the pitch channel.

4.5.1   Rigid Body 6-DOF Nonlinear Simulation Results

The Matlab-based program, employing a complete set of 6-DOF nonlinear models of Ares-I was used to validate the linear stability analysis result. The simulation results are shown in Figure 4.34-Figure 4.37. A dispersed, but stable, ascent trajectory can be seen in Figure 4.37 for the case with a simple gain adjustment but without active roll control.

Note that after changing the control gain, structural filters also need to be adjusted. The design methodology and design tool are mentioned in Chapter 3. A design example is given here. Flexible-body 6-DOF Nonlinear Simulation Results are similar to Figure 4.34- Figure 4.37.
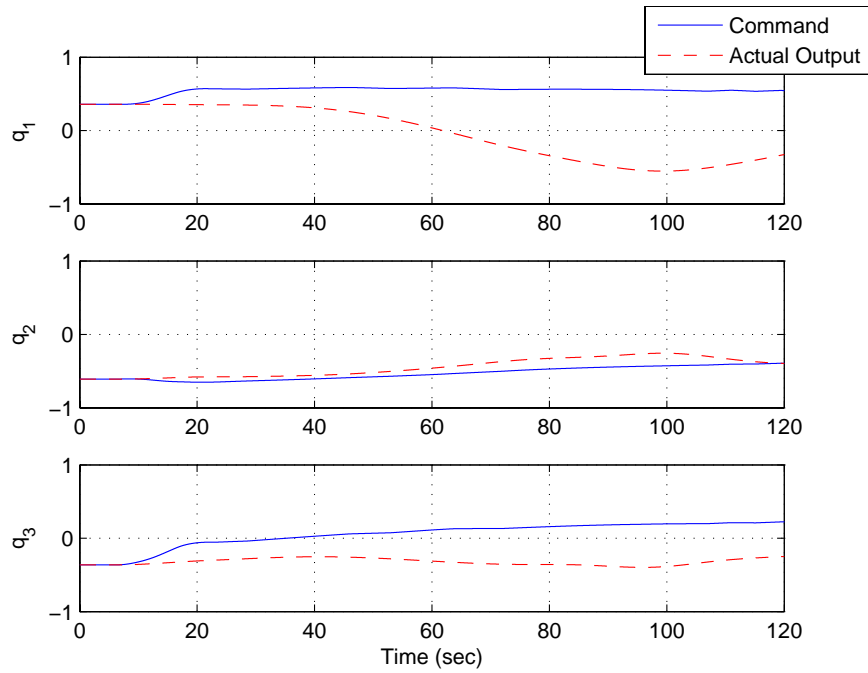
Figure 4.34   Attitude quaternion of 6-DOF nonlinear simulation with $\hat{K}_d = 4K_d$.
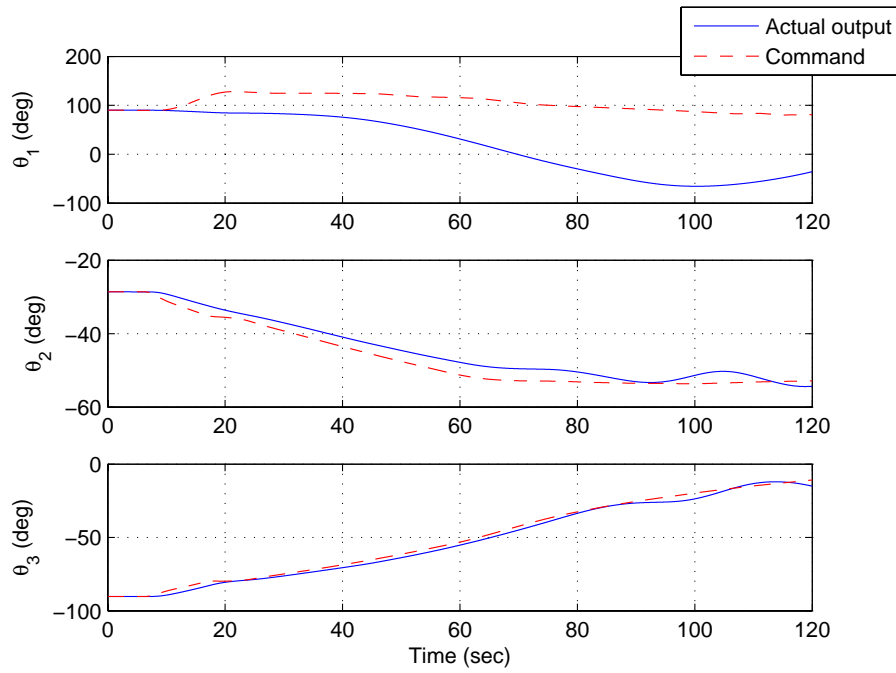
Figure 4.35   Euler angles of 6-DOF nonlinear simulation with $\hat{K}_d = 4K_d$.
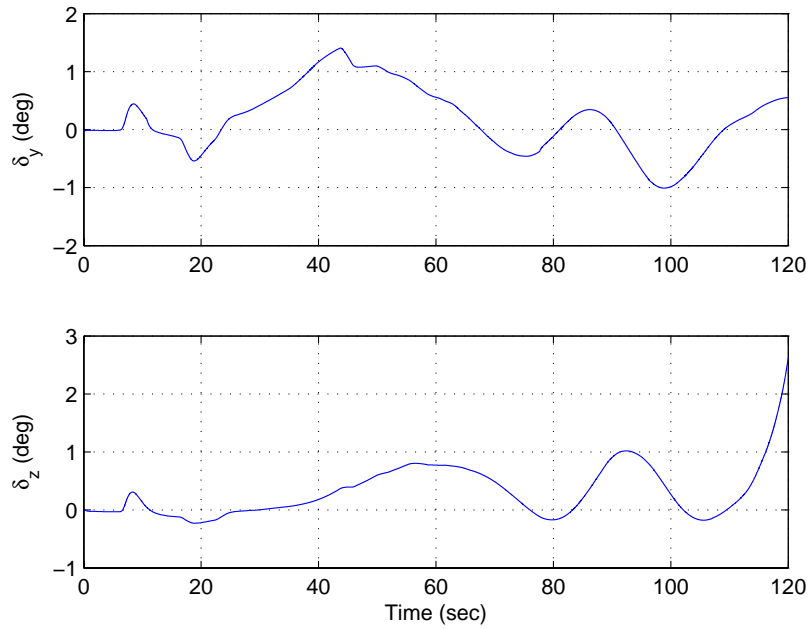
Figure 4.36   Gimbal angles of 6-DOF nonlinear simulation with $\hat{K}_d = 4K_d$.
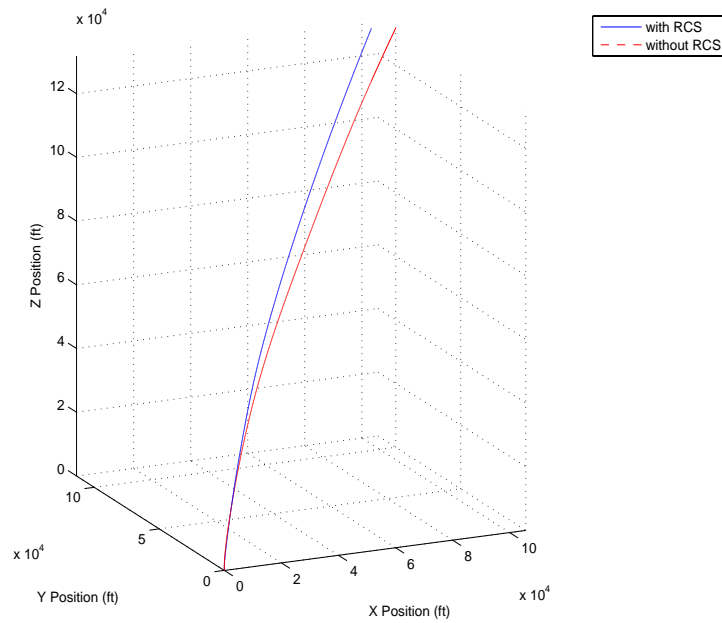
Figure 4.37   Comparison of ascent trajectories.

CHAPTER 5. UNDERACTUATED CONTROL PROBLEM OF AN AXISYMMETRIC RIGID BODY

5.1 Introduction

The problem of ascent flight control in the event of uncontrolled roll drift can be generalized as an underactuated control problem. Specifically, it is the problem of attitude stabilization with less than three independent control torques. System equations for a rigid body rotation can be written as follows:

$$
\begin{pmatrix} \dot{p} \\ \dot{q} \\ \dot{r} \end{pmatrix} = \begin{pmatrix} \frac{I_y - I_z}{I_x} qr \\ \frac{I_z - I_x}{I_y} rp \\ \frac{I_x - I_y}{I_z} pq \end{pmatrix} + \begin{pmatrix} \frac{u_1}{I_x} \\ \frac{u_2}{I_y} \\ \frac{u_3}{I_z} \end{pmatrix}
\tag{5.1}
$$

$$
\begin{pmatrix} \dot{q_1} \\ \dot{q_2} \\ \dot{q_3} \\ \dot{q_4} \end{pmatrix} = \frac{1}{2} \begin{pmatrix} 0 & r & -q & p \\ -r & 0 & p & q \\ q & -p & 0 & r \\ -p & -q & -r & 0 \end{pmatrix} \begin{pmatrix} q_1 \\ q_2 \\ q_3 \\ q_4 \end{pmatrix}
\tag{5.2}
$$

Note that the attitude kinematic differential equation can also be written in terms of Euler angles as follows:

$$
\begin{pmatrix} \dot{\theta}_1 \\ \dot{\theta}_2 \\ \dot{\theta}_3 \end{pmatrix} = \frac{1}{\cos\theta_2} \begin{pmatrix} \cos\theta_2 & \sin\theta_1\sin\theta_2 & \cos\theta_1\sin\theta_2 \\ 0 & \cos\theta_1\cos\theta_2 & -\sin\theta_1\cos\theta_2 \\ 0 & \sin\theta_1 & \cos\theta_1 \end{pmatrix} \begin{pmatrix} p \\ q \\ r \end{pmatrix}
\tag{5.3}
$$

We have the following relationship for the rotational sequence of $\mathbf{C}_1(\theta_1) \leftarrow \mathbf{C}_2(\theta_2) \leftarrow \mathbf{C}_3(\theta_3)$

$$\theta_1 = \text{sgn}\{2(q_2q_3 + q_1q_4)\} \cos^{-1}\left\{\frac{1 - 2(q_1^2 + q_2^2)}{\sqrt{1 - 4(q_1q_3 - q_2q_4)^2}}\right\} \tag{5.4a}$$

$$\theta_2 = \sin^{-1}\{-2(q_1q_3 - q_2q_4)\} \tag{5.4b}$$

$$\theta_3 = \text{sgn}\{2(q_1q_2 + q_3q_4)\} \cos^{-1}\left\{\frac{1 - 2(q_2^2 + q_3^2)}{\sqrt{1 - 4(q_1q_3 - q_2q_4)^2}}\right\} \tag{5.4c}$$

The underactuated control problem has been dealt with [23, 24, 25, 26, 27]. Necessary and sufficient conditions for controllability of the systems (Equation. (5.1) and Equation. (5.2)) in the case that the gas jet actuators yield one, two, or three independent torques are given in [23]. Particularly, the problem of attitude stabilization of an axisymmetric ($I_y = I_z$) spacecraft using two pairs of gas jet actuators is considered in [25, 26]. A new kinematic formulation is used to derive the feedback control law.

Without loss of generality, we consider the commanded quaternion to be $(0, 0, 0, 1)$. Then the attitude quaternion (q_1, q_2, q_3, q_4) becomes the attitude error quaternion $(q_{1e}, q_{2e}, q_{3e}, q_{4e})$. Therefore

$$u_2 = -K_{py}q_2 - K_{dy}q \tag{5.5a}$$

$$u_3 = -K_{pz}q_3 - K_{dz}r \tag{5.5b}$$

Since the rigid body is assumed to be axisymmetric ($I_y = I_z$), we have $K_{py} = K_{pz} = K_p$ and $K_{dy} = K_{dz} = K_d$.

Based on the analysis of Ares-I ascent flight control system in chapters 3 and 4, a modified attitude quaternion feedback control law is derived in the next section. It can stabilize an axisymmetric rigid body to the subsystem M (Equation. (4.20)). Moreover, a new kinematic formulation is not needed.

5.2 Steady-State Oscillations

The equations of motion of an axisymmetric rigid body with a PD-type attitude quaternion feedback control law can be expressed as

$$
\begin{pmatrix} \dot{q} \\ \dot{r} \\ \dot{q}_1 \\ \dot{q}_2 \\ \dot{q}_3 \\ \dot{q}_4 \end{pmatrix} = \begin{pmatrix} arp - \hat{K}_p q_2 - \hat{K}_d q \\ -apq - \hat{K}_p q_3 - \hat{K}_d r \\ \frac{r}{2}q_2 - \frac{q}{2}q_3 + \frac{p}{2}q_4 \\ -\frac{r}{2}q_1 + \frac{p}{2}q_3 + \frac{q}{2}q_4 \\ \frac{q}{2}q_1 - \frac{p}{2}q_2 + \frac{r}{2}q_4 \\ -\frac{p}{2}q_1 - \frac{q}{2}q_2 - \frac{r}{2}q_3 \end{pmatrix} \tag{5.6}
$$

where $a = \frac{I-I_x}{I}$, $I = I_y = I_z$, $\hat{K}_p = K_p/I$ and $\hat{K}_d = K_d/I$.

For this autonomous system $\dot{\mathbf{x}} = f(\mathbf{x})$, where $\mathbf{x} = (q,\ r,\ q_1,\ q_2,\ q_3,\ q_4)^T$, there is one steady-state oscillation which has the form

$$
M_1 = \{(q,\ r,\ q_1,\ q_2,\ q_3\ q_4):\ q = r = 0,\ q_2 = q_3 = 0\} \tag{5.7}
$$

$$
\begin{pmatrix} \dot{q}_1 \\ \dot{q}_4 \end{pmatrix} = \begin{pmatrix} \frac{p}{2}q_4 \\ -\frac{p}{2}q_1 \end{pmatrix} \tag{5.8}
$$

In this oscillation, the rigid body is rotating around its symmetry axis with the angular velocity p. At the same time, the symmetry axis has the orientation by quaternion $(q_1,\ 0,\ 0,\ q_4)$, or by Euler angles $(\theta_1,\ 0,\ 0)$. Note that it presents the orientation we want to achieve by a feedback control law when there are only two independent control inputs u_2 and u_3.

The autonomous system Equation. (5.6) may have another steady-state oscillation, when p is not zero. It has the form

$$
M_2 = \{(q,\ r,\ q_1,\ q_2,\ q_3\ q_4):\ q_1 = c_1,\ q_4 = c_4\} \tag{5.9}
$$

$$
\begin{pmatrix} \dot{q} \\ \dot{r} \end{pmatrix} = \begin{pmatrix} 0 & \omega \\ -\omega & 0 \end{pmatrix} \begin{pmatrix} q \\ r \end{pmatrix} \tag{5.10}
$$

$$
\begin{pmatrix} \dot{q}_2 \\ \dot{q}_3 \end{pmatrix} = \begin{pmatrix} 0 & \omega \\ -\omega & 0 \end{pmatrix} \begin{pmatrix} q_2 \\ q_3 \end{pmatrix} \tag{5.11}
$$

$$\begin{pmatrix} q \\ r \end{pmatrix} = \tau \begin{pmatrix} \cos\theta & \sin\theta \\ -\sin\theta & \cos\theta \end{pmatrix} \begin{pmatrix} q_2 \\ q_3 \end{pmatrix} \tag{5.12}$$

where c_1, c_4, ω, τ and θ are constants as follows:

$$c_1 = \frac{\hat{K}_d(q^2 + r^2)}{\hat{K}_p p} \tag{5.13a}$$

$$c_4 = \frac{[(2a-1)p^2 - q^2 - r^2](q^2 + r^2)}{2\hat{K}_p p^2} \tag{5.13b}$$

$$\omega = \frac{p^2 + q^2 + r^2}{2p} \tag{5.13c}$$

$$\tau = \frac{-\hat{K}_p}{\sqrt{(\frac{(2a-1)p^2 - (q^2+r^2)}{2p})^2 + (\hat{K}_d)^2}} \tag{5.13d}$$

$$\theta = \tan^{-1} \frac{(2a-1)p^2 - q^2 - r^2}{2p\hat{K}_d} \tag{5.13e}$$

The magnitude of vectors $(q_2, \ q_3)^T$ and $(q, \ r)^T$ are $\sqrt{q_2^2 + q_3^2} = R$ and $\sqrt{q^2 + r^2} = \hat{R}$, respectively, where $\hat{R} = |\tau|R$. Note that $\hat{R}$ is a positive real zero of a 4th-order polynomial

$$f(x) = x^4 + (3-4a)p^2 x^3 + [(2a-1)(2a-3)p^2 + 4\hat{K}_d^2]p^2 x^2 + [(2a-1)^2 p^2 + 4\hat{K}_d^2]p^4 x - 4p^4\hat{K}_p^2 \tag{5.14}$$

Since $f(0) = -4p^4\hat{K}_p^2$, $f(x) \to \infty$ as $x \to \infty$ and $f(x)$ is continuous in x, $f(x)$ has at least one positive real zero. Thus M_2 always exists when p is not zero. The derivation of the steady-state oscillation M_2 can be found in Appendix F.

A numerical example of those oscillations is provided below, using data for Ares-I CLV at $t = 60$ sec (see Table 5.1). The constants in Equation. (5.13) are listed in Table 5.2 with $p = 0.005$ rad/sec ≈ 0.2865 deg/sec.

Table 5.1   Ares-I reference parameters at $t = 60$ sec

Parameters	Values	Unit
a	0.9958	
p	0.005	rad/s
$\hat{K}_p$	1.5441	s^{-2}
$\hat{K}_d$	0.8607	s^{-1}

The steady-state oscillations M_1 and M_2 can be visualized in Figures 5.1 and 5.2. M_2 is illustrated from Figure 5.1 to 5.9.

Table 5.2   Parameters of steady-state oscillation M_2

Parameters	Values	Unit
c_1	0.7768	rad
c_4	0.6242	rad
ω	0.6994	rad/s
τ	-1.3963	s^{-1}
θ	-36.90	deg
R	0.05979	rad
$\hat{R}$	0.08348	rad/s
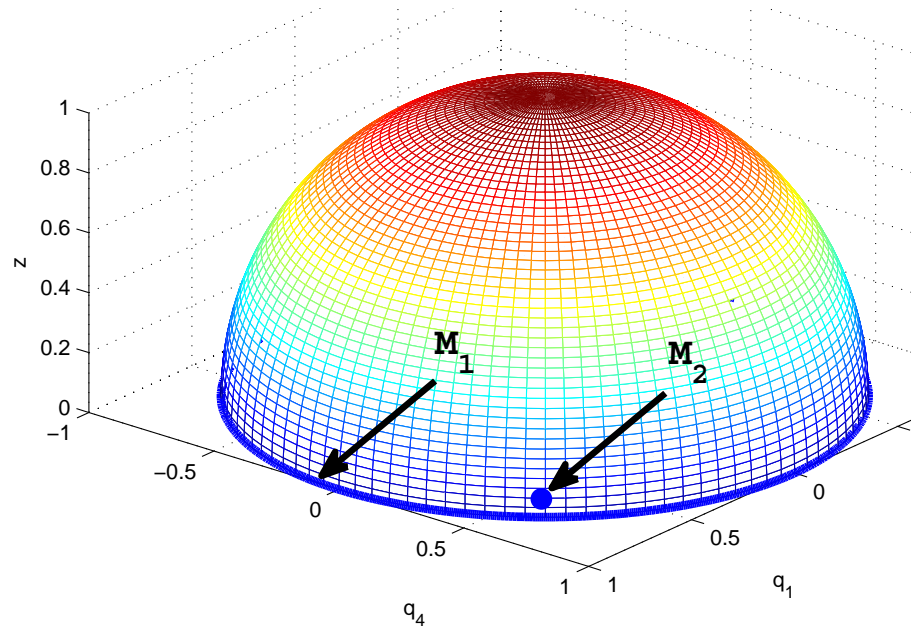
Figure 5.1   Steady-state oscillations M_1 and M_2 on the spherical surface $q_1^2 + q_4^2 + z^2 = 1$.
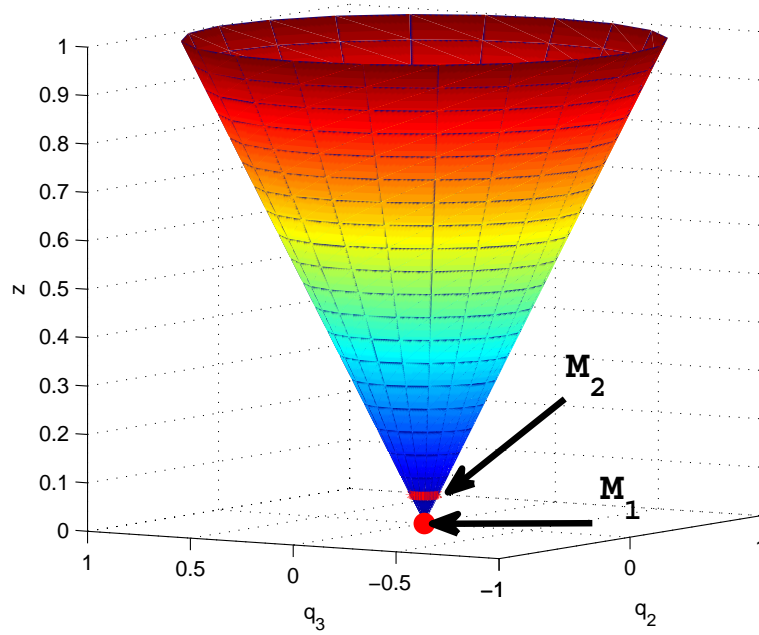
Figure 5.2 Steady-state oscillations M_1 and M_2 on the surface of cone $z = \sqrt{q_2^2 + q_3^2}$.
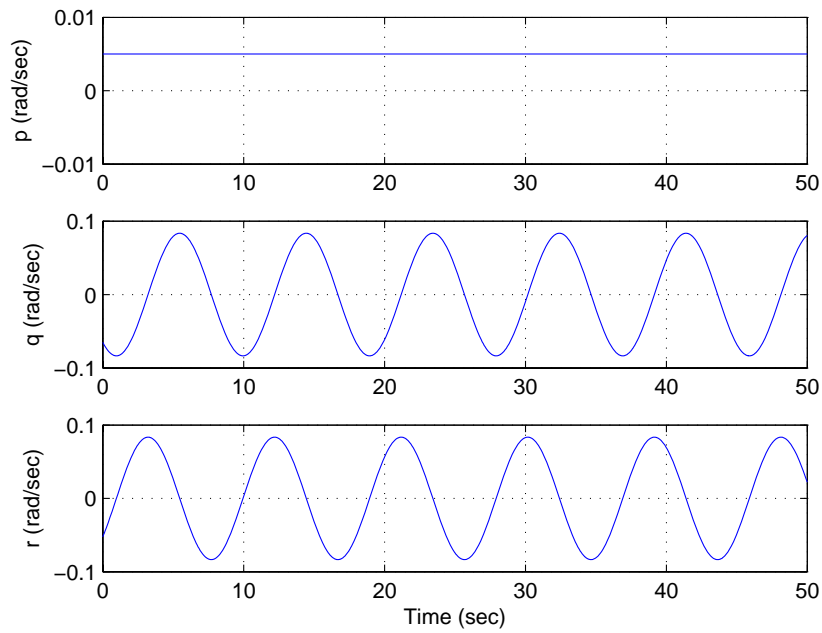
Figure 5.3 Angular velocity of steady-state oscillation M_2.
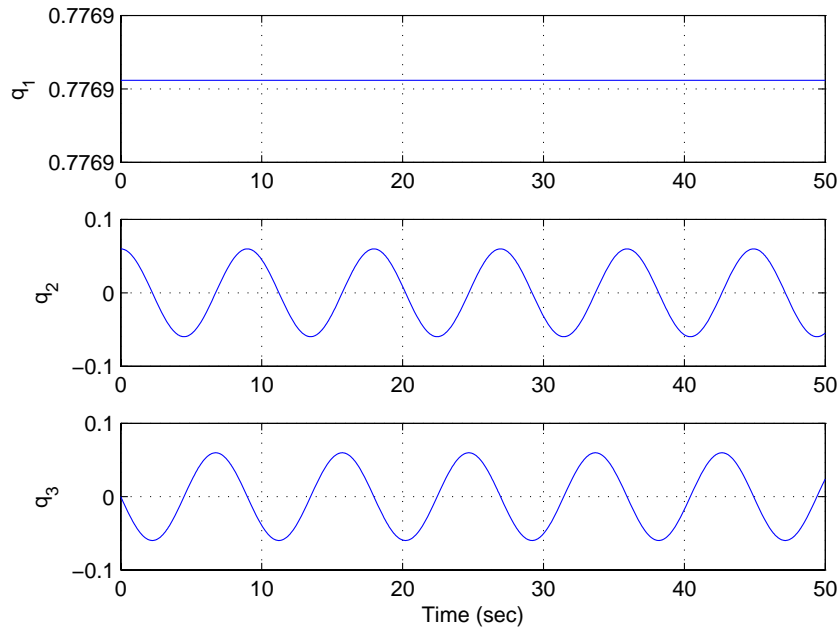
Figure 5.4   Attitude quaternion of steady-state oscillation M_2.
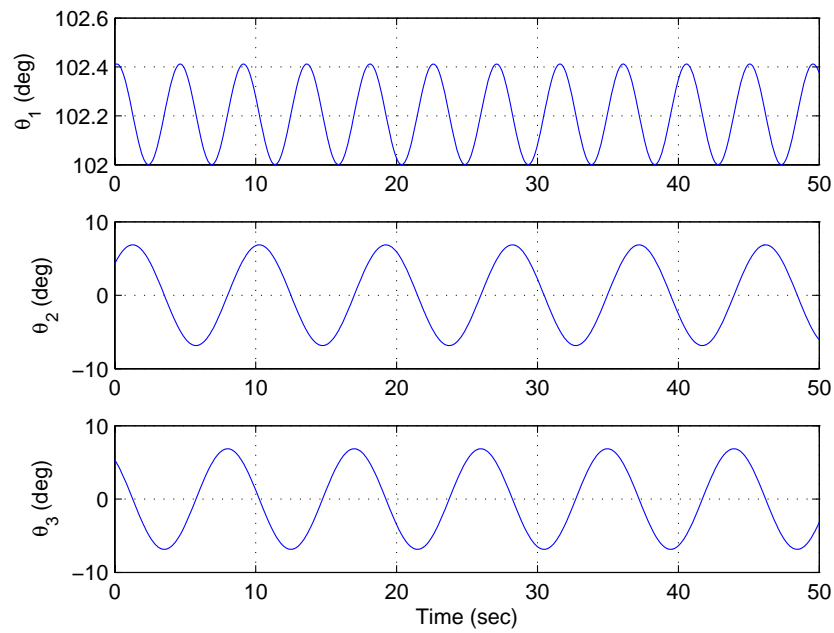
Figure 5.5   Euler angles of steady-state oscillation M_2.
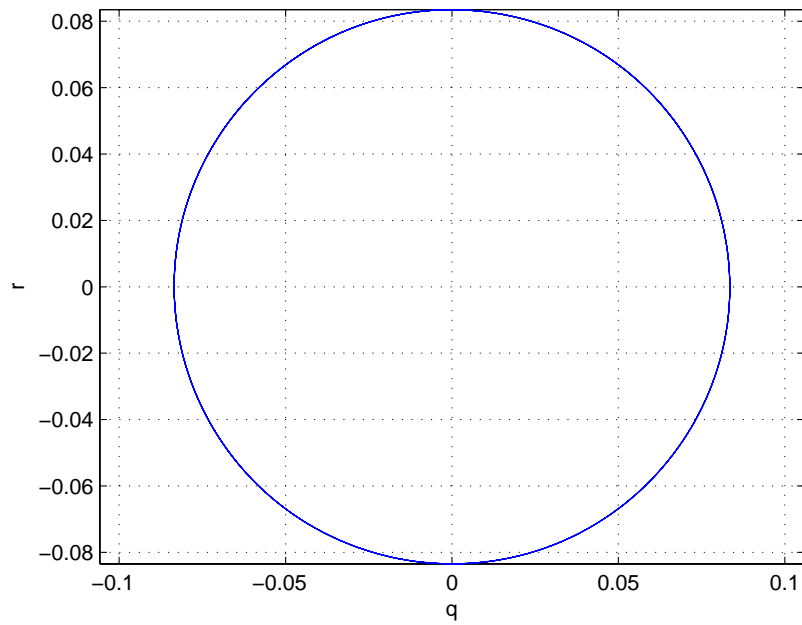
Figure 5.6　Phase portrait of q and r of steady-state oscillation M_2.
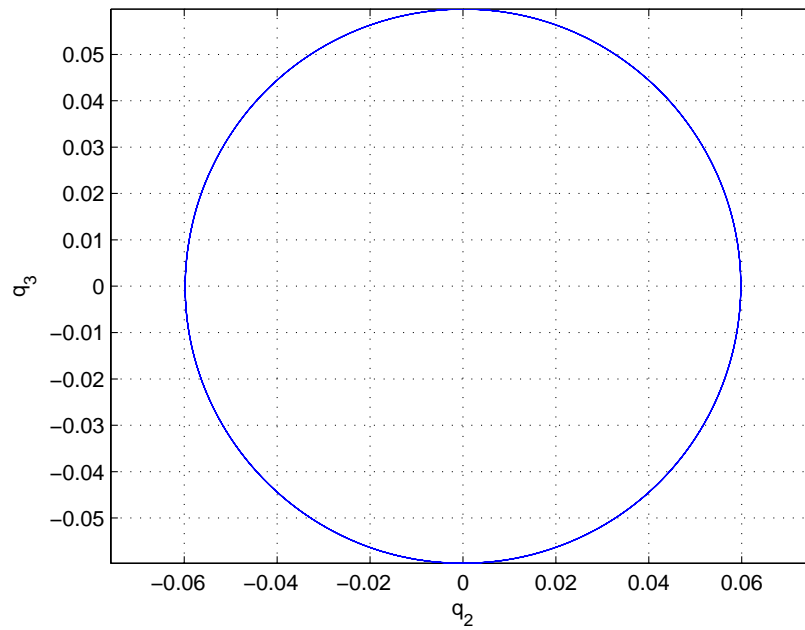
Figure 5.7　Phase portrait of q_2 and q_3 of steady-state oscillation M_2.
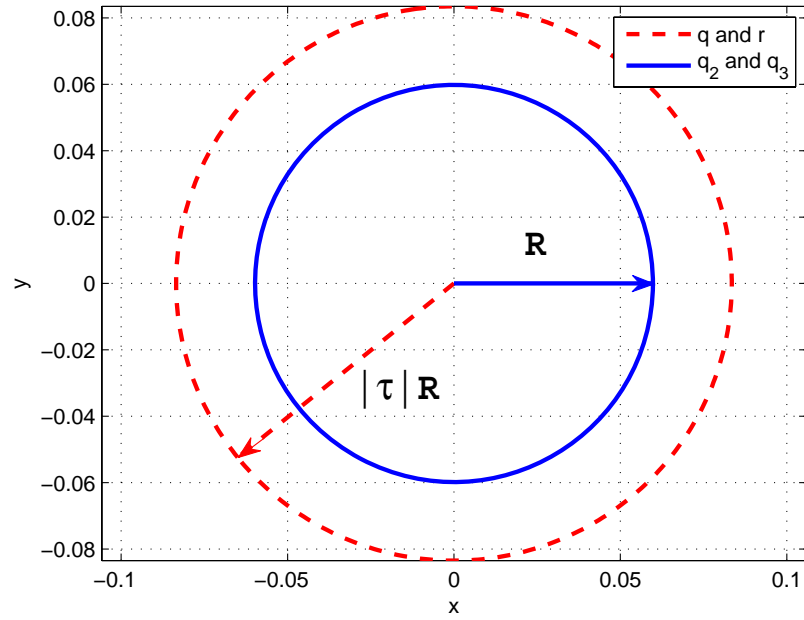
Figure 5.8   The relation between vectors $(q,\ r)^T$ and $(q_2,\ q_3)^T$ of steady-state oscillation M_2.
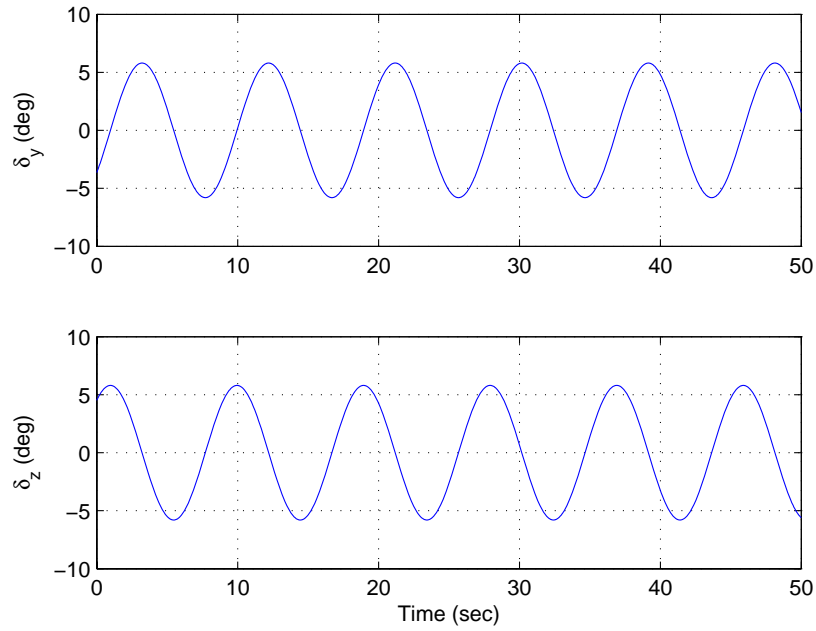
Figure 5.9   Gimbal angles of steady-state oscillation M_2.

5.3   Modified Attitude Quaternion Feedback Control Law

In the last section, it was shown that there are at least two steady-state oscillations of the autonomous system Equation. (5.6). Thus the original attitude quaternion feedback law can not always drive Equations. (5.1) and (5.2) to M_1. A new feedback control law is needed. Define a new state variable λ, such that $\dot{\lambda} = p$. A modified attitude quaternion feedback control law has the form

$$u_2 = -K_p[\cos(\lambda/2)q_2 + \sin(\lambda/2)q_3] - K_d q \tag{5.15a}$$

$$u_3 = -K_p[-\sin(\lambda/2)q_2 + \cos(\lambda/2)q_3] - K_d r \tag{5.15b}$$

where K_p and K_d are control gains designed to stabilize a rigid body by attitude quaternion feedback law [16]. λ is used to catch the angular velocity p.

We may obtain a new autonomous system, $\dot{\mathbf{x}} = f(\mathbf{x})$ as follows:

$$\begin{pmatrix} \dot{q} \\ \dot{r} \\ \dot{q}_1 \\ \dot{q}_2 \\ \dot{q}_3 \\ \dot{q}_4 \\ \dot{\lambda} \end{pmatrix} = \begin{pmatrix} arp - \hat{K}_p[\cos(\lambda/2)q_2 + \sin(\lambda/2)q_3] - \hat{K}_d q \\ -apq - \hat{K}_p[-\sin(\lambda/2)q_2 + \cos(\lambda/2)q_3] - \hat{K}_d r \\ \frac{r}{2}q_2 - \frac{q}{2}q_3 + \frac{p}{2}q_4 \\ -\frac{r}{2}q_1 + \frac{p}{2}q_3 + \frac{q}{2}q_4 \\ \frac{q}{2}q_1 - \frac{p}{2}q_2 + \frac{r}{2}q_4 \\ -\frac{p}{2}q_1 - \frac{q}{2}q_2 - \frac{r}{2}q_3 \\ p \end{pmatrix} \tag{5.16}$$

where $I = I_y = I_z$, $a = \frac{I - I_x}{I}$, $\lambda(0) = \theta_1$, $\hat{K}_p = K_p/I$ and $\hat{K}_d = K_d/I$.

5.4   Nonlinear Stability Analysis

A Lyapunov function candidate can be taken as the energy-like function

$$V(\mathbf{x}) = \frac{1}{2\hat{K}_p}q^2 + \frac{1}{2\hat{K}_p}r^2 + [q_1 - \sin(\lambda/2)]^2 + q_2^2 + q_3^2 + [q_4 - \cos(\lambda/2)]^2 \tag{5.17}$$

and $V(\mathbf{x}) = 0$ when $\mathbf{x} = (0,\ 0,\ \sin(\lambda/2),\ 0,\ 0,\ \cos(\lambda/2))^T$, otherwise $V(\mathbf{x}) > 0$.

The derivative of $V(\mathbf{x})$ can be found as

$$\dot{V}(\mathbf{x}) = -\frac{\hat{K}_d}{\hat{K}_p}(q^2 + r^2) + [q_1\cos(\lambda/2) - q_4\sin(\lambda/2)](p - \dot{\lambda}) \tag{5.18}$$

Since $\dot{\lambda} = p$, we have

$$\dot{V}(\mathbf{x}) = -\frac{K_d}{K_p}(q^2 + r^2) \leq 0 \qquad (5.19)$$

which is negative semidefinite. Detailed derivation can be found in Appendix G.

The set M_1 is a positive invariant set, since

$$\mathbf{x}(0) \in M_1 \Rightarrow \mathbf{x}(t) \in M_1, \forall t \geq 0 \qquad (5.20)$$

By LaSalle's theorem (Invariance Principle) [52], all trajectories approach M_1 as $t \to \infty$. In addition, we have

$$V(\mathbf{x}) \to \infty \ \ \text{as} \ \ \|\mathbf{x}\| \to \infty \qquad (5.21)$$

The Lyapunov function $V(\mathbf{x})$ is radially unbounded. Thus the modified quaternion feedback control law Equation. (5.15) can reorient the symmetry axis to the desired direction from an arbitrary initial orientation. Moreover, the new control law has no restriction on the spinning rate p, which could be an arbitrary value. Even if p keeps changing due to some disturbance torque, the new control law still works.

5.5 Simulation Results

Two simulation cases are performed to compare the effect of original and modified quaternion feedback laws. Assuming that the initial spinning rate is $p = 0.005$ rad/sec.

Table 5.3 Simulation cases with $p = 0.005$ rad/sec

Case numbers	Initial values $(q,\ r,\ q_1,\ q_2,\ q_3,\ q_4)$	Control law
1	$(0,\ 0,\ 0.7769,\ 0.0598,\ 0,\ 0.6268,)$	Original attitude quaternion feedback
2	$(0,\ 0,\ 0.7769,\ 0.0598,\ 0,\ 0.6268,)$	Modified attitude quaternion feedback

The effect of M_2 can be seen from Figure. 5.10 to Figure. 5.18. The trajectory converges to M_2 in a oscillation behavior. Furthermore, the modified quaternion feedback control law eliminates this effect. The trajectory is driven to M_1, which represents the commanded orientation of the axis of symmetry.
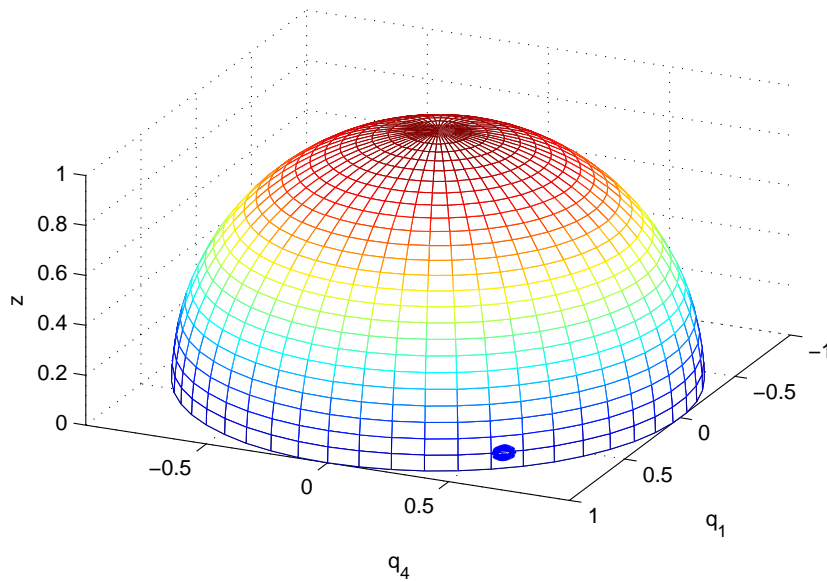
Figure 5.10   Trajectory on the spherical surface $q_1^2 + q_4^2 + z^2 = 1$ for Case 1.

Start Point
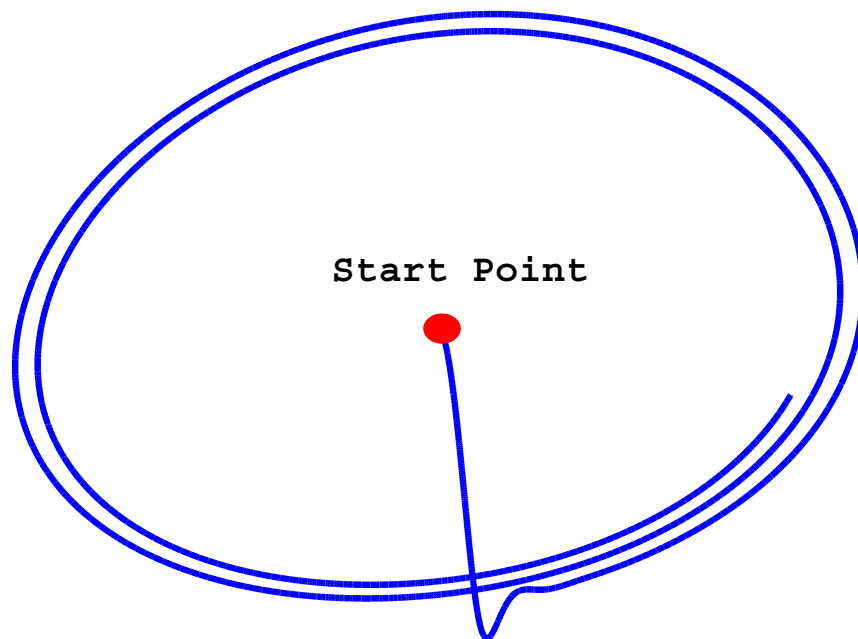
Figure 5.11   Detailed trajectory on the spherical surface $q_1^2 + q_4^2 + z^2 = 1$ for Case 1.
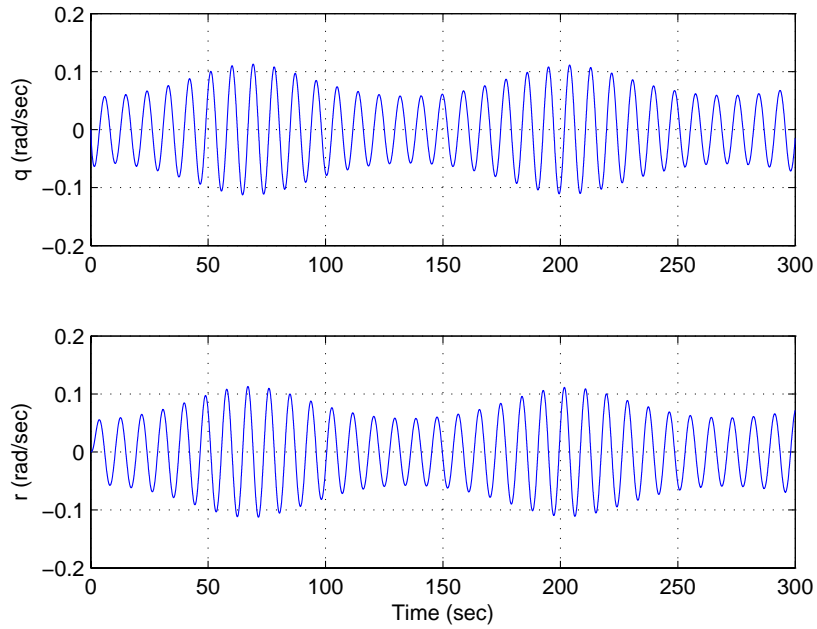
Figure 5.12   Angular velocity components q and r for Case 1.
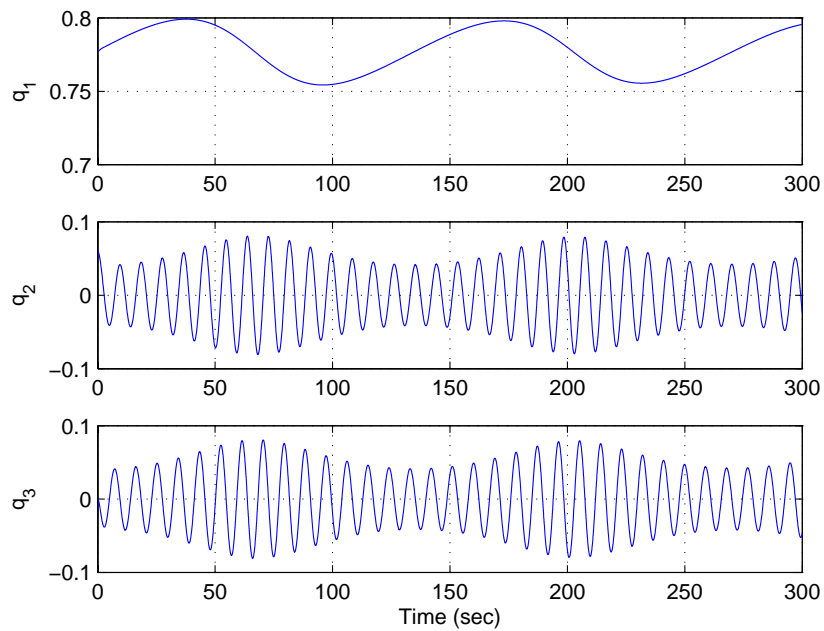
Figure 5.13   Quaternion q_1, q_2 and q_3 for Case 1.
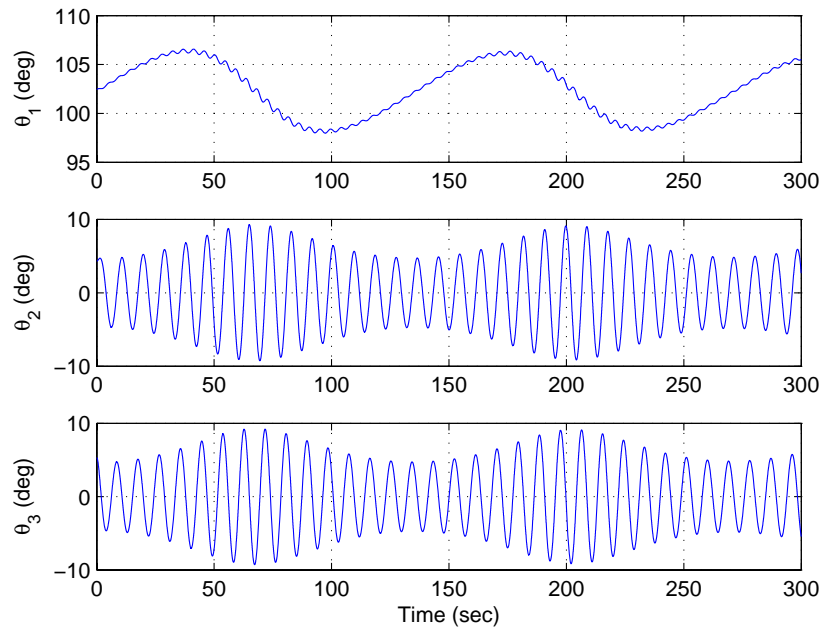
Figure 5.14 Euler angles for Case 1.
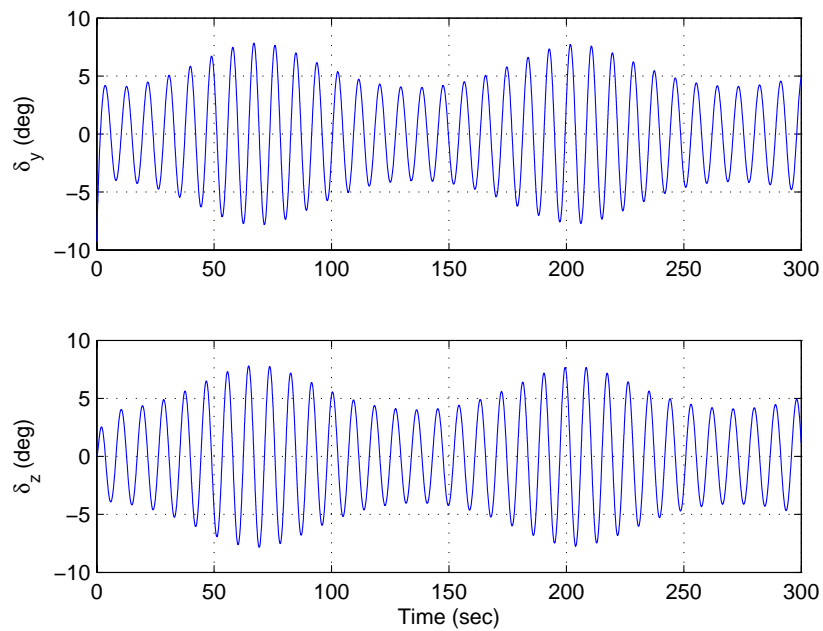
Figure 5.15 Gimbal angles for Case 1.
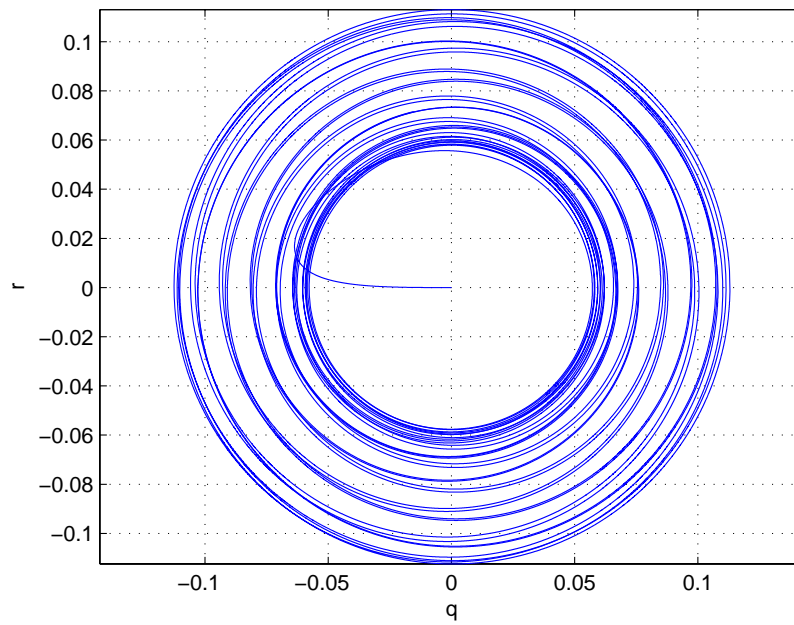
Figure 5.16   Phase portrait of q and r for Case 1.
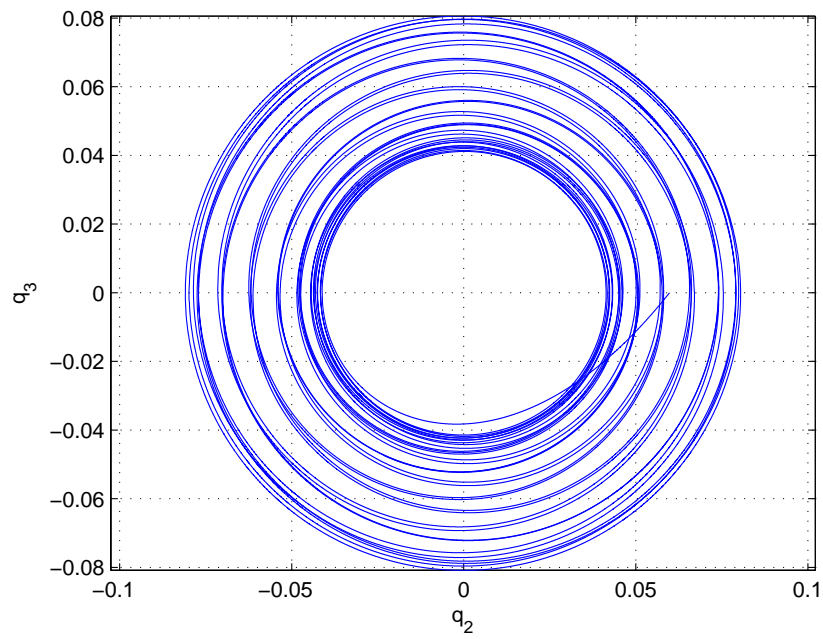
Figure 5.17   Phase portrait of q_2 and q_3 for Case 1.
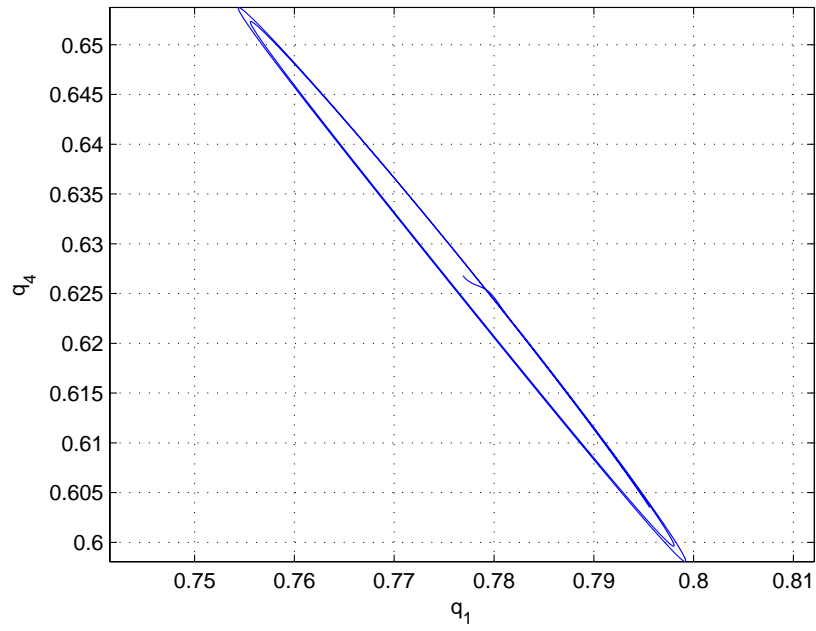
Figure 5.18   Phase portrait of q_1 and q_4 for Case 1.
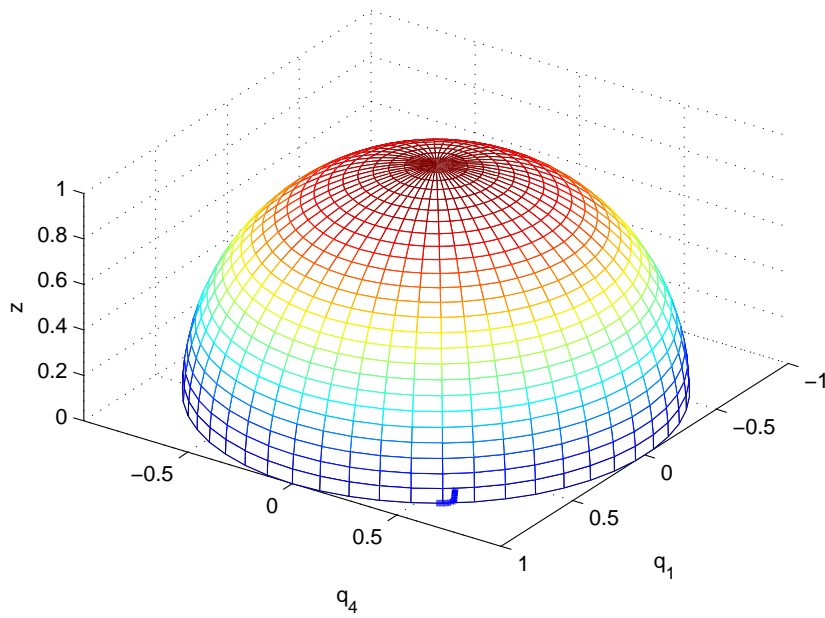
Figure 5.19   Trajectory on the spherical surface $q_1^2 + q_4^2 + z^2 = 1$ for Case 2.
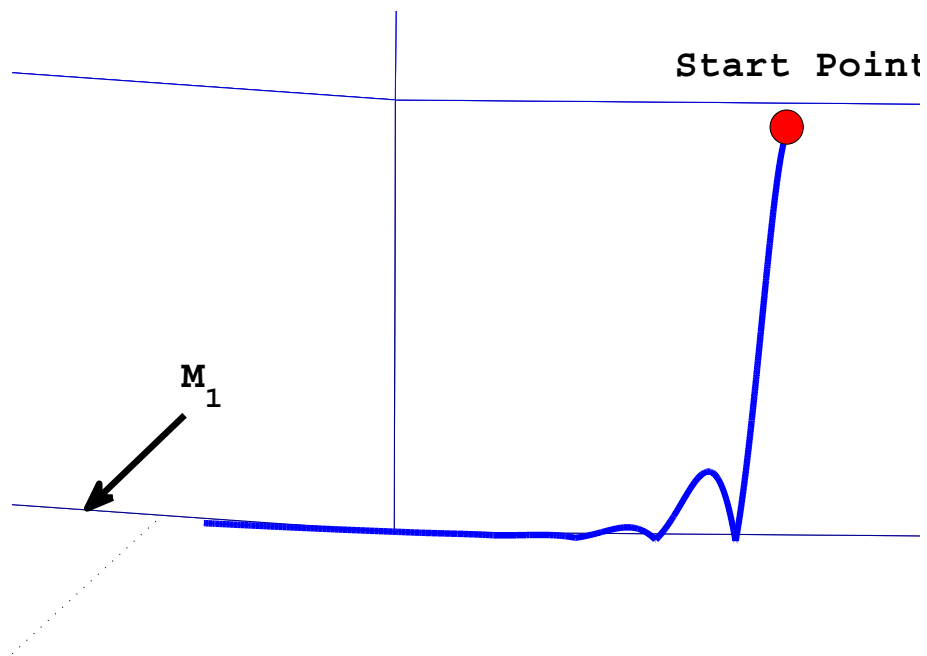
Figure 5.20   Detailed trajectory on the spherical surface $q_1^2 + q_4^2 + z^2 = 1$
for Case 2.
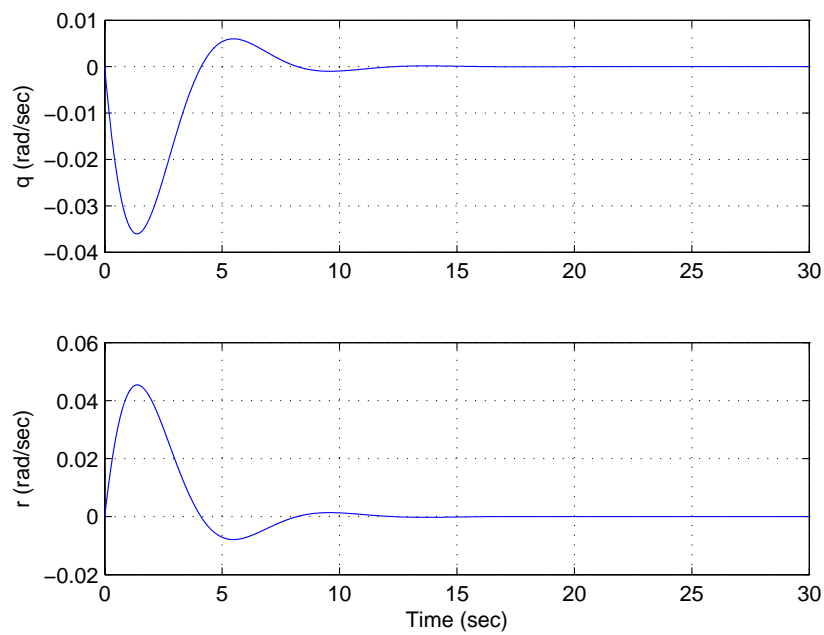
Figure 5.21   Angular velocity components q and r for Case 2.
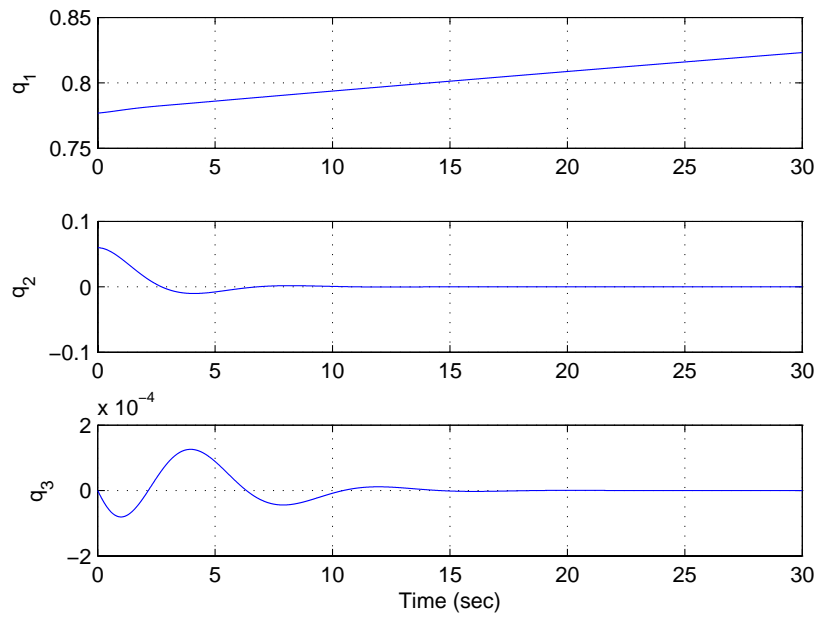
Figure 5.22 Quaternion q_1, q_2 and q_3 for Case 2.
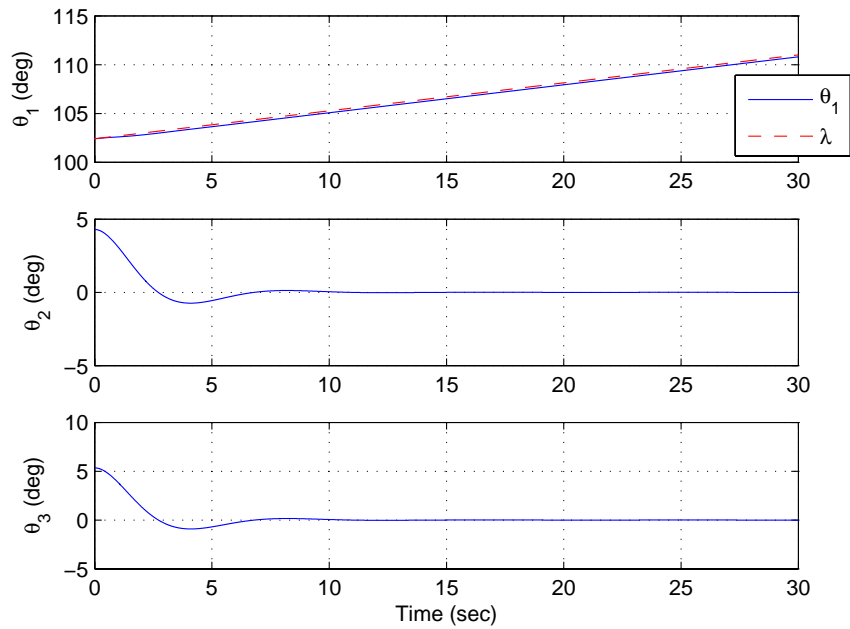
Figure 5.23 Euler angles for Case 2.
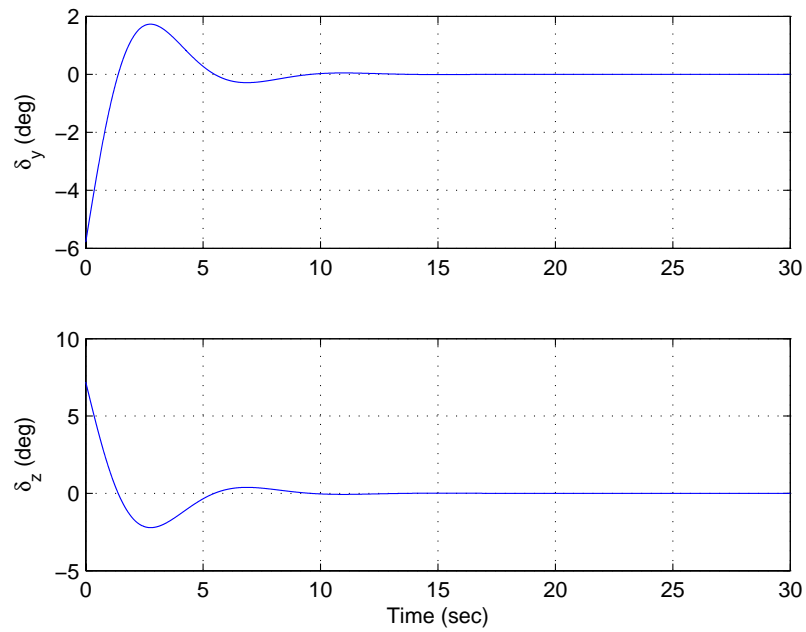
Figure 5.24   Gimbal angles for Case 2.

5.6 A Special Case

When $p = 0$, $\lambda = \theta_1(0)$ is a constant. The modified attitude quaternion feedback control law is equivalent to a quaternion command adjustment.

For a typical attitude quaternion feedback law, we have

$$\begin{pmatrix} q_{1e} \\ q_{2e} \\ q_{3e} \\ q_{4e} \end{pmatrix} = \begin{pmatrix} q_{4c} & q_{3c} & -q_{2c} & -q_{1c} \\ -q_{3c} & q_{4c} & q_{1c} & -q_{2c} \\ q_{2c} & -q_{1c} & q_{4c} & -q_{3c} \\ q_{1c} & q_{2c} & q_{3c} & q_{4c} \end{pmatrix} \begin{pmatrix} q_1 \\ q_2 \\ q_3 \\ q_4 \end{pmatrix} \tag{5.22}$$

The command Euler angles are $(\theta_{1c}, \theta_{2c}, \theta_{3c}) = (\theta_1, 0, 0)$, where

$$q_{1c} = \sin(\theta_{1c}/2)\cos(\theta_{2c}/2)\cos(\theta_{3c}/2) - \cos(\theta_{1c}/2)\sin(\theta_{2c}/2)\sin(\theta_{3c}/2)$$
$$q_{2c} = \cos(\theta_{1c}/2)\sin(\theta_2 c/2)\cos(\theta_{3c}/2) + \sin(\theta_{1c}/2)\cos(\theta_{2c}/2)\sin(\theta_{3c}/2)$$
$$q_{3c} = \cos(\theta_{1c}/2)\cos(\theta_{2c}/2)\sin(\theta_{3c}/2) - \sin(\theta_{1c}/2)\sin(\theta_{2c}/2)\cos(\theta_{3c}/2)$$
$$q_{4c} = \cos(\theta_{1c}/2)\cos(\theta_{2c}/2)\cos(\theta_{3c}/2) + \sin(\theta_{1c}/2)\sin(\theta_{2c}/2)\sin(\theta_{3c}/2)$$
$$\tag{5.23}$$

The new command quaternion is

$$q_{1c} = \sin(\theta_1/2)$$
$$q_{2c} = 0$$
$$q_{3c} = 0$$
$$q_{4c} = \cos(\theta_1/2)$$
$$\tag{5.24}$$

The attitude-error quaternion becomes

$$\begin{pmatrix} q_{1e} \\ q_{2e} \\ q_{3e} \\ q_{4e} \end{pmatrix} = \begin{pmatrix} \cos(\theta_1/2) & 0 & 0 & -\sin(\theta_1/2) \\ 0 & \cos(\theta_1/2) & \sin(\theta_1/2) & 0 \\ 0 & -\sin(\theta_1/2) & \cos(\theta_1/2) & 0 \\ \sin(\theta_1/2) & 0 & 0 & \cos(\theta_1/2) \end{pmatrix} \begin{pmatrix} q_1 \\ q_2 \\ q_3 \\ q_4 \end{pmatrix} \tag{5.25}$$

By the attitude quaternion feedback law, we have

$$u_2 = -K_p q_{2e} - K_d q = -K_p[\cos(\theta_1/2)q_2 + \sin(\theta_1/2)q_3] - K_d q \tag{5.26a}$$

$$u_3 = -K_p q_{3e} - K_d r = -K_p[-\sin(\theta_1/2)q_2 + \cos(\theta_1/2)q_3] - K_d r \tag{5.26b}$$

109

The quaternion command adjustment is a special case of the modified attitude quaternion feedback control law, when $p = 0$.

$$
\begin{aligned}
q_{1e} &= -\sin(\theta_2/2)\sin(\theta_3/2) \\
q_{2e} &= \cos(\theta_1)\sin(\theta_2/2)\cos(\theta_3/2) + \sin(\theta_1)\cos(\theta_2/2)\sin(\theta_3/2) \\
q_{3e} &= \cos(\theta_1)\cos(\theta_2/2)\sin(\theta_3/2) - \sin(\theta_1)\sin(\theta_2/2)\cos(\theta_3/2) \\
q_{4e} &= \cos(\theta_2/2)\cos(\theta_3/2)
\end{aligned}
\tag{5.27}
$$

When $\theta_2 \approx 0$, $\theta_3 \approx 0$, we have

$$
\begin{aligned}
q_{1e} &\approx 0 \\
q_{2e} &\approx \cos(\theta_1)\theta_2/2 + \sin(\theta_1)\theta_3/2 \\
q_{3e} &\approx -\sin(\theta_1)\theta_2/2 + \cos(\theta_1)\theta_3/2 \\
q_{4e} &\approx 1
\end{aligned}
\tag{5.28}
$$

CHAPTER 6.   CONCLUSIONS

A set of dynamic models of the Ares-I Crew Launch Vehicle, incorporating its propulsion, aerodynamics, guidance and control, and structural flexibility, has been described in this dissertation. The results of developing a Matlab-based simulation and linearization program by utilizing NASA's SAVANT Simulink-based program have been discussed. The purpose of the study was to develop an independent validation tool for the performance and stability analysis of the ascent flight control system of the Ares-I. A linearized model of the Ares-I was obtained as a test case of an independent validation of the ascent flight control design and analysis of the Ares-I.

The fundamental principles of flight control analysis and design for flexible launch vehicles have also been examined. In particular, the classical "drift-minimum" and "load-minimum" control principles were re-examined, and the performance and stability of launch vehicle ascent flight control with an additional feedback of angle-of-attack was demonstrated. For a typical "non-collocated actuator and sensor" control problem of large flexible launch vehicles, non-minimum-phase filtering of "unstably interacting" bending modes was shown to be effective and robust.

Two distinct approaches to the ascent flight control of Ares-I in the event of uncontrolled roll drift have been investigated. The first approach exploits the inherent versatility of a quaternion-based attitude control system, and it only requires the desired inertial attitude quaternion to be re-computed using the actual uncontrolled roll angle information. This approach achieved an ascent flight trajectory identical as the nominal flight case with active roll control. The second approach only requires a simple adjustment of the proportional-derivative gains of the quaternion-based flight control system. The first approach is recommended for the Ares-I as

well as other launch vehicles in the event of no active roll control.

Finally, an undesired steady-state oscillation is found when the spinning rate is a constant. Inspired by the method derived to stabilize a large flexible launch vehicle in the event of uncontrolled roll drift, a modified attitude quaternion feedback law is presented in this dissertation. It is used to stabilize an axisymmetric rigid body by two independent control torques. By Lyapunov's stability analysis, it is proved that the new control law can achieve an arbitrary orientation of the symmetry axis with arbitrary spinning rate.

APPENDIX A.   A SUMMARY OF THE 6-DOF EQUATIONS OF MOTION

Total force expressed in the body frame:

$$
\begin{pmatrix} F_{total.xb} \\ F_{total.yb} \\ F_{total.zb} \end{pmatrix} = \begin{pmatrix} F_{aero.xb} \\ F_{aero.yb} \\ F_{aero.zb} \end{pmatrix} + \begin{pmatrix} F_{rkt.xb} \\ F_{rkt.yb} \\ F_{rkt.zb} \end{pmatrix} + \begin{pmatrix} F_{rcs.xb} \\ F_{rcs.yb} \\ F_{rcs.zb} \end{pmatrix}
\tag{A.1}
$$

Total force expressed in the inertial frame:

$$
\begin{pmatrix} F_{total.xi} \\ F_{total.yi} \\ F_{total.zi} \end{pmatrix} = \boldsymbol{C}^{I/B} \begin{pmatrix} F_{total.xb} \\ F_{total.yb} \\ F_{total.zb} \end{pmatrix}
\tag{A.2}
$$

Translational equation in the inertial frame:

$$
\begin{pmatrix} \ddot{x} \\ \ddot{y} \\ \ddot{z} \end{pmatrix} = \frac{1}{m} \begin{pmatrix} F_{total.xi} \\ F_{total.yi} \\ F_{total.zi} \end{pmatrix} + \begin{pmatrix} g_x \\ g_y \\ g_z \end{pmatrix}
\tag{A.3}
$$

Rotational equation in the body frame:

$$
\begin{pmatrix} I_{xx} & I_{xy} & I_{xz} \\ I_{xy} & I_{yy} & I_{yz} \\ I_{xz} & I_{yz} & I_{zz} \end{pmatrix} \begin{pmatrix} \dot{p} \\ \dot{q} \\ \dot{r} \end{pmatrix} = - \begin{pmatrix} 0 & -r & q \\ r & 0 & -p \\ -q & p & 0 \end{pmatrix} \begin{pmatrix} I_{xx} & I_{xy} & I_{xz} \\ I_{xy} & I_{yy} & I_{yz} \\ I_{xz} & I_{yz} & I_{zz} \end{pmatrix} \begin{pmatrix} p \\ q \\ r \end{pmatrix}
$$
$$
+ \begin{pmatrix} T_{aero.xb} \\ T_{aero.yb} \\ T_{aero.zb} \end{pmatrix} + \begin{pmatrix} T_{rkt.xb} \\ T_{rkt.yb} \\ T_{rkt.zb} \end{pmatrix} + \begin{pmatrix} T_{rcs.xb} \\ 0 \\ 0 \end{pmatrix}
\tag{A.4}
$$

$$
\begin{pmatrix} \dot{q}_1 \\ \dot{q}_2 \\ \dot{q}_3 \\ \dot{q}_4 \end{pmatrix} = \frac{1}{2} \begin{pmatrix} 0 & r & -q & p \\ -r & 0 & p & q \\ q & -p & 0 & r \\ -p & -q & -r & 0 \end{pmatrix} \begin{pmatrix} q_1 \\ q_2 \\ q_3 \\ q_4 \end{pmatrix}
\tag{A.5}
$$

APPENDIX B.   ADDITIONAL FIGURES FROM 6-DOF SIMULATION

B.1   Atmospheric Model
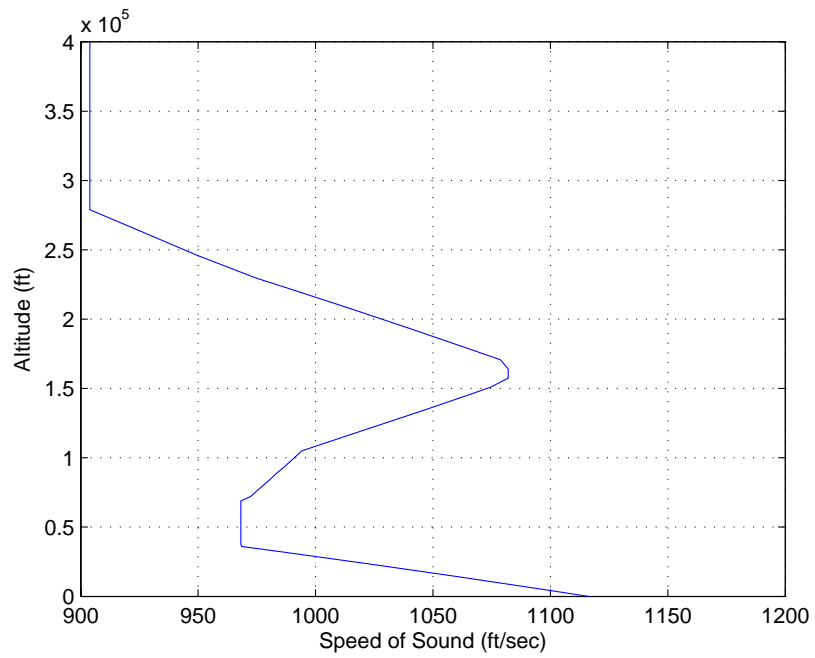
Figure B.1   Speed of sound
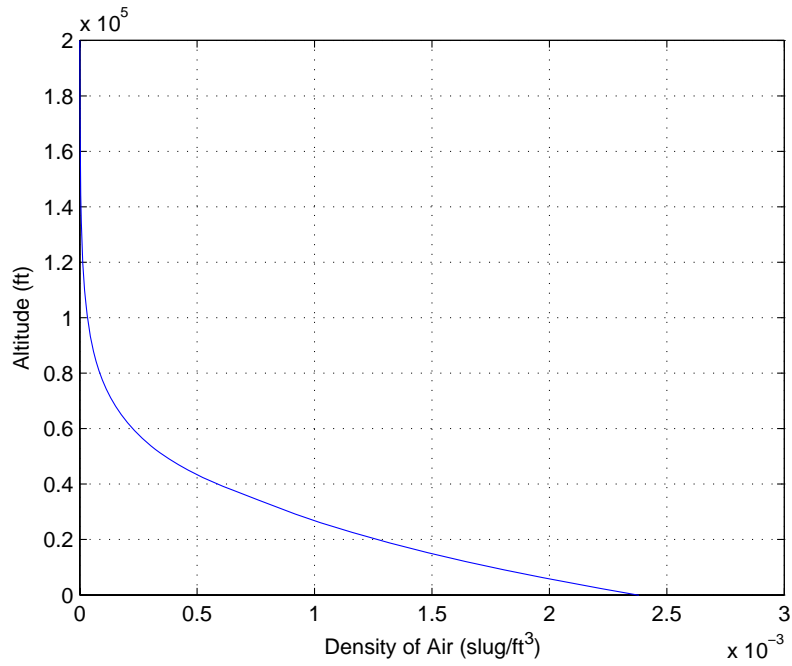
Figure B.2   Density of air
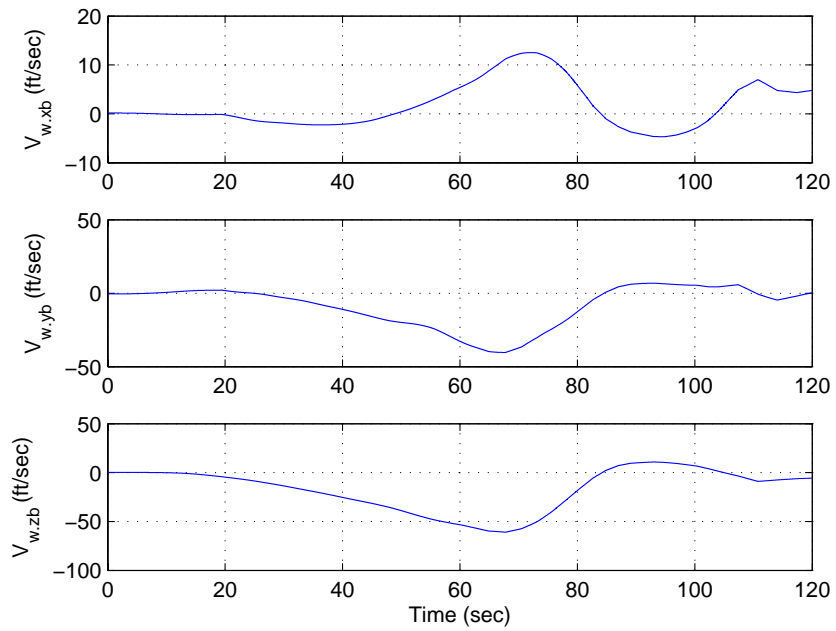
Figure B.3   Wind profile
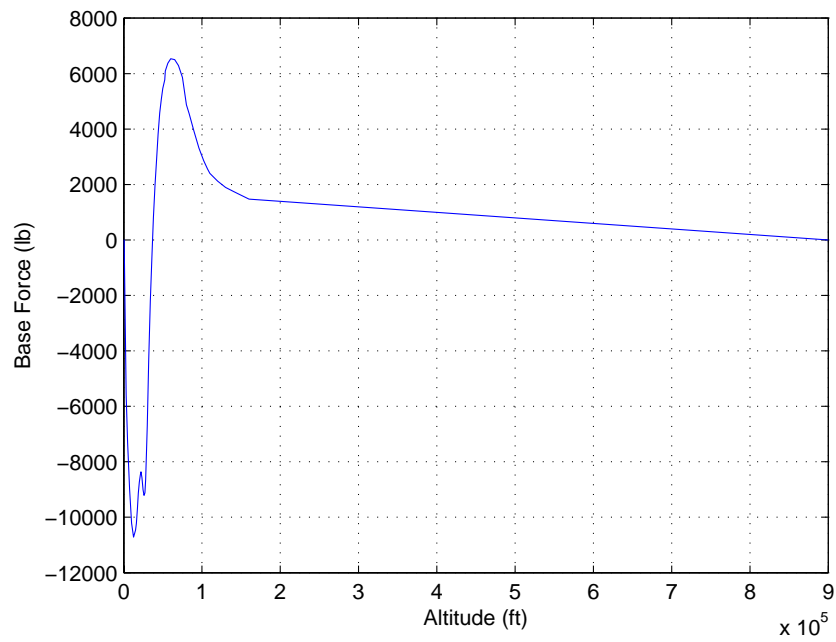
Figure B.4   Base force

B.2   Aerodynamic Coefficient
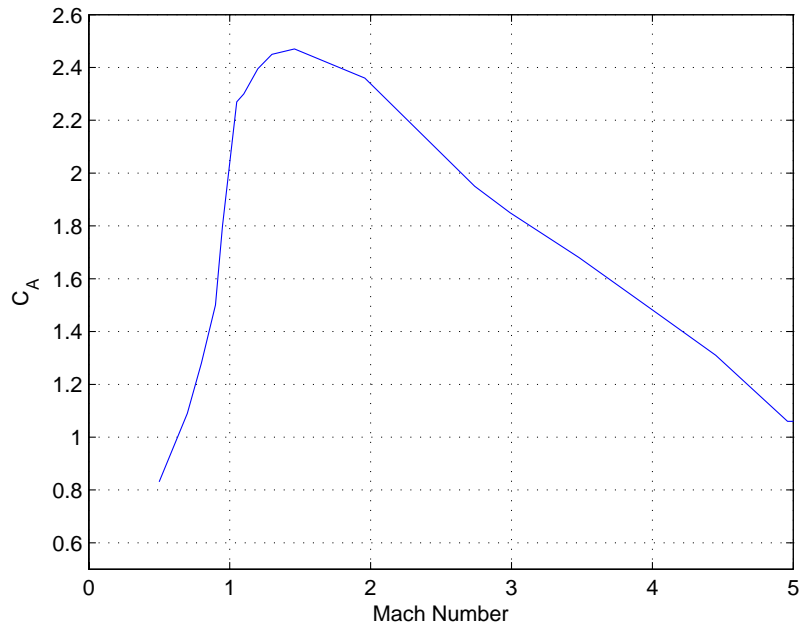
Figure B.5 C_A
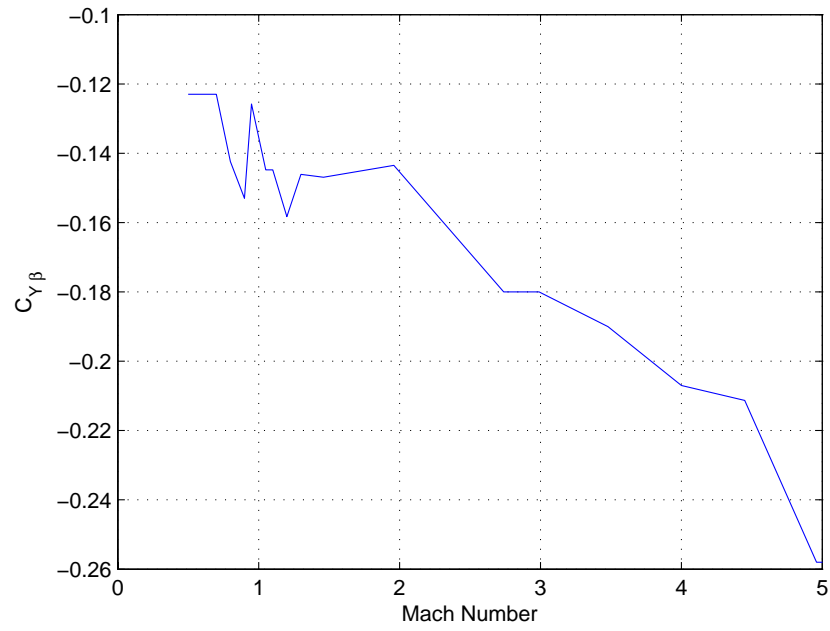
Figure B.6 $C_{Y\beta}$
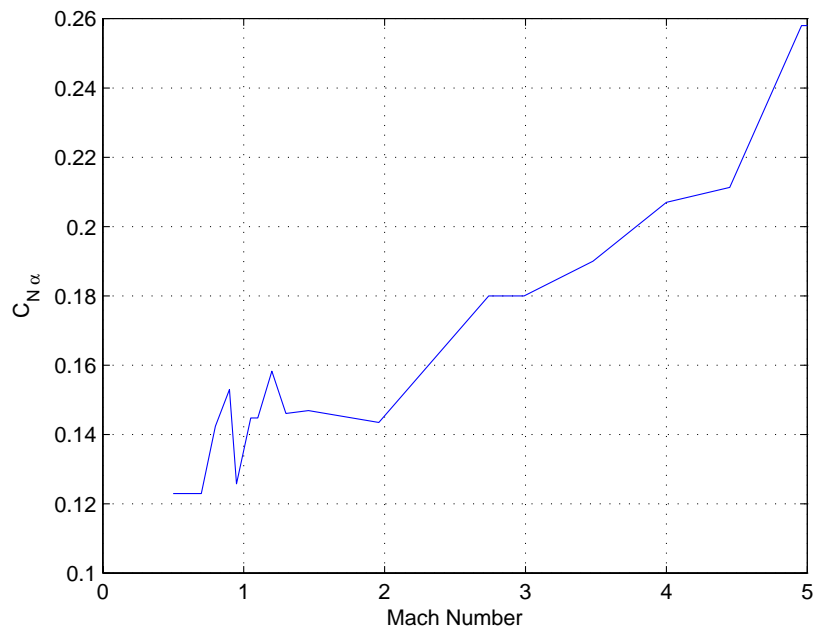
Figure B.7 $C_{N\alpha}$
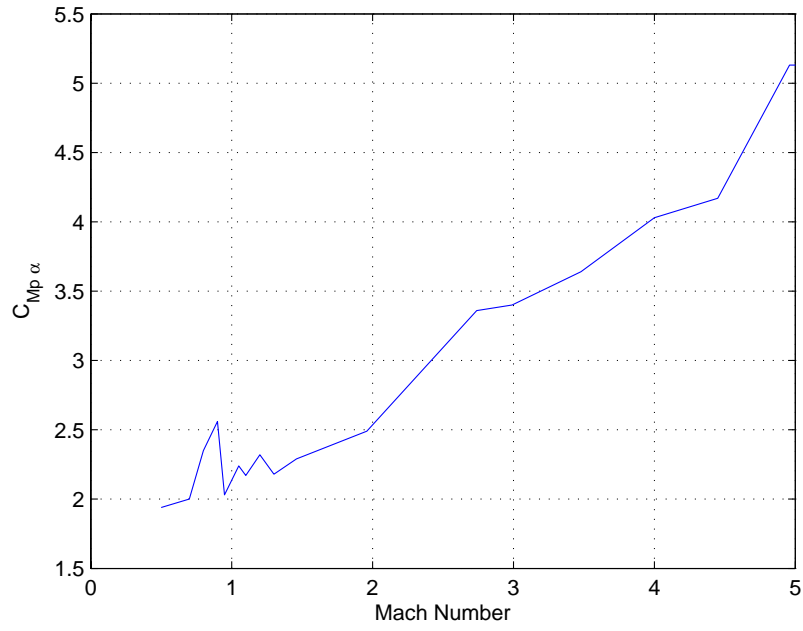
Figure B.8 $C_{Mp\alpha}$
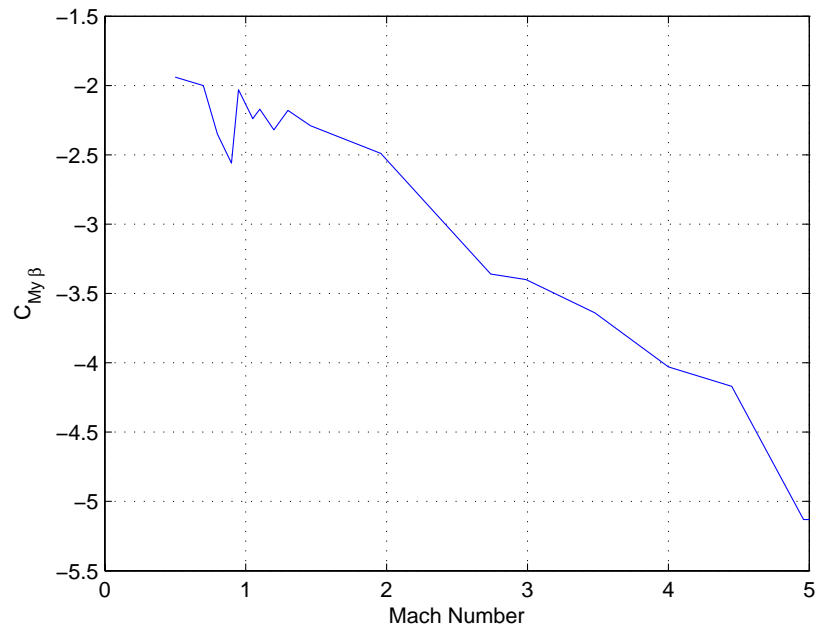
Figure B.9 $C_{My\beta}$

Rocket Parameters
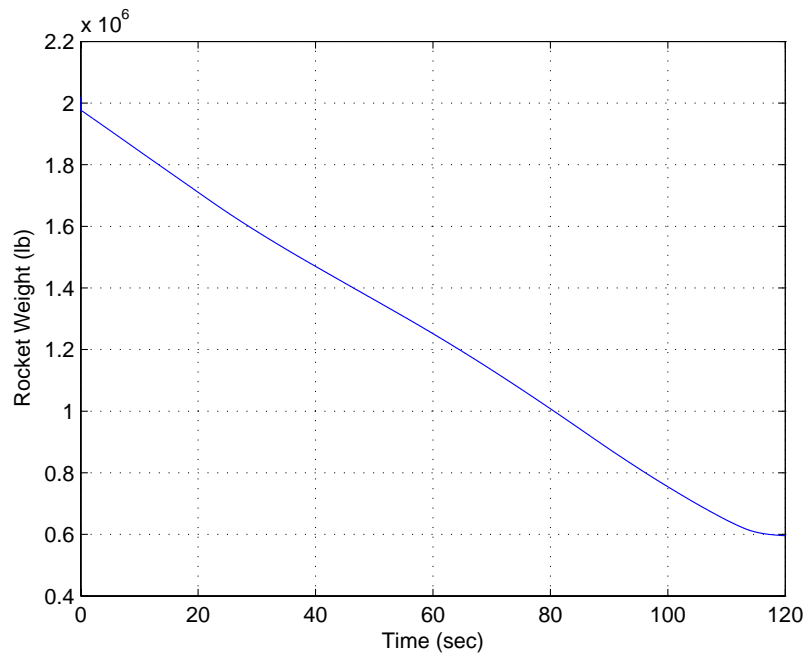
Figure B.10   Rocket weight.
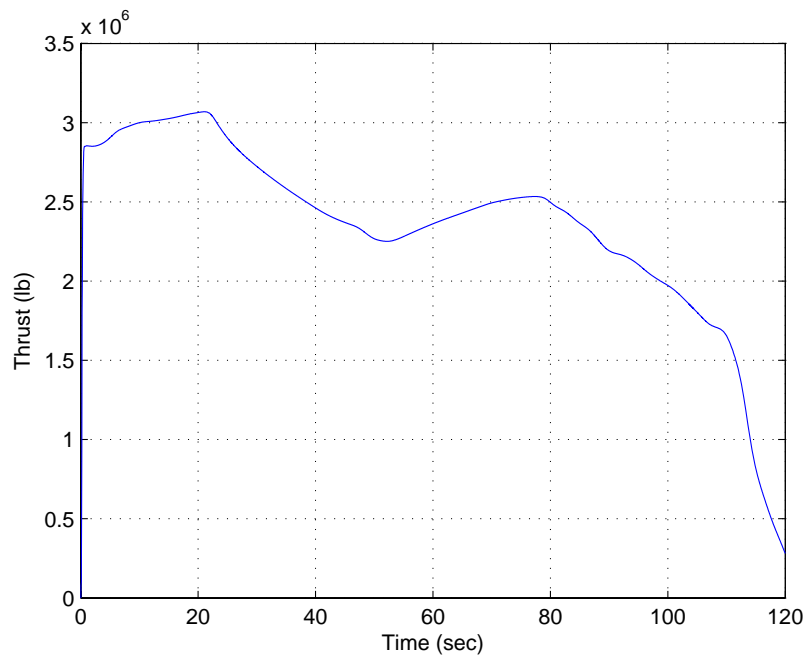
Figure B.11   Rocket thrust.
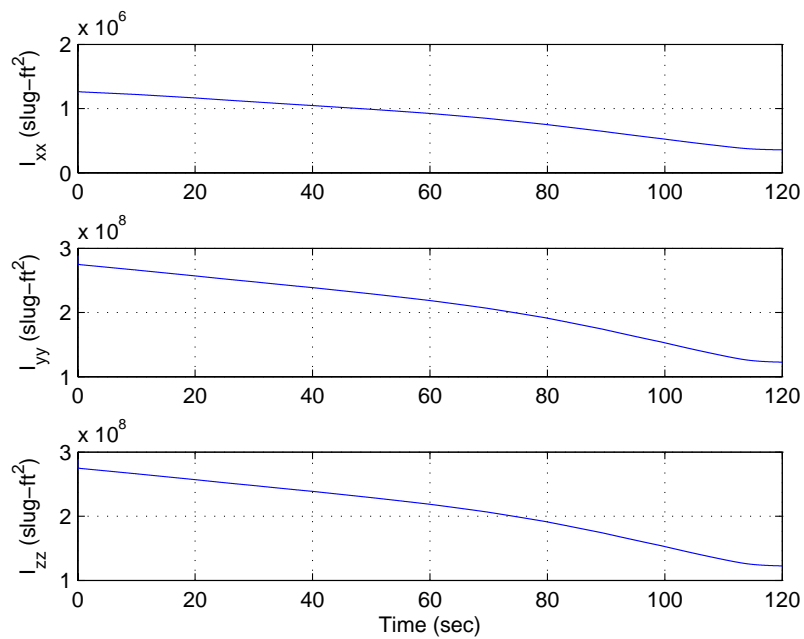
Figure B.12   Moments of inertia.

APPENDIX C.   LINEARIZATION RESULTS

C.1   Nonlinear 6-DOF Equations

Translational equations in the body frame:

$$
\begin{pmatrix} \dot{u} \\ \dot{v} \\ \dot{w} \end{pmatrix} = - \begin{pmatrix} 0 & -r & q \\ r & 0 & -p \\ -q & p & 0 \end{pmatrix} \begin{pmatrix} u \\ v \\ w \end{pmatrix} + \boldsymbol{C}^{B/I} \begin{pmatrix} g_x \\ g_y \\ g_z \end{pmatrix} + \frac{1}{m} \begin{pmatrix} F_{aero.xb} \\ F_{aero.yb} \\ F_{aero.zb} \end{pmatrix} + \frac{1}{m} \begin{pmatrix} T \\ -T\delta_z \\ T\delta_y \end{pmatrix}
$$
(C.1)

where

$$
\mathbf{C}^{B/I} = \begin{pmatrix} 1 - 2(q_2^2 + q_3^2) & 2(q_1 q_2 + q_3 q_4) & 2(q_1 q_3 - q_2 q_4) \\ 2(q_1 q_2 - q_3 q_4) & 1 - 2(q_1^2 + q_3^2) & 2(q_2 q_3 + q_1 q_4) \\ 2(q_1 q_3 + q_2 q_4) & 2(q_2 q_3 - q_1 q_4) & 1 - 2(q_1^2 + q_2^2) \end{pmatrix}
$$
(C.2)

Rotational equation in the body frame:

$$
\begin{pmatrix} I_{xx} & I_{xy} & I_{xz} \\ I_{xy} & I_{yy} & I_{yz} \\ I_{xz} & I_{yz} & I_{zz} \end{pmatrix} \begin{pmatrix} \dot{p} \\ \dot{q} \\ \dot{r} \end{pmatrix} = - \begin{pmatrix} 0 & -r & q \\ r & 0 & -p \\ -q & p & 0 \end{pmatrix} \begin{pmatrix} I_{xx} & I_{xy} & I_{xz} \\ I_{xy} & I_{yy} & I_{yz} \\ I_{xz} & I_{yz} & I_{zz} \end{pmatrix} \begin{pmatrix} p \\ q \\ r \end{pmatrix}
$$
$$
+ \begin{pmatrix} T_{aero.xb} \\ T_{aero.yb} \\ T_{aero.zb} \end{pmatrix} + \begin{pmatrix} T_{rkt.xb} \\ T_{rkt.yb} \\ T_{rkt.zb} \end{pmatrix} + \begin{pmatrix} T_{rcs.xb} \\ 0 \\ 0 \end{pmatrix}
$$
(C.3)

C.2 Linear Rigid-Body Model

$$\Delta\dot{u} = r_0\Delta v - q_0\Delta w - w_0\Delta q + v_0\Delta r + (2g_y q_{2c} + 2g_z q_{3c})\Delta q_1 + (-4g_x q_{2c} + 2g_y q_{1c} - 2g_z q_{4c})\Delta q_2$$
$$+ (-4g_x q_{3c} + 2g_y q_{4c} + 2g_z q_{1c})\Delta q_3 + (2g_y q_{3c} - 2g_z q_{2c})\Delta q_4 + \frac{1}{m}\Delta F_{aero.xb}$$

$$\text{(C.4)}$$

$$\Delta\dot{v} = -r_0\Delta u + p_0\Delta w + w_0\Delta p - u_0\Delta r + (2g_x q_{2c} - 4g_y q_{1c} + 2g_z q_{4c})\Delta q_1$$
$$+ (2g_x q_{1c} + 2g_z q_{3c})\Delta q_2 + (-2g_x q_{4c} - 4g_y q_{3c} + 2g_z q_{2c})\Delta q_3 + (-2g_x q_{3c} + 2g_z q_{1c})\Delta q_4$$
$$+ \frac{1}{m}\Delta F_{aero.yb} + (-\frac{T}{m})\Delta\delta_z$$

$$\text{(C.5)}$$

$$\Delta\dot{w} = q_0\Delta u - p_0\Delta v - v_0\Delta p + u_0\Delta q + (2g_x q_{3c} - 2g_y q_{4c} - 4g_z q_{1c})\Delta q_1$$
$$+ (2g_x q_{4c} + 2g_y q_{3c} - 4g_z q_{2c})\Delta q_2 + (2g_x q_{1c} + 2g_y q_{2c})\Delta q_3 + (2g_x q_{2c} - 2g_y q_{1c})\Delta q_4 \quad\text{(C.6)}$$
$$+ \frac{1}{m}\Delta F_{aero.zb} + (\frac{T}{m})\Delta\delta_y$$

$$\begin{pmatrix} I_{xx} & 0 & 0 \\ 0 & I_{yy} & 0 \\ 0 & 0 & I_{zz} \end{pmatrix} \begin{pmatrix} \Delta\dot{p} \\ \Delta\dot{q} \\ \Delta\dot{r} \end{pmatrix} = \begin{pmatrix} b_1 \\ b_2 \\ b_3 \end{pmatrix} \quad\text{(C.7)}$$

where the relatively small products of inertia are ignored, and

$$b_1 = (r_0 I_{yy} - I_{zz}r_0)\Delta q + (I_{yy}q_0 - q_0 I_{zz})\Delta r + \Delta T_{aero.xb}$$
$$+ (-c_y T)\Delta\delta_y + (-c_z T)\Delta\delta_z + \Delta T_{rcs} \quad\text{(C.8a)}$$

$$b_2 = (-r_0 I_{yy} + I_{zz}r_0))\Delta p + (-(I_{xx}p_0 + p_0 I_{zz})\Delta r + \Delta T_{aero.yb} + (c_x - X_g)T\Delta\delta_y \quad\text{(C.8b)}$$

$$b_3 = (q_0 I_{xx} - I_{yy}q_0)\Delta p + (I_{xx}p_0 - p_0 I_{yy})\Delta q + \Delta T_{aero.zb} + (X_g - c_x)(-T)\Delta\delta_z \quad\text{(C.8c)}$$

$$\Delta \dot{q_1} = \frac{1}{2}(q_{4c}\Delta p - q_{3c}\Delta q + q_{2c}\Delta r + r_0\Delta q_2 - q_0\Delta q_3 + p_0\Delta q_4) \tag{C.9a}$$

$$\Delta \dot{q_2} = \frac{1}{2}(q_{3c}\Delta p + q_{4c}\Delta q - q_{1c}\Delta r - r_0\Delta q_1 + p_0\Delta q_3 + q_0\Delta q_4) \tag{C.9b}$$

$$\Delta \dot{q_3} = \frac{1}{2}(-q_{2c}\Delta p + q_{1c}\Delta q + q_{4c}\Delta r + q_0\Delta q_1 - p_0\Delta q_2 + r_0\Delta q_4) \tag{C.9c}$$

$$\Delta \dot{q_4} = \frac{1}{2}(-q_{1c}\Delta p - q_{2c}\Delta q - q_{3c}\Delta r - p_0\Delta q_1 - q_0\Delta q_2 - r_0\Delta q_3) \tag{C.9d}$$

Linearization of the aerodynamic forces and moments:

$$\begin{pmatrix} \Delta F_{aero.xb} \\ \Delta F_{aero.yb} \\ \Delta F_{aero.zb} \end{pmatrix} = \begin{pmatrix} 0 & 0 & 0 \\ 0 & C_{Y\beta}QS/V_m & 0 \\ 0 & 0 & -C_{N\alpha}QS/V_{m.xb} \end{pmatrix} \begin{pmatrix} \Delta u \\ \Delta v \\ \Delta w \end{pmatrix} \tag{C.10}$$

$$\begin{pmatrix} \Delta T_{aero.xb} \\ \Delta T_{aero.yb} \\ \Delta T_{aero.zb} \end{pmatrix} = \begin{pmatrix} 0 & c_z & -c_y \\ -c_z & 0 & -X_a + c_x \\ c_y & X_a - c_x & 0 \end{pmatrix} \begin{pmatrix} \Delta F_{aero.xb} \\ \Delta F_{aero.yb} \\ \Delta F_{aero.zb} \end{pmatrix}$$
$$+ \begin{pmatrix} 0 & 0 & 0 \\ 0 & 0 & C_{Mp\alpha}QSb/V_{m.xb} \\ 0 & C_{My\beta}QSb/V_m & 0 \end{pmatrix} \begin{pmatrix} \Delta u \\ \Delta v \\ \Delta w \end{pmatrix} \tag{C.11}$$

Linearization of α and β:

$$\Delta \alpha = \frac{1}{V_{m.xb}}\Delta w \tag{C.12}$$

$$\Delta \beta = \frac{1}{V_m}\Delta v \tag{C.13}$$

Linearization of the thrust force and moment:

$$\begin{pmatrix} \Delta F_{rkt.xb} \\ \Delta F_{rkt.yb} \\ \Delta F_{rkt.zb} \end{pmatrix} = \begin{pmatrix} 0 \\ -T\Delta\delta_z \\ T\Delta\delta_y \end{pmatrix} \tag{C.14}$$

$$\begin{pmatrix} \Delta T_{rkt.xb} \\ \Delta T_{rkt.yb} \\ \Delta T_{rkt.zb} \end{pmatrix} = \begin{pmatrix} 0 & c_z & -c_y \\ -c_z & 0 & -X_g + c_x \\ c_y & X_g - c_x & 0 \end{pmatrix} \begin{pmatrix} \Delta F_{rkt.xb} \\ \Delta F_{rkt.yb} \\ \Delta F_{rkt.zb} \end{pmatrix} \tag{C.15}$$

Quaternion errors:

$$
\begin{pmatrix} q_{1e} \\ q_{2e} \\ q_{3e} \\ q_{4e} \end{pmatrix} = \begin{pmatrix} q_{4c} & q_{3c} & -q_{2c} & -q_{1c} \\ -q_{3c} & q_{4c} & q_{1c} & -q_{2c} \\ q_{2c} & -q_{1c} & q_{4c} & -q_{3c} \\ q_{1c} & q_{2c} & q_{3c} & q_{4c} \end{pmatrix} \begin{pmatrix} \Delta q_1 \\ \Delta q_2 \\ \Delta q_3 \\ \Delta q_4 \end{pmatrix} \tag{C.16}
$$

C.3   Linear State-Space Equations

A linearized state-space model of a rigid vehicle is described by

$$
\begin{aligned} \dot{\mathbf{x}} &= \mathbf{A}\mathbf{x} + \mathbf{B}\mathbf{u} \\ \mathbf{y} &= \mathbf{C}\mathbf{x} \end{aligned} \tag{C.17}
$$

where $\mathbf{x} = (\Delta u,\ \Delta v,\ \Delta w,\ \Delta p,\ \Delta q,\ \Delta r,\ \Delta q_1,\ \Delta q_2,\ \Delta q_3,\ \Delta q_4)^T$, $\mathbf{u} = (\Delta T_{rcs},\ \Delta \delta_y,\ \Delta \delta_z)^T$, $\mathbf{y} = (2q_{1e},\ 2q_{2e},\ 2q_{3e},\ p,\ q,\ r)^T$,

$$
\mathbf{A} = \left(\begin{array}{c|c|c} \mathbf{A}_{11} & \mathbf{A}_{12} & \mathbf{A}_{13} \\ \hline \mathbf{A}_{21} & \mathbf{A}_{22} & 0 \\ \hline 0 & \mathbf{A}_{32} & \mathbf{A}_{33} \end{array} \right) \tag{C.18}
$$

$$
\mathbf{A}_{11} = \begin{pmatrix} 0 & r_0 & -q_0 \\ -r_0 & C_{Y\beta}QS/(mV_m) & p_0 \\ q_0 & -p_0 & -C_{N\alpha}QS/(mV_{m.xb}) \end{pmatrix} \tag{C.19}
$$

$$
\mathbf{A}_{12} = \begin{pmatrix} 0 & -w_0 & v_0 \\ w_0 & 0 & -u_0 \\ -v_0 & u_0 & 0 \end{pmatrix} \tag{C.20}
$$

$$
\mathbf{A}_{13} = \begin{pmatrix} (2g_y q_{2c} + 2g_z q_{3c}) & (-4g_x q_{2c} + 2g_y q_{1c} - 2g_z q_{4c}) \\ (2g_x q_{2c} - 4g_y q_{1c} + 2g_z q_{4c}) & (2g_x q_{1c} + 2g_z q_{3c}) \\ (2g_x q_{3c} - 2g_y q_{4c} - 4g_z q_{1c}) & (2g_x q_{4c} + 2g_y q_{3c} - 4g_z q_{2c}) \\ (-4g_x q_{3c} + 2g_y q_{4c} + 2g_z q_{1c}) & (2g_y q_{3c} - 2g_z q_{2c}) \\ (-2g_x q_{4c} - 4g_y q_{3c} + 2g_z q_{2c}) & (-2g_x q_{3c} + 2g_z q_{1c}) \\ (2g_x q_{1c} + 2g_y q_{2c}) & (2g_x q_{2c} - 2g_y q_{1c}) \end{pmatrix} \tag{C.21}
$$

$$\mathbf{A}_{21} = \begin{pmatrix} I_{xx} & 0 & 0 \\ 0 & I_{yy} & 0 \\ 0 & 0 & I_{zz} \end{pmatrix}^{-1} \begin{pmatrix} 0 & 0 & 0 \\ 0 & 0 & \left[-\frac{(-X_a+c_x)C_{N\alpha}QS}{V_{m.xb}} + \frac{C_{Mp\alpha}QSb}{V_{m.xb}} \right] \\ 0 & \left[-\frac{(X_a+c_x)C_{Y\beta}QS}{V_m} + \frac{C_{My\beta}QSb}{V_m} \right] & 0 \end{pmatrix} \quad (C.22)$$

$$\mathbf{A}_{22} = \begin{pmatrix} I_{xx} & 0 & 0 \\ 0 & I_{yy} & 0 \\ 0 & 0 & I_{zz} \end{pmatrix}^{-1} \begin{pmatrix} 0 & r_0 I_{yy} + I_{zz}r_0 & I_{yy}q_0 - q_0 I_{zz} \\ -r_0 I_{yy} + I_{zz}r_0 & 0 & -I_{xx}p_0 + p_0 I_{zz} \\ q_0 I_{xx} - I_{yy}q_0 & I_{xx}p_0 - p_0 I_{yy} & 0 \end{pmatrix} \quad (C.23)$$

$$\mathbf{A}_{32} = \frac{1}{2} \begin{pmatrix} q_{4c} & -q_{3c} & q_{2c} \\ q_{3c} & q_{4c} & -q_{1c} \\ -q_{2c} & q_{1c} & q_{4c} \\ -q_{1c} & -q_{2c} & -q_{3c} \end{pmatrix} \quad (C.24)$$

$$\mathbf{A}_{33} = \frac{1}{2} \begin{pmatrix} 0 & r_0 & -q_0 & p_0 \\ -r_0 & 0 & p_0 & q_0 \\ q_0 & -p_0 & 0 & r_0 \\ -p_0 & -q_0 & -r_0 & 0 \end{pmatrix} \quad (C.25)$$

$$\mathbf{B} = \begin{pmatrix} \mathbf{B}_1 \\ \mathbf{B}_2 \\ 0 \end{pmatrix} \quad (C.26)$$

$$\mathbf{B}_1 = \begin{pmatrix} 0 & 0 & 0 \\ 0 & 0 & -T/m \\ 0 & T/m & 0 \end{pmatrix} \quad (C.27)$$

$$\mathbf{B}_2 = \begin{pmatrix} I_{xx} & 0 & 0 \\ 0 & I_{yy} & 0 \\ 0 & 0 & I_{zz} \end{pmatrix}^{-1} \begin{pmatrix} 1 & -c_y T & -c_z T + c_y T \\ 0 & (c_x - X_g)T & 0 \\ 0 & 0 & (c_x - X_g)T \end{pmatrix} \quad (C.28)$$

$$\mathbf{C} = \begin{pmatrix} 0 & 0 & 0 & 0 & 0 & 0 & 2q_{4c} & 2q_{3c} & -2q_{2c} & -2q_{1c} \\ 0 & 0 & 0 & 0 & 0 & 0 & -2q_{3c} & 2q_{4c} & 2q_{1c} & -2q_{2c} \\ 0 & 0 & 0 & 0 & 0 & 0 & 2q_{2c} & -2q_{1c} & 2q_{4c} & -2q_{3c} \\ 0 & 0 & 0 & 1 & 0 & 0 & 0 & 0 & 0 & 0 \\ 0 & 0 & 0 & 0 & 1 & 0 & 0 & 0 & 0 & 0 \\ 0 & 0 & 0 & 0 & 0 & 1 & 0 & 0 & 0 & 0 \end{pmatrix} \tag{C.29}$$

Assuming that $p_0 = q_0 = r_0 = 0$, $v_0 = w_0 = 0$, $\theta \approx 2q_{2e}$ and V_m is a constant, then we get the rigid-body dynamic model of Ares-I CLV in the pitch plane as follows:

$$\dot{\alpha} = \dot{\theta} + \frac{g_x}{V_m}\theta + \frac{-C_{N\alpha}QS}{mV_m}\alpha + \frac{T}{mu_0}\delta_y \tag{C.30a}$$

$$\dot{\theta} = \frac{-(-X_a + c_x)C_{N\alpha}QS + C_{Mp\alpha}QSb}{I_{yy}}\alpha + \frac{(c_x - X_g)T}{I_{yy}}\delta_y \tag{C.30b}$$

where $\alpha = \frac{\Delta w}{V_m}$.

C.4 Linear Flexible-Body Model

The linear state-space equation of the Ares-I including the flexible-body modes is described by

$$\begin{aligned} \dot{\mathbf{x}} &= \hat{\mathbf{A}}\mathbf{x} + \hat{\mathbf{B}}\mathbf{u} \\ \mathbf{y} &= \hat{\mathbf{C}}\mathbf{x} \end{aligned} \tag{C.31}$$

where

$$\mathbf{x} = (\Delta u,\ \Delta v,\ \Delta w,\ \Delta p,\ \Delta q,\ \Delta r,\ \Delta q_1,\ \Delta q_2,\ \Delta q_3,\ \Delta q_4,\ \eta_1,\ \eta_2,\ \eta_3,\ \eta_4,\ \eta_5,\ \eta_6,\ \dot{\eta}_1,\ \dot{\eta}_2,\ \dot{\eta}_3,\ \dot{\eta}_4,\ \dot{\eta}_5,\ \dot{\eta}_6)^T \tag{C.32}$$

and

$$\hat{\mathbf{A}} = \left(\begin{array}{c|cc} \mathbf{A} & & 0 \\ \hline & 0 & \mathbf{I} \\ 0 & & \\ & -\mathbf{\Omega}^2 & -2\zeta\mathbf{\Omega} \end{array} \right) \tag{C.33}$$

$$\hat{\mathbf{B}} = \left(\begin{array}{c} \mathbf{B} \\ \hline 0 \\ \hline \mathbf{\Phi}^T m\mathbf{B}_1 \end{array} \right) \tag{C.34}$$

$$\hat{\mathbf{C}} = \left(\begin{array}{cccccccccc|c|c} 0 & 0 & 0 & 0 & 0 & 0 & 2q_{4c} & 2q_{3c} & -2q_{2c} & -2q_{1c} & & \\ 0 & 0 & 0 & 0 & 0 & 0 & -2q_{3c} & 2q_{4c} & 2q_{1c} & -2q_{2c} & \boldsymbol{\Psi} & 0 \\ 0 & 0 & 0 & 0 & 0 & 0 & 2q_{2c} & -2q_{1c} & 2q_{4c} & -2q_{3c} & & \\ \hline & 0 & 0 & 0 & 1 & 0 & 0 & 0 & 0 & 0 & & \\ & 0 & 0 & 0 & 0 & 1 & 0 & 0 & 0 & 0 & 0 & \boldsymbol{\Psi} \\ & 0 & 0 & 0 & 0 & 0 & 1 & 0 & 0 & 0 & & \end{array} \right) \tag{C.35}$$

APPENDIX D.   ATTITUDE ERROR QUATERNION KINEMATIC DIFFERENTIAL EQUATIONS

Equations. (2.12) and (2.46) can be written as

$$\dot{\mathbf{q}} = \frac{1}{2}\mathbf{\Omega}\mathbf{q} \tag{D.1}$$

$$\mathbf{q_e} = \mathbf{Q_c}\mathbf{q} \tag{D.2}$$

where $\mathbf{q} = (q_1,\ q_2,\ q_3,\ q_4)^T$, $\mathbf{q_e} = (q_{1e},\ q_{2e},\ q_{3e},\ q_{4e})^T$, and

$$\mathbf{\Omega} = \begin{pmatrix} 0 & r & -q & p \\ -r & 0 & p & q \\ q & -p & 0 & r \\ -p & -q & -r & 0 \end{pmatrix} \tag{D.3}$$

$$\mathbf{Q_c} = \begin{pmatrix} q_{4c} & q_{3c} & -q_{2c} & -q_{1c} \\ -q_{3c} & q_{4c} & q_{1c} & -q_{2c} \\ q_{2c} & -q_{1c} & q_{4c} & -q_{3c} \\ q_{1c} & q_{2c} & q_{3c} & q_{4c} \end{pmatrix} \tag{D.4}$$

Note that $\mathbf{Q_c}$ is an orthonormal matrix; that is, $\mathbf{Q_c}\mathbf{Q_c^T} = \mathbf{I}$ and $\mathbf{Q_c^{-1}} = \mathbf{Q_c^T}$. Differentiating Equation. (D.2) with constant commanded quaternions, we obtain

$$\dot{\mathbf{q}}_e = \mathbf{Q_c}\dot{\mathbf{q}} \tag{D.5}$$

Substituting Equation. (D.1) into Equation. (D.5), we obtain

$$\dot{\mathbf{q}}_e = \frac{1}{2}\mathbf{Q_c}\mathbf{\Omega}\mathbf{Q_c^{-1}}\mathbf{q_e} \tag{D.6}$$

By substituting Equations. (D.3) and (D.4) into $\mathbf{Q_c\Omega Q_c^{-1}}$, we can show that $\mathbf{Q_c\Omega Q_c^{-1} = \Omega}$. An indirect approach to obtaining this relationship is provided as follows.

Let

$$\mathbf{Q_c} = q_{4c}\mathbf{I} + \mathbf{Q} \tag{D.7}$$

where

$$\mathbf{Q} = \begin{pmatrix} 0 & q_{3c} & -q_{2c} & -q_{1c} \\ -q_{3c} & 0 & q_{1c} & -q_{2c} \\ q_{2c} & -q_{1c} & 0 & -q_{3c} \\ q_{1c} & q_{2c} & q_{3c} & 0 \end{pmatrix} \tag{D.8}$$

Note that $\mathbf{Q}$ and $\mathbf{\Omega}$ are skew-symmetric matrices; that is, $\mathbf{Q} = -\mathbf{Q^T}$ and $\mathbf{\Omega} = -\mathbf{\Omega^T}$. Consequently, $\mathbf{Q\Omega}$ is a symmetric matrix; that is, $\mathbf{Q\Omega} = (\mathbf{Q\Omega})^T$. Then we have

$$\mathbf{Q\Omega} = (\mathbf{Q\Omega})^T = \mathbf{\Omega^T Q^T} = -\mathbf{\Omega Q^T} = \mathbf{\Omega Q} \tag{D.9}$$

By using these properties, we can rewrite $\mathbf{Q_c\Omega Q_c^{-1}}$ as

$$\mathbf{Q_c\Omega Q_c^{-1}} = \mathbf{Q_c\Omega Q_c^{-1}} = (q_{4c}\mathbf{I} + \mathbf{Q})\mathbf{\Omega Q_c^{-1}} \tag{D.10}$$

which becomes

$$(q_{4c}\mathbf{I} + \mathbf{Q})\mathbf{\Omega Q_c^{-1}} = (q_{4c}\mathbf{I\Omega} + \mathbf{Q\Omega})\mathbf{Q_c^{-1}} = \mathbf{\Omega}(q_{4c}\mathbf{I} + \mathbf{Q})\mathbf{Q_c^{-1}} = \mathbf{\Omega Q_c Q_c^{-1}} \tag{D.11}$$

Finally, we have

$$\mathbf{Q_c\Omega Q_c^{-1}} = \mathbf{\Omega} \tag{D.12}$$

and

$$\begin{pmatrix} \dot{q}_{1e} \\ \dot{q}_{2e} \\ \dot{q}_{3e} \\ \dot{q}_{4e} \end{pmatrix} = \frac{1}{2} \begin{pmatrix} 0 & r & -q & p \\ -r & 0 & p & q \\ q & -p & 0 & r \\ -p & -q & -r & 0 \end{pmatrix} \begin{pmatrix} q_{1e} \\ q_{2e} \\ q_{3e} \\ q_{4e} \end{pmatrix} \tag{D.13}$$

Note that the constant commanded quaternions are assumed here.

APPENDIX E. LINEAR MODEL OF UNCONTROLLED ROLL DRIFT WITH AERODYNAMIC DISTURBANCE

$$\dot{v} = -u_0 r - g_x \psi + \frac{C_{Y\beta} Q S}{m} \beta - \frac{T}{m} \delta_z \qquad (E.1)$$

$$\dot{w} = u_0 q - g_x \theta - \frac{C_{N\alpha} Q S}{m} \alpha + \frac{T}{m} \delta_y \qquad (E.2)$$

$$\dot{q} = M_\alpha \alpha + M_\delta \delta_y \qquad (E.3)$$

$$\dot{r} = M_\beta \beta + M_\delta \delta_z \qquad (E.4)$$

$$\dot{q}_{2e} = \frac{q_{4e}}{2} q - \frac{q_{1e}}{2} r \qquad (E.5)$$

$$\dot{q}_{3e} = \frac{q_{1e}}{2} q + \frac{q_{4e}}{2} r \qquad (E.6)$$

where $\alpha = \frac{w}{u_0}$, $\beta = \frac{v}{u_0}$.

When attitude error quaternion are small, we have $\theta \approx 2q_{2e}$ and $\psi \approx 2q_{3e}$.

$$
\begin{pmatrix} \dot{v} \\ \dot{w} \\ \dot{q} \\ \dot{r} \\ \dot{q}_{2e} \\ \dot{q}_{3e} \end{pmatrix} = \begin{pmatrix} \frac{C_{Y\beta}QS}{mu_0} & 0 & 0 & -u_0 & 0 & -2g_x \\ 0 & -\frac{C_{N\alpha}QS}{mu_0} & u_0 & 0 & 2g_x & 0 \\ 0 & M_\alpha/u_0 & 0 & 0 & 0 & 0 \\ M_\beta/u_0 & 0 & 0 & 0 & 0 & 0 \\ 0 & 0 & q_{4e}/2 & -q_{1e}/2 & 0 & 0 \\ 0 & 0 & q_{1e}/2 & q_{4e}/2 & 0 & 0 \end{pmatrix} \begin{pmatrix} v \\ w \\ q \\ r \\ q_{2e} \\ q_{3e} \end{pmatrix} + \begin{pmatrix} 0 & -T/m \\ T/m & 0 \\ M_\delta & 0 \\ 0 & M_\delta \\ 0 & 0 \\ 0 & 0 \end{pmatrix} \begin{pmatrix} \delta_y \\ \delta_z \end{pmatrix}
$$

$$\text{(E.7)}$$

APPENDIX F. DERIVATION OF A STEADY-STATE OSCILLATION

F.1 A Steady-State Oscillation of the Autonomous System

For this autonomous system $\dot{\mathbf{x}} = f(\mathbf{x})$, we have

$$
\begin{pmatrix} \dot{q} \\ \dot{r} \\ \dot{q}_1 \\ \dot{q}_2 \\ \dot{q}_3 \\ \dot{q}_4 \end{pmatrix} = \begin{pmatrix} arp - \hat{K}_p q_2 - \hat{K}_d q \\ -apq - \hat{K}_p q_3 - \hat{K}_d r \\ \frac{r}{2} q_2 - \frac{q}{2} q_3 + \frac{p}{2} q_4 \\ -\frac{r}{2} q_1 + \frac{p}{2} q_3 + \frac{q}{2} q_4 \\ \frac{q}{2} q_1 - \frac{p}{2} q_2 + \frac{r}{2} q_4 \\ -\frac{p}{2} q_1 - \frac{q}{2} q_2 - \frac{r}{2} q_3 \end{pmatrix} \tag{F.1}
$$

Assume that there is a steady-state oscillation. q_1 and q_4 are constants and it has the following relation between two vectors $(q, \ r)^T$ and $(q_2, \ q_3)^T$ is

$$
\begin{pmatrix} q \\ r \end{pmatrix} = X \begin{pmatrix} q_2 \\ q_3 \end{pmatrix} \tag{F.2}
$$

$$
X = \tau \begin{pmatrix} \cos\theta & \sin\theta \\ -\sin\theta & \cos\theta \end{pmatrix} \tag{F.3}
$$

where $|\tau|$ is the magnitude ratio and θ is the phase shift between those two vectors. Note that the matrix X is invertible. Therefore

$$
\begin{pmatrix} q_2 \\ q_3 \end{pmatrix} = X^{-1} \begin{pmatrix} q \\ r \end{pmatrix} = \frac{1}{\tau} \begin{pmatrix} \cos\theta & -\sin\theta \\ \sin\theta & \cos\theta \end{pmatrix} \begin{pmatrix} q \\ r \end{pmatrix} \tag{F.4}
$$

Since τ and θ are constants, the relation between $(\dot{q}, \ \dot{r})^T$ and $(\dot{q}_2, \ \dot{q}_3)^T$ is

$$
\begin{pmatrix} \dot{q} \\ \dot{r} \end{pmatrix} = X \begin{pmatrix} \dot{q}_2 \\ \dot{q}_3 \end{pmatrix} \tag{F.5}
$$

Equation. (F.1) can be expressed in terms of $(q,\ r)^T$, $(q_2,\ q_3)^T$ and $(q_1,\ q_4)^T$ as

$$\begin{pmatrix} \dot{q} \\ \dot{r} \end{pmatrix} = \begin{pmatrix} -\hat{K}_d & ap \\ -ap & -\hat{K}_d \end{pmatrix} \begin{pmatrix} q \\ r \end{pmatrix} + (-\hat{K}_p) \begin{pmatrix} q_2 \\ q_3 \end{pmatrix} \tag{F.6a}$$

$$\begin{pmatrix} \dot{q}_2 \\ \dot{q}_3 \end{pmatrix} = \frac{1}{2}\begin{pmatrix} q_4 & -q_1 \\ q_1 & q_4 \end{pmatrix} \begin{pmatrix} q \\ r \end{pmatrix} + \frac{1}{2}\begin{pmatrix} 0 & p \\ -p & 0 \end{pmatrix} \begin{pmatrix} q_2 \\ q_3 \end{pmatrix} \tag{F.6b}$$

$$\begin{pmatrix} \dot{q}_1 \\ \dot{q}_4 \end{pmatrix} = \frac{1}{2}\begin{pmatrix} 0 & p \\ -p & 0 \end{pmatrix} \begin{pmatrix} q_1 \\ q_4 \end{pmatrix} + \frac{1}{2}\begin{pmatrix} r & -q \\ -q & -r \end{pmatrix} \begin{pmatrix} q_2 \\ q_3 \end{pmatrix} \tag{F.6c}$$

Substituting Equation. (F.4) into Equation. (F.6a), we get

$$\begin{pmatrix} \dot{q} \\ \dot{r} \end{pmatrix} = \left[\begin{pmatrix} -\hat{K}_d & ap \\ -ap & -\hat{K}_d \end{pmatrix} + (-\hat{K}_p)X^{-1} \right] \begin{pmatrix} q \\ r \end{pmatrix} = M \begin{pmatrix} q \\ r \end{pmatrix} \tag{F.7}$$

Similarly, substituting Equation. (F.2) into Equation. (F.6b), we get

$$\begin{pmatrix} \dot{q}_2 \\ \dot{q}_3 \end{pmatrix} = \left[\frac{1}{2}\begin{pmatrix} q_4 & -q_1 \\ q_1 & q_4 \end{pmatrix} X + \frac{1}{2}\begin{pmatrix} 0 & p \\ -p & 0 \end{pmatrix} \right] \begin{pmatrix} q_2 \\ q_3 \end{pmatrix} = N \begin{pmatrix} q_2 \\ q_3 \end{pmatrix} \tag{F.8}$$

According to Equations. (F.5), (F.7) and (F.8), we obtain

$$\begin{pmatrix} \dot{q} \\ \dot{r} \end{pmatrix} = X \begin{pmatrix} \dot{q}_2 \\ \dot{q}_3 \end{pmatrix} = XN \begin{pmatrix} q_2 \\ q_3 \end{pmatrix} = M \begin{pmatrix} q \\ r \end{pmatrix} = MX \begin{pmatrix} q_2 \\ q_3 \end{pmatrix} \tag{F.9}$$

Therefore, the relation between M, N and X must be

$$MX = XN \tag{F.10}$$

In the matrix form, we have

$$\left[\begin{pmatrix} -\hat{K}_d & ap \\ -ap & -\hat{K}_d \end{pmatrix} + (-\hat{K}_p)X^{-1} \right] X = X \left[\frac{1}{2}\begin{pmatrix} q_4 & -q_1 \\ q_1 & q_4 \end{pmatrix} X + \frac{1}{2}\begin{pmatrix} 0 & p \\ -p & 0 \end{pmatrix} \right] \tag{F.11}$$

Note that the preceding equation is a quadratic matrix equation as follows:

$$XAX + BX + XC = D \tag{F.12}$$

In the matrix form, the preceding equation can be written as

$$\frac{1}{2}X \begin{pmatrix} q_4 & -q_1 \\ q_1 & q_4 \end{pmatrix} X + \frac{1}{2}X \begin{pmatrix} 0 & p \\ -p & 0 \end{pmatrix} + \begin{pmatrix} \hat{K}_d & -ap \\ ap & \hat{K}_d \end{pmatrix} X = (-\hat{K}_p)I \quad \text{(F.13)}$$

We are going to find out expressions of q_1 and q_4. According to the assumption that q_1 and q_4 are constant, we have

$$\begin{pmatrix} \dot{q}_1 \\ \dot{q}_4 \end{pmatrix} = \frac{1}{2} \begin{pmatrix} 0 & p \\ -p & 0 \end{pmatrix} \begin{pmatrix} q_1 \\ q_4 \end{pmatrix} + \frac{1}{2} \begin{pmatrix} r & -q \\ -q & -r \end{pmatrix} \begin{pmatrix} q_2 \\ q_3 \end{pmatrix} = \begin{pmatrix} 0 \\ 0 \end{pmatrix} \quad \text{(F.14)}$$

therefore,

$$\frac{1}{2} \begin{pmatrix} 0 & p \\ -p & 0 \end{pmatrix} \begin{pmatrix} q_1 \\ q_4 \end{pmatrix} = -\frac{1}{2} \begin{pmatrix} r & -q \\ -q & -r \end{pmatrix} \begin{pmatrix} q_2 \\ q_3 \end{pmatrix} \quad \text{(F.15)}$$

Substituting Equation. (F.4) into the preceding equation, we obtain

$$\frac{1}{2} \begin{pmatrix} 0 & p \\ -p & 0 \end{pmatrix} \begin{pmatrix} q_1 \\ q_4 \end{pmatrix} = -\frac{1}{2} \begin{pmatrix} r & -q \\ -q & -r \end{pmatrix} \frac{1}{\tau} \begin{pmatrix} \cos\theta & -\sin\theta \\ \sin\theta & \cos\theta \end{pmatrix} \begin{pmatrix} q \\ r \end{pmatrix} \quad \text{(F.16)}$$

The right side of the preceding equation can be simplified

$$\frac{1}{2\tau} \begin{pmatrix} r\cos\theta - q\sin\theta & -r\sin\theta - q\cos\theta \\ -q\cos\theta - r\sin\theta & q\sin\theta - r\cos\theta \end{pmatrix} \begin{pmatrix} q \\ r \end{pmatrix} = \frac{1}{2\tau} \begin{pmatrix} qr\cos\theta - q^2\sin\theta - r^2\sin\theta - qr\cos\theta \\ -q^2\cos\theta - rq\sin\theta + qr\sin\theta - r^2\cos\theta \end{pmatrix}$$

$$= -\frac{q^2 + r^2}{2\tau} \begin{pmatrix} \sin\theta \\ \cos\theta \end{pmatrix}$$

(F.17)

Hence,

$$\begin{pmatrix} q_1 \\ q_4 \end{pmatrix} = \frac{q^2 + r^2}{\tau p} \begin{pmatrix} -\cos\theta \\ \sin\theta \end{pmatrix} = \Omega \begin{pmatrix} -\cos\theta \\ \sin\theta \end{pmatrix} \quad \text{(F.18)}$$

where $\Omega = \frac{q^2 + r^2}{\tau p}$

F.2 Solution of the Quadratic Matrix Equation

The matrix X is the solution of the Equation. (F.13)

$$\frac{1}{2}X \begin{pmatrix} q_4 & -q_1 \\ q_1 & q_4 \end{pmatrix} X + \frac{1}{2}X \begin{pmatrix} 0 & p \\ -p & 0 \end{pmatrix} + \begin{pmatrix} \hat{K}_d & -ap \\ ap & \hat{K}_d \end{pmatrix} X = (-\hat{K}_p)I \quad \text{(F.19)}$$

where

$$\begin{pmatrix} q_1 \\ q_4 \end{pmatrix} = \Omega \begin{pmatrix} -\cos\theta \\ \sin\theta \end{pmatrix} \tag{F.20}$$

The first term on the left side of Equation. (F.13) can be written as

$$\frac{1}{2}X \begin{pmatrix} q_4 & -q_1 \\ q_1 & q_4 \end{pmatrix} X = \frac{\tau^2\Omega}{2} \begin{pmatrix} \cos\theta & \sin\theta \\ -\sin\theta & \cos\theta \end{pmatrix} \begin{pmatrix} \sin\theta & \cos\theta \\ -\cos\theta & \sin\theta \end{pmatrix} \begin{pmatrix} \cos\theta & \sin\theta \\ -\sin\theta & \cos\theta \end{pmatrix}$$
$$= \frac{\tau^2\Omega}{2} \begin{pmatrix} 0 & 1 \\ -1 & 0 \end{pmatrix} \begin{pmatrix} \cos\theta & \sin\theta \\ -\sin\theta & \cos\theta \end{pmatrix}$$
$$= \frac{\tau^2\Omega}{2} \begin{pmatrix} -\sin\theta & \cos\theta \\ -\cos\theta & -\sin\theta \end{pmatrix} \tag{F.21}$$

The second term on the left side of Equation. (F.13) can be written as

$$\frac{1}{2}X \begin{pmatrix} 0 & p \\ -p & 0 \end{pmatrix} = \frac{\tau}{2} \begin{pmatrix} \cos\theta & \sin\theta \\ -\sin\theta & \cos\theta \end{pmatrix} \begin{pmatrix} 0 & p \\ -p & 0 \end{pmatrix} = \frac{\tau p}{2} \begin{pmatrix} -\sin\theta & \cos\theta \\ -\cos\theta & -\sin\theta \end{pmatrix} \tag{F.22}$$

The third term on the left side of Equation. (F.13) can be written as

$$\begin{pmatrix} \hat{K}_d & -ap \\ ap & \hat{K}_d \end{pmatrix} X = \begin{pmatrix} \hat{K}_d & -ap \\ ap & \hat{K}_d \end{pmatrix} \tau \begin{pmatrix} \cos\theta & \sin\theta \\ -\sin\theta & \cos\theta \end{pmatrix}$$
$$= \tau\hat{K}_d \begin{pmatrix} \cos\theta & \sin\theta \\ -\sin\theta & \cos\theta \end{pmatrix} + \tau ap \begin{pmatrix} \sin\theta & -\cos\theta \\ \cos\theta & \sin\theta \end{pmatrix} \tag{F.23}$$

Substituting Equations. (F.21), (F.22) and (F.23) into Equation. (F.13), the quadratic matrix equation becomes

$$(\frac{\tau^2\Omega}{2}+\frac{\tau p}{2}) \begin{pmatrix} -\sin\theta & \cos\theta \\ -\cos\theta & -\sin\theta \end{pmatrix} + \tau ap \begin{pmatrix} \sin\theta & -\cos\theta \\ \cos\theta & \sin\theta \end{pmatrix} + \tau\hat{K}_d \begin{pmatrix} \cos\theta & \sin\theta \\ -\sin\theta & \cos\theta \end{pmatrix} = (-\hat{K}_p)I \tag{F.24}$$

or

$$(\frac{\tau(2a-1)p}{2} - \frac{\tau^2\Omega}{2}) \begin{pmatrix} \sin\theta & -\cos\theta \\ \cos\theta & \sin\theta \end{pmatrix} + \tau\hat{K}_d \begin{pmatrix} \cos\theta & \sin\theta \\ -\sin\theta & \cos\theta \end{pmatrix} = (-\hat{K}_p)I \tag{F.25}$$

Therefore, τ and θ must satisfy the following equation

$$\begin{pmatrix} \frac{\tau(2a-1)p-\tau^2\Omega}{2}\sin\theta + \tau\hat{K}_d\cos\theta & -\frac{\tau(2a-1)p-\tau^2\Omega}{2}\cos\theta + \tau\hat{K}_d\sin\theta \\ \frac{\tau(2a-1)p-\tau^2\Omega}{2}\cos\theta - \tau\hat{K}_d\sin\theta & \frac{\tau(2a-1)p-\tau^2\Omega}{2}\sin\theta + \tau\hat{K}_d\cos\theta \end{pmatrix} = (-\hat{K}_p)I \qquad \text{(F.26)}$$

Note that the preceding equation can be reduced to only two equations

$$\frac{\tau(2a-1)p-\tau^2\Omega}{2}\sin\theta + \tau\hat{K}_d\cos\theta = -\hat{K}_p \qquad \text{(F.27)}$$

and

$$\frac{\tau(2a-1)p-\tau^2\Omega}{2}\cos\theta - \tau\hat{K}_d\sin\theta = 0 \qquad \text{(F.28)}$$

In the matrix form, we get

$$\begin{pmatrix} \frac{\tau(2a-1)p-\tau^2\Omega}{2} & \tau\hat{K}_d \\ -\tau\hat{K}_d & \frac{\tau(2a-1)p-\tau^2\Omega}{2} \end{pmatrix} \begin{pmatrix} \sin\theta \\ \cos\theta \end{pmatrix} = \begin{pmatrix} -\hat{K}_p \\ 0 \end{pmatrix} \qquad \text{(F.29)}$$

Since $\Omega = \frac{q^2+r^2}{\tau p}$, we find

$$\tau \begin{pmatrix} \frac{(2a-1)p^2-(q^2+r^2)}{2p} & \hat{K}_d \\ -\hat{K}_d & \frac{(2a-1)p^2-(q^2+r^2)}{2p} \end{pmatrix} \begin{pmatrix} \sin\theta \\ \cos\theta \end{pmatrix} = \begin{pmatrix} -\hat{K}_p \\ 0 \end{pmatrix} \qquad \text{(F.30)}$$

or

$$\tau \begin{pmatrix} \sin\theta \\ \cos\theta \end{pmatrix} = \frac{-\hat{K}_p}{(\frac{(2a-1)p^2-(q^2+r^2)}{2p})^2 + (\hat{K}_d)^2} \begin{pmatrix} \frac{(2a-1)p^2-(q^2+r^2)}{2p} \\ \hat{K}_d \end{pmatrix} \qquad \text{(F.31)}$$

If τ is chosen as

$$\tau = \frac{-\hat{K}_p}{\sqrt{(\frac{(2a-1)p^2-(q^2+r^2)}{2p})^2 + (\hat{K}_d)^2}} \qquad \text{(F.32)}$$

Finally, solving Equation. (F.13) yields

$$\begin{pmatrix} \sin\theta \\ \cos\theta \end{pmatrix} = \frac{1}{\sqrt{(\frac{(2a-1)p^2-(q^2+r^2)}{2p})^2 + (\hat{K}_d)^2}} \begin{pmatrix} \frac{(2a-1)p^2-(q^2+r^2)}{2p} \\ \hat{K}_d \end{pmatrix} \qquad \text{(F.33)}$$

F.3 State Equations of the Steady-State Oscillation

Substituting Equations. (F.18) and (F.33) into Equation. (F.8) yields

$$\begin{pmatrix} \dot{q}_2 \\ \dot{q}_3 \end{pmatrix} = N \begin{pmatrix} q_2 \\ q_3 \end{pmatrix} = \frac{p^2+q^2+r^2}{2p} \begin{pmatrix} 0 & 1 \\ -1 & 0 \end{pmatrix} \begin{pmatrix} q_2 \\ q_3 \end{pmatrix} \qquad \text{(F.34)}$$

From Equation. (F.7) we have

$$M = \begin{pmatrix} -\hat{K}_d & ap \\ -ap & -\hat{K}_d \end{pmatrix} + (-\hat{K}_p)X^{-1} \tag{F.35}$$

According to Equations. (F.18) and (F.32), we have

$$M = \begin{pmatrix} -\hat{K}_d & ap \\ -ap & -\hat{K}_d \end{pmatrix} + \sqrt{(\frac{(2a-1)p^2 - (q^2+r^2)}{2p})^2 + (\hat{K}_d)^2} \begin{pmatrix} \cos\theta & -\sin\theta \\ \sin\theta & \cos\theta \end{pmatrix}$$

$$= \begin{pmatrix} -\hat{K}_d + \sqrt{(\frac{(2a-1)p^2-(q^2+r^2)}{2p})^2 + (\hat{K}_d)^2}\cos\theta & ap - \sqrt{(\frac{(2a-1)p^2-(q^2+r^2)}{2p})^2 + (\hat{K}_d)^2}\sin\theta \\ -ap + \sqrt{(\frac{(2a-1)p^2-(q^2+r^2)}{2p})^2 + (\hat{K}_d)^2}\sin\theta & -\hat{K}_d + \sqrt{(\frac{(2a-1)p^2-(q^2+r^2)}{2p})^2 + (\hat{K}_d)^2}\cos\theta \end{pmatrix} \tag{F.36}$$

Substituting Equation. (F.33) into the preceding equation yields

$$M = \begin{pmatrix} 0 & ap - \frac{(2a-1)p^2-(q^2+r^2)}{2p} \\ -ap + \frac{(2a-1)p^2-(q^2+r^2)}{2p} & 0 \end{pmatrix} = \frac{(p^2+q^2+r^2)}{2p} \begin{pmatrix} 0 & 1 \\ -1 & 0 \end{pmatrix} \tag{F.37}$$

Finally, state equations of the steady-state oscillation are listed here

$$\begin{pmatrix} \dot{q}_2 \\ \dot{q}_3 \end{pmatrix} = \frac{p^2+q^2+r^2}{2p} \begin{pmatrix} 0 & 1 \\ -1 & 0 \end{pmatrix} \begin{pmatrix} q_2 \\ q_3 \end{pmatrix} \tag{F.38}$$

$$\begin{pmatrix} \dot{q} \\ \dot{r} \end{pmatrix} = \frac{p^2+q^2+r^2}{2p} \begin{pmatrix} 0 & 1 \\ -1 & 0 \end{pmatrix} \begin{pmatrix} q \\ r \end{pmatrix} \tag{F.39}$$

and

$$\begin{pmatrix} q \\ r \end{pmatrix} = \tau \begin{pmatrix} \cos\theta & \sin\theta \\ -\sin\theta & \cos\theta \end{pmatrix} \begin{pmatrix} q_2 \\ q_3 \end{pmatrix} \tag{F.40}$$

where

$$\tau = \frac{-\hat{K}_p}{\sqrt{(\frac{(2a-1)p^2-(q^2+r^2)}{2p})^2 + (\hat{K}_d)^2}} \tag{F.41}$$

$$\begin{pmatrix} q_1 \\ q_4 \end{pmatrix} = \frac{q^2+r^2}{\tau p} \begin{pmatrix} -\cos\theta \\ \sin\theta \end{pmatrix} \tag{F.42}$$

$$\begin{pmatrix} \sin\theta \\ \cos\theta \end{pmatrix} = \frac{1}{\sqrt{(\frac{(2a-1)p^2-(q^2+r^2)}{2p})^2 + (\hat{K}_d)^2}} \begin{pmatrix} \frac{(2a-1)p^2-(q^2+r^2)}{2p} \\ \hat{K}_d \end{pmatrix} \tag{F.43}$$

$$\theta = \tan^{-1}\frac{(2a-1)p^2 - q^2 - r^2}{2p\hat{K}_d} \tag{F.44}$$

Since there is another constraint

$$q_1^2 + q_2^2 + q_3^2 + q_4^2 = 1 \tag{F.45}$$

From Equation. (F.18) we have

$$q_1^2 + q_4^2 = (\frac{q^2 + r^2}{\tau p})^2 \tag{F.46}$$

From Equation. (F.2) we get

$$q^2 + r^2 = \tau^2(q_2^2 + q_3^2) \tag{F.47}$$

Define the magnitude square of the vector $(q,\ r)^T$ as x

$$q^2 + r^2 = x \tag{F.48}$$

and

$$q_2^2 + q_3^2 = \frac{x}{\tau^2} \tag{F.49}$$

Therefore, x must satisfy the constraint

$$q_1^2 + q_2^2 + q_3^2 + q_4^2 = (\frac{x}{\tau p})^2 + \frac{x}{\tau^2} = 1 \tag{F.50}$$

Substituting Equation. (F.32) into the preceding equation yields

$$x^4 + (3-4a)p^2x^3 + [(2a-1)(2a-3)p^2 + 4\hat{K}_d^2]p^2x^2 + [(2a-1)^2p^2 + 4\hat{K}_d^2]p^4x - 4p^4\hat{K}_p^2 = 0 \tag{F.51}$$

Define a function $f(x)$ as the left side of equal sign of the preceding equation

$$f(x) = x^4 + (3-4a)p^2x^3 + [(2a-1)(2a-3)p^2 + 4\hat{K}_d^2]p^2x^2 + [(2a-1)^2p^2 + 4\hat{K}_d^2]p^4x - 4p^4\hat{K}_p^2 \tag{F.52}$$

Since x is the magnitude square of the vector $(q,\ r)^T$, all real positive zeros of the function $f(x)$ could be x.

APPENDIX G. DERIVATION OF THE DERIVATIVE OF A LYAPUNOV FUNCTION CANDIDATE

A Lyapunov function candidate is given in Equation. (5.17),

$$V(\mathbf{x}) = \frac{1}{2\hat{K}_p}q^2 + \frac{1}{2\hat{K}_p}r^2 + [q_1 - \sin(\lambda/2)]^2 + q_2^2 + q_3^2 + [q_4 - \cos(\lambda/2)]^2 \qquad \text{(G.1)}$$

Expanding the square terms of quaternion, we get

$$V(\mathbf{x}) = \frac{1}{2\hat{K}_p}q^2 + \frac{1}{2\hat{K}_p}r^2 + q_1^2 - 2q_1\sin(\lambda/2) + \sin^2(\lambda/2)$$
$$+ q_2^2 + q_3^2 + q_4^2 - 2q_4\cos(\lambda/2) + \cos^2(\lambda/2) \quad \text{(G.2)}$$

Therefore, the Lyapunov function can be rewritten as

$$V(\mathbf{x}) = \frac{1}{2\hat{K}_p}(q^2 + r^2) + 2 - 2q_1\sin(\lambda/2) - 2q_4\cos(\lambda/2) \qquad \text{(G.3)}$$

The derivative of $V(\mathbf{x})$ is

$$\dot{V}(\mathbf{x}) = \frac{1}{\hat{K}_p}(q\dot{q} + r\dot{r}) - 2\dot{q}_1\sin(\lambda/2) - q_1\cos(\lambda/2)\dot{\lambda} - 2\dot{q}_4\cos(\lambda/2) + q_4\sin(\lambda/2)\dot{\lambda} \qquad \text{(G.4)}$$

Substituting Equation. (5.16) into the preceding equation yields the derivative of $V(\mathbf{x})$ along the trajectories of the system, then

$$\dot{V}(\mathbf{x}) = \frac{q}{\hat{K}_p}\{arp - \hat{K}_p[\cos(\lambda/2)q_2 + \sin(\lambda/2)q_3] - \hat{K}_d q\}$$
$$+ \frac{r}{\hat{K}_p}\{-apq - \hat{K}_p[-\sin(\lambda/2)q_2 + \cos(\lambda/2)q_3] - \hat{K}_d r\}$$
$$- (rq_2 - qq_3 + pq_4)\sin(\lambda/2) - (-pq_1 - qq_2 - rq_3)\cos(\lambda/2) \qquad \text{(G.5)}$$
$$- q_1\cos(\lambda/2)\dot{\lambda} + q_4\sin(\lambda/2)\dot{\lambda}$$

Expanding the preceding equation yields

$$\dot{V}(\mathbf{x}) = \frac{apqr}{\hat{K}_p} - qq_2\cos(\lambda/2) - qq_3\sin(\lambda/2) - \frac{\hat{K}_d}{\hat{K}_p}q^2 - \frac{apqr}{\hat{K}_p} + rq_2\sin(\lambda/2) - rq_3\cos(\lambda/2) - \frac{\hat{K}_d}{\hat{K}_p}r^2$$
$$- rq_2\sin(\lambda/2) + qq_3\sin(\lambda/2) - pq_4\sin(\lambda/2) + pq_1\cos(\lambda/2) + qq_2\cos(\lambda/2) + rq_3\cos(\lambda/2)$$
$$- [q_1\cos(\lambda/2) - q_4\sin(\lambda/2)]\dot{\lambda}$$

$$(G.6)$$

Hence,

$$\dot{V}(\mathbf{x}) = -\frac{\hat{K}_d}{\hat{K}_p}q^2 - \frac{\hat{K}_d}{\hat{K}_p}r^2 + [q_1\cos(\lambda/2) - q_4\sin(\lambda/2)]p - [q_1\cos(\lambda/2) - q_4\sin(\lambda/2)]\dot{\lambda} \quad (G.7)$$

Finally, we obtain a compact form the the derivative of $V(\mathbf{x})$

$$\dot{V}(\mathbf{x}) = -\frac{\hat{K}_d}{\hat{K}_p}(q^2 + r^2) + [q_1\cos(\lambda/2) - q_4\sin(\lambda/2)](p - \dot{\lambda}) \quad (G.8)$$

Since $\dot{\lambda} = p$, we have

$$\dot{V}(\mathbf{x}) = -\frac{\hat{K}_d}{\hat{K}_p}(q^2 + r^2) \quad (G.9)$$

BIBLIOGRAPHY

[1] Cook, S., "Ares Project Status," Presented at *2nd AIAA Space Exploration Conference*, December 4-6, 2006.

[2] Sumrall, P., "The Ares Projects: Progress Toward Exploration," Presented at *AIAA Space 2008 Conference*, September 10, 2008.

[3] Butt, A., Popp, C. G., Pitts, H. M. and Sharp, D. J., "NASA Ares I Launch Vehicle Roll and Reaction Control Systems Design Status," *NASA Technical Reports Server*, August 2009.

[4] Norris, L., Tao, Y. C., Hall, R., Chuang, J., and Whorton, M., "Analysis of Ares-I Ascent Navigation Options," AIAA 2008-6290, *AIAA Guidance, Navigation, and Control Conference*, Honolulu, Hawaii, August 18-21, 2008.

[5] Pinson, R. M., Schmitt, T. L., and Hanson, J. M., "Development of a Smooth Trajectory Maneuver Method to Accommodate the Ares I Flight Control Constrains," AIAA 2008-6292, *AIAA Guidance, Navigation, and Control Conference*, Honolulu, Hawaii, August 18-21, 2008.

[6] Pitman, G. R., *Inertial Guidance*, New York, John Wiley and Sons, 1962, pp. 260-261.

[7] Dukeman, G. A., and Hill, A. D., "Rapid Trajectory Optimization for the Ares-I Launch Vehicle," AIAA 2008-6288, *AIAA Guidance, Navigation, and Control Conference*, Honolulu, Hawaii, August 18-21, 2008.

[8] Seifert, H., *Space Technology*, New York, John Wiley and Sons, 1959, Chapter 4.

[9] Leondes, C. T., *Guidance and Control of Aerospace Vehicles*, New York, McGraw-Hill Book Company, 1963, pp. 191-249.

[10] Greensite, A. L., *Analysis and Design of Space Vehicle Flight Control Systems*, Spartan Books, New York, 1970, pp. 44-108, pp. 194-372.

[11] Whorton, M., Hall, C., and Cook, S., "Ascent Flight Control and Structural Interaction for the Ares-I Crew Launch Vehicle," AIAA 2007-1780, April 2007.

[12] Haeussermann, W., "Description and Performance of the Saturn Launch Vehicle's Navigation, Guidance, and Control System," *NASA Technical Reports Server*, NASA TN D-5869, July 1970.

[13] Frosch, J. A. and Valley, D. P., "Saturn AS-501/S-IC Flight Control System Design," *Journal of Spacecraft*, Vol. 4, No. 8, 1967, pp. 1003-1009.

[14] Blakelock, J., *Automatic Control of Aircraft and Missiles*, John Wiley & Sons, New York, 1991. pp. 429-437.

[15] Blackburn, T. R. and Vaughan, D. R., "Application of Linear Optimal Control and Filtering Theory to the Saturn V Launch Vehicle," *IEEE Transactions on Automatic Control*, Vol. AC-16, No. 6, December 1971, pp. 799-806.

[16] Wie, B., *Space Vehicle Dynamics and Control*, AIAA Education Series, 1998, pp. 129-145, pp. 381-418.

[17] Wie, B., and Barba, P. M., "Quaternion Feedback for Spacecraft Large Angle Maneuvers," *Journal of Guidance, Control, and Dynamics*, Vol. 8, No. 3, 1985, pp. 360-365.

[18] Wie, B., Weiss, H., and Arapostathis, A., "Quaternion Feedback Regulator for Spacecraft Eigenaxis Rotations," *Journal of Guidance, Control, and Dynamics*, Vol. 12, No. 3, 1989, pp. 375-380.

[19] Weiss, H., "Quaternion-Based Rate/Attitude racking System with Application to Gimbal Attitude Control," *Journal of Guidance, Control, and Dynamics*, Vol. 16, No. 4, 1993, pp. 609-616.

[20] Wie, B. and Byun, K. W., "New Generalized Structural Filtering Concept for Active Vibration Control Synthesis," *Journal of Guidance, Control, and Dynamics*, Vol. 12, No. 2, 1989, pp. 147-154.

[21] Byun, K. W., Wie, B. and Sunkel, J., "Robust Non-Minimum-Phase Compensation for a Class of Uncertain Dynamical Systems," *Journal of Guidance, Control, and Dynamics*, Vol. 14, No. 6, 1991, pp. 1191-1199.

[22] Davis, S., "Ares I-X Flight Test-The Future Begins Here," AIAA 2008-7806, *AIAA space 2008 Conference and Exposition*, San Diego, California, September 9-11, 2008.

[23] Crouch, P. E., "Spacecraft Attitude Control and Stabilization: Applications of Geometric Control Theory to Rigid Body Models," *IEEE Transactions on Automatic Control*, Vol. 29, No. 4, 1984, pp. 321-331.

[24] Krishnan, H., McClamroch, N. H., and Reyhanoglu, M., "Attitude Stabilization of a Rigid Spacecraft Using Gas Jet Actuators Operating in a Failure Mode," *IEEE Conference on Decision and Control*, Tucson, Arizona, pp. 1612-1617.

[25] Tsiotras, P., and Longuski, J. M., "Spin-axis stabilization of symmetric spacecraft with two control torques," *Systems & Control Letters*, Vol. 23, 1994, pp. 395-402.

[26] Tsiotras, P., Corless, M., and Longuski, J. M., "A Novel Approach to the Attitude Control of Axisymmetric Spacecraft," *Automatica*, Vol. 31, No. 6, 1995, pp. 1099-1112.

[27] Bymes, C.I., and Isidori. A., "On the attitude stabilization of rigid spacecraft," *Automatica*, Vol. 27, No. 1, 1991, pp. 87-95.

[28] Betts, K. M., Rutherford, R. C., McDuffie, J., Johnson, M. D., Jackson, M., and Hall, C., "Time Domain Simulation of the NASA Crew Launch Vehicle," AIAA 2007-6621, August 2007.

[29] Betts, K. M., Rutherford, R. C., McDuffie, J., Johnson, M. D., Jackson, M., and Hall, C., "Stability Analysis of the NASA Ares-I Crew Launch Vehicle Control System," AIAA 2007-6776, August 2007.

[30] James, R. L., "A Three-Dimensional Trajectory Simulation Using Six Degrees of Freedom with Arbitrary Wind," NASA TN D-641, 1961.

[31] Harris, R. J., "Trajectory Simulation Applicable to Stability and Control Studies of Large Multi-Engine Vehicles," NASA TN D-1838, 1963.

[32] Zipfel, P. H., *Modeling and Simulation of Aerospace Vehicle Dynamics*, AIAA Education Series, 1998, pp. 367-427.

[33] Stuelpnagel, J., "On the parameterization of the three-dimensional rotation group," *SLAM Review*, Vol. 6, No. 4, October 1964.

[34] Brandon, J. M., Derry, S. D., Heim, E. H., Hueschen, R. M., and Bacon, B. J., "Ares-I-X Stability and Control Flight Test: Analysis and Plans," *NASA Technical Reports Server*, September 2008.

[35] Hall, C., Lee, C., Jackson, M., Whorton, M., West, M., Brandon, J., Hall, R. A., Jang, J., Bedrossian, N., Compton, J., and Rutherford, C., "Ares-I Flight Control System Overview," AIAA 2008-6287, *AIAA Guidance, Navigation, and Control Conference*, Honolulu, Hawaii, August 18-21, 2008.

[36] Chopra, A. K., *Dynamics of Structures*, Prentice Hall, New Jersey, 1995, pp. 585-600.

[37] Hoelkner, R. F., "The Principle of Artificial Stabilization of Aerodynamically Unstable Missiles," ABMA DA-TR-64-59, September 25, 1959.

[38] Hoelkner, R. F., "Theory of Artificial Stabilization of Missiles and Space Vehicles with Exposition of Four Control Principles," *NASA Technical Reports Server*, NASA TN D-555, June 1961.

[39] Harvey, C. A., "An Alternate Derivation and Interpretation of the Drift-Minimum Principle," NASA Contract NASw-563, MH MPG Report 1541-TR 15, Minneapolis-Honeywell, November 22, 1963.

[40] Garner, D., "Control Theory Handbook," NASA TM X-53036, April 22, 1964.

[41] Rheinfurth, M. H., "The Alleviation of Aerodynamic Loads on Rigid Space Vehicles," NASA TM X-53397, February 21, 1966.

[42] Martin, D. T., Sievers , R. F., O'Brien, R. M., and Rice, A. F., "Saturn V Guidance, Navigation, and Targeting," *J. Spacecraft*, Vol. 4, No. 7, 1967, pp. 891-898.

[43] Wie, B., and Du, W., "Analysis and Design of Launch Vehicle Flight Control Systems," AIAA 2008-6291, *AIAA Guidance, Navigation, and Control Conference*, August 2008.

[44] Doyle, J. C., Francis, B. A. and Tannenbaum A. R., *Feedback Control Theory*, Dover Publication, New York, 1992, pp. 45-62.

[45] Skogestad, S. and Postlethwaite, I., *Multivariable Feedback Control: Analysis and Design*, John Wiley & Sons, 2nd ed., 2005, pp. 259-338.

[46] Zhou, K., Doyle, J. C. and Glover. K., *Robust and Optimal Control*, Prentice Hall, New Jersey, 1995, pp. 213-300.

[47] "Effects of Structural Flexibility on Launch Vehicle Control Systems," *NASA Technical Reports Server*, NASA SP-8036, February 1970.

[48] Balas, G. J., and Doyle, J. C., "Robustness and Performance Tradeoffs in Control Design for Flexible Structures," *IEEE Transactions on Control Systems Technology*, Vol. 2, No. 4, 1994, pp. 352-361.

[49] Balas, G. J., and Doyle, J. C., "Control of Lightly Damped, Flexible Modes in the Controller Crossover Region," *Journal of Guidance, Control, and Dynamics*, Vol. 17, No. 2, 1994, pp. 370-377.

[50] Smith, R. S., Chu, C. C., and Fanson, J. L., "The Design of H_∞ Controllers for an Experimental Non-collocated Flexible Structure Problem," *IEEE Transactions on Control Systems Technology*, Vol. 2, No. 2, 1994, pp. 101-109.

[51] Franklin, G. F., Powell, J. D., and Naeini, A. E., *Feedback Control of Dynamic Systems*, 5th ed., Prentice Hall, New Jersey, 2006, pp. 131-139.

[52] Khalil, H. K., *Nonlinear Systems*, 3rd ed., Prentice Hall, New Jersey, 2010, pp. 126-129.

[53] Sastry, S. S., *Nonlinear Systems: Analysis, Stability, and Control*, 1st ed., Springer, New York, 1999, pp. 287-288.